

AD-764 646

THE NET CIRCULATION IN THE WEST PASSAGE
OF NARRAGANSETT BAY

Robert H. Weisberg, et al

Rhode Island University

Prepared for:

Office of Naval Research

March 1973

DISTRIBUTED BY:

NTIS

National Technical Information Service
U. S. DEPARTMENT OF COMMERCE
5285 Port Royal Road, Springfield Va. 22151

AD-764-646

GRADUATE SCHOOL OF OCEANOGRAPHY
UNIVERSITY OF RHODE ISLAND
KINGSTON, RHODE ISLAND

Reproduction of the material contained in this report in
whole or in part is permitted for any purpose of the
United States Government

Distribution of this document is unlimited

The Net Circulation in the West Passage of
Narragansett Bay

Technical Report

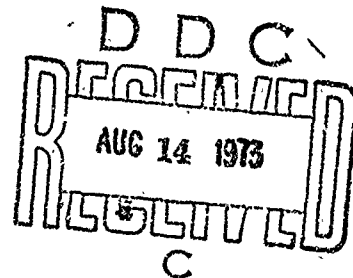
Ref. No. 3-73

by

Robert H. Weisberg

and

Wilton Sturges III



Approved for Distribution

John A. Krauss

Sponsored by Office of Naval Research

Report under Contract N00014-68-A-0215-0003

March 1973

Reproduced by
NATIONAL TECHNICAL
INFORMATION SERVICE
U S Department of Commerce
Springfield VA 22131

DOCUMENT CONTROL DATA - R & D

(Security classification of title, body of abstract and indexing annotation must be entered when the overall report is classified)

1. ORIGINATING ACTIVITY (Corporate author)		2a. REPORT SECURITY CLASSIFICATION	
G. aduate School of Oceanography, University of Rhode Island, Kingston, R.I. 02881		Unclassified	
		2b. GROUP	
		n/a	
3. REPORT TITLE			
The Net Circulation in the West Passage of Narragansett Bay			
4. DESCRIPTIVE NOTES (Type of report and inclusive dates)			
Technical Report			
5. AUTHOR(S) (First name, middle initial, last name)			
Robert H. Weisberg and Wilton Sturges III			
6. REPORT DATE		7a. TOTAL NO. OF PAGES	7b. NO. OF REFS
March 1973		98/09	25
8a. CONTRACT OR GRANT NO.		9a. ORIGINATOR'S REPORT NUMBER(S)	
N00014-68-A-0215-0003		3-73	
b. PROJECT NO. n/a			
c. n/a		9b. OTHER REPORT NO(S) (Any other numbers that may be assigned this report)	
d. n/a		n/a	
10. DISTRIBUTION STATEMENT			
Approved for public release; distribution unlimited.			
11. SUPPLEMENTARY NOTES		12. SPONSORING MILITARY ACTIVITY	
This report was initiated under state of R.I. funding. Partial support was also obtained from the Narragansett Electric Co; URI #98-20-7057; and CTR Contract # N00014-68-A-0215-0003.		n/a	
13. ABSTRACT			
<p>Narragansett Bay is a weakly stratified estuary comprised of three connecting passages of varying depths. The vertical distribution of horizontal velocity was observed in the West Passage using moored current meters. The instantaneous motion was characterized by semi-diurnal tidal currents of amplitude 25-60 cm/s. These currents exhibited a phase advance with depth (total water depth=12.8 m) ranging with lunar phase from 0-3 hrs. The primary objective of the study was the analysis of the net circulation, i.e., the motion exclusive of the periodic tides. The net current time series obtained by filtering out the tidal periodicities were found to be an order of magnitude less than the instantaneous motion and well correlated to the prevailing 2-10 m/s wind. For periodicities about two days, the squared coherence and phase between the longitudinal components of wind and net near surface current were 0.7 and 3 hours respectively. The mean near surface speed, obtained by averaging over one month, was 1.2 ± 1.6 cm/s. The large error bounds were a result of the large variability of the net current time series (and not a result of inadequate sampling). A measure of this variability due to day to day changes in weather is given by the root mean square deviation of the net current time series or 2.6 cm/s. The net transport of water through the West Passage was observed to be seaward or landward over the entire water column for several days duration, with typical wind induced transport fluctuations of ± 500 m³/s. Hence, a net communication of water exists between the East and West Passages with water flowing either way in response to the wind. Wind is concluded to be the dominant mechanism driving the net circulation in the West Passage of Narragansett Bay. This is in contrast with the classical views of gravitationally convected net estuarine circulation.</p>			

14 KEY WORDS	LINK A		LINK B		LINK C	
	ROLE	WT	ROLE	WT	ROLE	WT
Estuary Narragansett Bay Physical Oceanography Currents Tidal Characteristics Net Circulation Net Transport.						

ia

ABSTRACT

Narragansett Bay is a weakly stratified estuary comprised of three connecting passages of varying depths. The vertical distribution of horizontal velocity was observed in the West Passage using moored current meters. The instantaneous motion was characterized by semi-diurnal tidal currents of amplitude 25-60 cm/s. These currents exhibited a phase advance with depth (total water depth = 12.8 m) ranging with lunar phase from 0-3 hrs. The primary objective of the study was the analysis of the net circulation, i.e., the motion exclusive of the periodic tides. The net current time series obtained by filtering out the tidal periodicities were found to be an order of magnitude less than the instantaneous motion and well correlated to the prevailing 2-10 m/s winds. For periodicities about two days, the squared coherence and phase between the longitudinal components of wind and net near surface current were 0.7 and 3 hours respectively. The mean near surface speed, obtained by averaging over one month, was 1.2 ± 1.6 cm/s. The large error bounds were a result of the large variability of the net current time series (and not a result of inadequate sampling). A measure of this variability due to day to day changes in weather is given by the root mean square deviation of the net current time series or 2.6 cm/s. The net transport of water through the West Passage was observed to be seaward or landward over the entire water column for several days duration, with typical wind induced transport fluctuations of $\pm 500 \text{ m}^3/\text{s}$. Hence, a net communication of water exists between the East and West Passages with water flowing either way in response to the wind. Wind is concluded to be the dominant mechanism driving the net circulation in the West Passage of Narragansett Bay. This is in contrast with the classical views of gravitationally convected net estuarine circulation.

Preface

A report in this form was submitted by Robert H. Weisberg in June 1972 as partial fulfillment for a Master of Science degree in Oceanography, at the University of Rhode Island. Several revisions appear in the present form. The work was planned and initiated with the assistance of State of Rhode Island funding. The authors were able to expand their project with the help of a grant from the Narragansett Electric Co., U.R.I. # 98-20-7057. Partial support was also given by the Office of Naval Research, grant # N00014-68-A-0215-0003.

TABLE OF CONTENTS

	Page
TITLE PAGE.....	i
ABSTRACT.....	ii
PREFACE.....	iii
TABLE OF CONTENTS.....	iv
LIST OF TABLES.....	vi
LIST OF FIGURES.....	viii
CHAPTER	
I. INTRODUCTION.....	1
II. MEASUREMENT PROGRAM.....	3
Station Location.....	3
Current Meter Distribution.....	6
Current Sampling.....	7
Subsidiary Data.....	8
Support Equipment.....	9
Rigidly Moored Array.....	9
Buoyantly Moored Array.....	9
Field Procedures.....	13
III. DATA PROCESSING AND RESULTS.....	14
Instantaneous Currents.....	14
Net Currents (Fall 1970).....	18
Averaging Technique.....	18
Results of Filtering.....	21
Digression on Estimating the Uncertainty of the Mean Values.....	25
Results of Filtering (cont'd).....	27
Qualitative Correlation Analysis.....	29
Vertical Distributions of the Net North Velocity Component at the Rome Point Station.....	32
Net Transport.....	37
Correlation Analysis between the North Components of Wind and Net Near Surface Current.....	39
Net Currents (Spring 1971).....	46

	Page
IV. DISCUSSION.....	49
Wind Induced Transport.....	49
Phase Advance of the Instantaneous Motion with Depth.....	52
V. SUMMARY AND CONCLUSIONS.....	57
ACKNOWLEDGEMENTS.....	59
BIBLIOGRAPHY.....	60
APPENDICES	
APPENDIX 1. Instancaneous Motion.....	63
APPENDIX 2. Error Analysis.....	73
APPENDIX 3. Fresh Water Input.....	84
APPENDIX 4. Stratification.....	88

LIST OF TABLES

Table	Page
1. Station locations and depths.....	3
2. Position, record number, and sampling duration for all current meters used during the fall 1970 and spring 1971 measurements.....	7
3. The r.m.s. current speed, percentage of energy contained in the M_2 and M_4 harmonics and the phase difference ($\Delta\phi_{M_2}$) of the M_2 harmonic for currents measured 2.1 m and 7.2 m below mean low water	16
4. The mean values and the root mean square deviations about the mean for the Gaussian filtered ($\sigma = 8$ hr) and the unfiltered north component time series obtained from the fall 1970 Rome Point station. Positive denotes flow to the north.....	25
5. The net transport of water through the West Passage as computed from the fall 1970 Rome Point station data. Estimates are given for the mean plus and minus two standard errors, the mean plus and minus one standard deviation (s.d.) and for various wind conditions. The river input rate (see Appendix 3) is also included for comparison. An asterisk indicates values that are not statistically different from zero.....	38
6. Squared coherence, phase, and transfer function for the bandpass filtered north component time series of wind and net near surface current (record 026). The data were obtained from the fall 1970 Rome Point station. A negative value of phase indicates that the net current lags the wind.....	44
7. The mean values and the root mean square deviations about the mean for the net currents obtained from the spring 1971 Rome Point station. Positive denotes flow toward the north.....	48

Table	Page
8. A sample calculation showing the surface elevation at the northern tip of Conanicut Island under the influence of a 10 m/s northward wind.....	52
9. Sample calculations showing the vertical extent of bottom frictional effects.....	54
A 2.1a. Calculated wave heights (cm) as a function of wind speed and fetch.....	78
A 2.1b. Calculated wavelengths (m) as a function of wind speed and fetch.....	78
A 2.1c. Calculated wave periods (sec) as a function of wind speed and fetch.....	78
A 2.2. The magnitude V_d (cm/s) of the wave induced water motions at a depth of 2 m (depth of the near surface current meter). The dashed line demarks the limit after which wave biasing may be troublesome.....	79
A 3. The average uncorrected volume flow rate for the rivers feeding the western side of Narragansett Bay and the corresponding fresh water input to the West Passage during the fall and spring measurement programs.....	85
A 4.1. Temperature, salinity, and σ_t at the Rome Point station during the fall program.....	91
A 4.2. Temperature, salinity, and σ_t at the Bonnet Shores station during the fall program.....	92
A 4.3. Temperature, salinity, and σ_t at the Rome Point station during the spring program.....	93
A 4.4. Temperature, salinity, and σ_t at the Bonnet Shores station during the spring program.....	95
A 4.5. Typical vertical and longitudinal density gradients in the West Passage during the fall and spring measurement programs.....	88

LIST OF FIGURES

Figure		Page
1.	A map of Narragansett Bay showing the station locations and the principal rivers.....	2
2.	The cross sectional area of the West Passage at the Rome Point station.....	4
3.	The cross sectional area of the West Passage at the Bonnet Shores station.....	5
4.	The rigidly moored array used at the Rome Point station.....	10
5.	The rigidly moored current meter mounting scheme.....	11
6.	The buoyantly moored array used at the Bonnet Shores station.....	12
7.	The kinetic energy spectrum of the near surface current (record 026) observed at the fall 1970 Rome Point station.....	15
8.	The north components of currents measured 2.1 m and 7.2 m below mean low water (records 026 and 023 respectively). The deeper current leads the near surface current.....	17
9.	The north component of instantaneous current at the Rome Point station as a function of depth for different stages of a tidal cycle.....	19
10.	The frequency response function of a Gaussian filter..	20
11 a, b, c.	The net current and smoothed wind time series obtained during the fall of 1970.....	22, 23, 24
12.	A comparison of the instantaneous and net near surface current (record 026) at the Rome Point station.....	26
13.	The autocovariance function of the net near surface current (record 026) at the Rome Point station.....	28
14.	A scatter plot of the north components of net near surface current (record 026) and wind.....	30

Figure		Page
15.	A scatter plot of the north component of net near surface current (record 026) and the east component of wind.....	31
16.	A vertical distribution of the net north component of velocity at the Rome Point station. Included are: the mean values averaged over the entire record length of one month (center curve), the mean plus and minus two standard errors of the mean (2σ), and the mean values plus and minus one standard deviation of the signal (σ).....	35
17.	The vertical distribution of the net north component of velocity at the Rome Point station comparing winds blowing toward the northwest and southwest...	34
18.	The vertical distribution of the net north component of velocity at the Rome Point station for two independent rebound events.....	35
19.	The vertical distribution of the net north component of velocity at the Rome Point station showing the response of the West Passage to a quick reversal in wind direction.....	36
20 a, b, c.	The bandpass filtered time series of the north components of wind and near surface current (record 026) at the Rome Point station.....	41, 42, 43
21.	The net current and smoothed wind time series obtained during the spring of 1971.....	47
22.	The vertical distribution of Ekman's elementary current system projected on a horizontal plane. Examples 7 and 8 apply to a wind blowing parallel to the axis of the West Passage. (From Ekman (1905)).....	50
23 a, b.	The depth distribution for the relative amplitude and phase of a simple harmonic oscillation over a flat plate. Curves are given for three different values of the eddy viscosity coefficient. The comparative data points are from Cannon (1969) and the present study.....	55

Figure		Page
A 1.1	Record 022, Position: Rome Point Station, 3.8 m from the bottom.....	64
A 1.2	Record 023, Position: Rome Point Station, 5.5 m from the bottom.....	65
A 1.3	Record 025, Position: Rome Point Station, 8.9 m from the bottom.....	66
A 1.4	Record 026, Position: Rome Point Station, 10.6 m from the bottom.....	67
A 1.5	Record 027, Position: Bonnet Shores Station, 3.7 m from the bottom.....	68
A 1.6	Record 028, Position: Bonnet Shores Station, 1.7 m from the bottom.....	69
A 1.7	Record 1, Position: Rome Point Station, 10.6 m from the bottom.....	70
A 1.8	Record 3, Position: Rome Point Station, 3.8 m from the bottom.....	71
A 1.9	Record 4, Position: Rome Point Station, 2.1 m from the bottom.....	72
A 2.1	The West Passage broken into eight regions, each with a characteristic fetch.....	75
A 2.2	Wave height, age, and period as a function of wind speed and fetch. (From Weigel 1964).....	76
A 2.3	Wave steepness as a function of wave age. (After Sverdrup and Munk (1947)).....	77
A 2.4	Progressive vector diagram of the wind during the fall 1970 experiment.....	81
A 2.5	Progressive vector diagram of the wind during the spring 1971 experiment.....	82
A 3.1	River input data obtained from a gauging station on the Blackstone River.....	86
A 3.2	River input data obtained from gauging stations on the Potowomut, Woonasquatucket, and Pawtuxet rivers.....	87

Figure		Page
A 4.1	Examples of Sigma-t as a function of depth during the fall 1970 measurement program.....	89
A 4.2	Examples of Sigma-t as a function of depth during the spring 1971 measurement program.....	90

I INTRODUCTION

The instantaneous motion in an estuary is strongly affected by tides. If velocity observations are averaged, or filtered, to remove the tidal currents then the remaining non-tidal motion may be termed the "net velocity" field. It is this net velocity field that is generally referred to as estuarine circulation.

The gravitational convection scheme of estuarine circulation has received considerable emphasis in the past. This particular driving mechanism arises from the density difference between the river and ocean ends of the estuary. The resulting net circulation is generally two layered with a seaward flow of fresher water in the upper layer and landward flow of saltier water in the lower layer, e.g., see Cameron and Pritchard (1963).

Narragansett Bay is a partially mixed estuary. It is comprised of three connecting passages as shown in Figure 1. Data concerning the instantaneous and net motion were first compiled by Haight (1938). Hicks (1959, 1963) offers a general description of the physical parameters in the bay.

The primary objective of the present study is the analysis of the net circulation and transport in the West Passage of Narragansett Bay. Based on the constraints of water and salt conservation, published estuarine literature contains several recipes for estimating the net circulation from rudimentary measurements of salinity and velocity. e.g., see Pritchard and Kent (1956), Rattray and Hansen (1962), and Hansen and Rattray (1966). These constraints cannot be invoked in the West Passage a priori because sources of both water and salt exist at the connection of the West and East Passages above Conanicut Island. Therefore, a program to measure the vertical distribution of horizontal velocity was initiated. Another reason for a direct measurement program was to study the effects of wind. A theoretical model by Hansen and Rattray (1965) implied that, along with gravitational convection, wind may also be an important driving mechanism of the net circulation. Except for short term observations by Pickard and Rodgers (1959) in the Knight Inlet, British Columbia, little attention has been given to the effects of wind on net estuarine circulation.

Some preliminary results of this study may be found in Sturges and Weisberg (1971).

II MEASUREMENT PROGRAM

Station Location

Transport determinations entail the integration of a velocity field over a cross sectional area. Excepting very wide estuaries, where the effect of the earth's rotation becomes important, lateral variability in the net motion has generally been thought to be negligible in comparison to that in the vertical direction. We therefore decided to measure the vertical distribution of horizontal velocity and assume lateral uniformity for subsequent net transport calculations. This assumption has been supported by the measurements in the West Passage of Kowalski et al. (1971).

Lateral cross sections of depth were measured in the spring of 1970. These were used in conjunction with published U.S.C. & G.S. charts to determine the position of the current meter stations and to calculate cross sectional areas.

Two stations were selected. The primary one was near Rome Point (see Figure 1 and Table 1) and a secondary station was near the mouth of the West Passage at Bonnet Shores. Both stations were near the deepest part of the channel and their positions were selected to minimize the effects of topographic irregularities. Their location with respect to the cross sectional areas may be seen in Figures 2 and 3.

Table 1. Station locations and depths.

Station	Location	Depth (m.l.w.)
Rome Point	41°32'27"N, 71°24'54"W	12.8 m
Bonnet Shores	41°28'40"N, 71°24'09"W	11.0 m

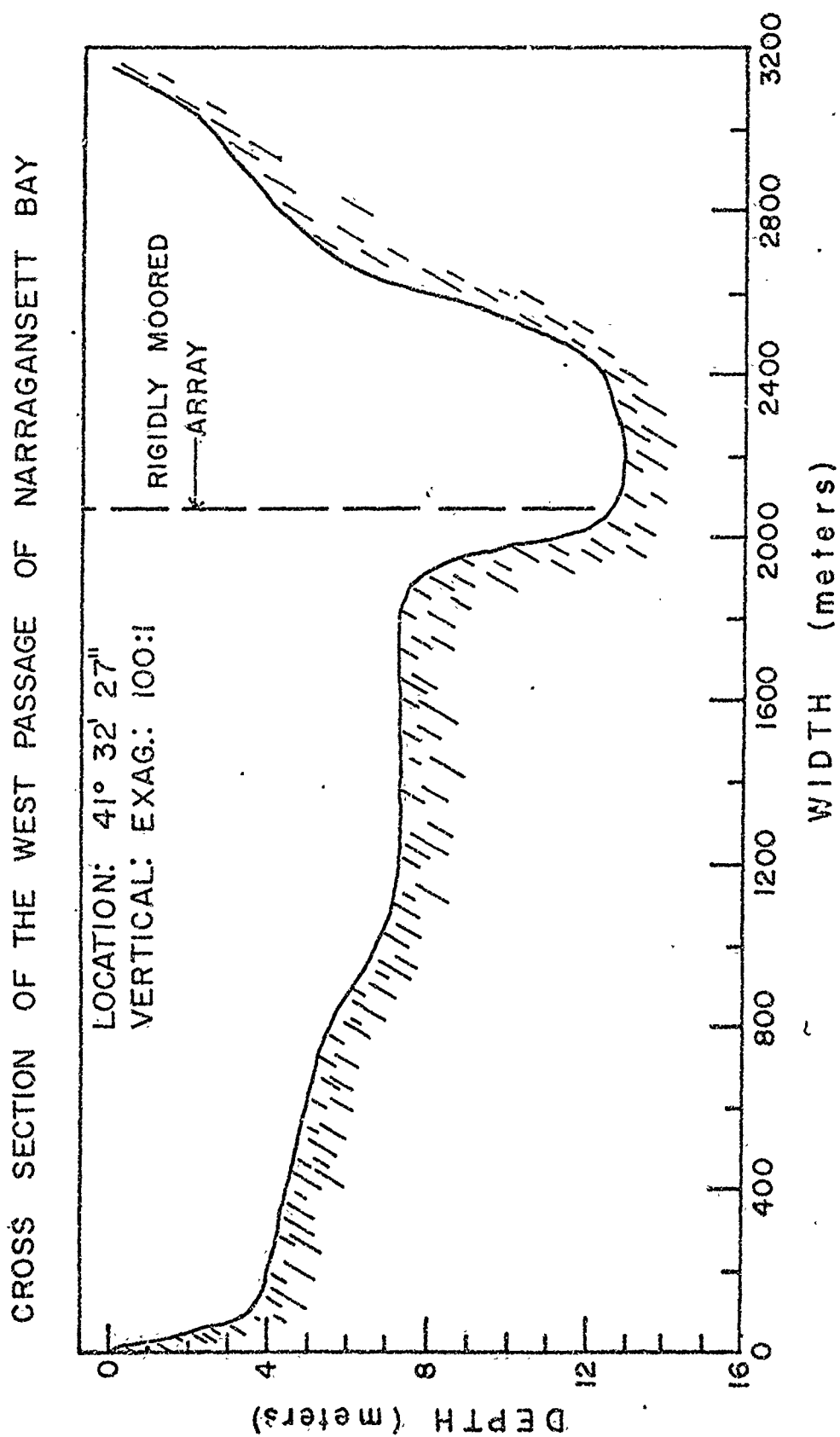


Figure 2. The cross sectional area of the West Passage at the Rome Point station.

CROSS SECTION OF THE WEST PASSAGE
OF NARRAGANSETT BAY

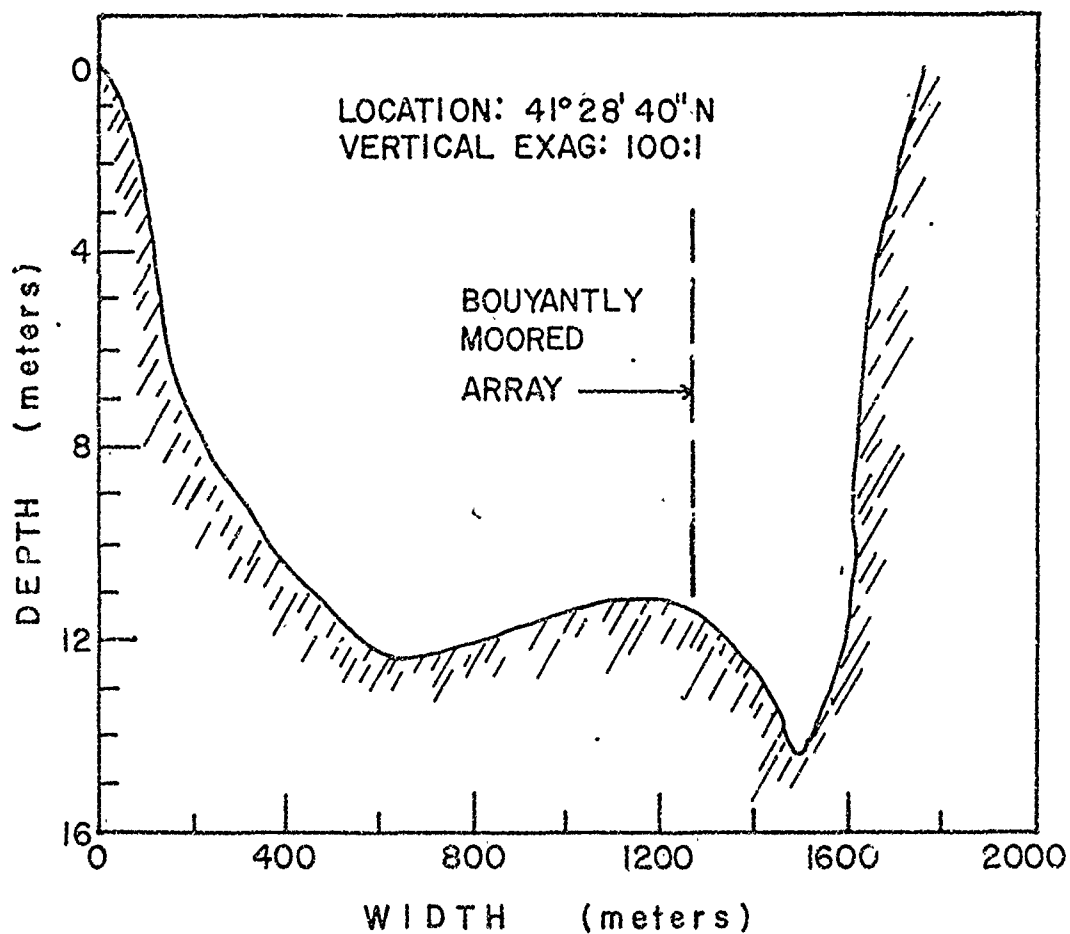


Figure 3. The cross sectional area of the West Passage at the Bonnet Shores station.

Current Meter Distribution

Distributing the current meters vertically entailed consideration of: (1) the bottom boundary condition, (2) interference by surface waves, and (3) the uncertainty of the shape of the net velocity distribution. The bottom boundary condition specifies that the velocity goes to zero at the bottom. Pritchard and Kent (1956), via observation and theoretical calculation in the James River estuary, found that the net horizontal velocity is substantially affected by the bottom boundary only within one to two meters from the bottom, and Cannon's (1969) observations in the Pawtuxent River estuary are consistent with that. Near surface measurements are complicated by the tendency of a Savonius rotor to rectify high frequency wave induced motions (see Appendix 2). These considerations led to the choice of a current meter distribution that was uniform in the vertical and excluded the top and bottom two meters of the water column.

The principal set of measurements was obtained during the fall of 1970. Six current meters were uniformly distributed in a rigidly mounted vertical array at the Rome Point station. As an independent comparison, two current meters were placed in a buoyantly moored vertical array at the Bonnet Shores station.

A supplementary set of measurements was made during the spring of 1971 using four rigidly mounted current meters at the Rome Point station. Their purpose was to examine the effect of increased stratification on the net flow. Table 2 gives the location and sampling duration of all the current meters used.

Table 2. Position, record number, and sampling duration for all current meters used during the fall 1970 and spring 1971 experiments.

Height (m) measured from the bottom	Record number	Duration
Rome Point Station		
10.6	026	19 Oct - 25 Nov 1970
8.9	025	19 Oct - 25 Nov 1970
7.2	024	19 Oct - 25 Nov 1970
5.5	023	19 Oct - 25 Nov 1970
3.8	022	19 Oct - 25 Nov 1970
2.1	021	19 Oct - 25 Nov 1970
10.6	1	19 Mar - 1 Apr 1971
8.9	2	19 Mar - 1 Apr 1971
3.8	3	17 Mar - 1 Apr 1971
2.1	4	17 Mar - 1 Apr 1971
Bonnet Shores Station		
3.7	027	29 Oct - 5 Dec 1970
1.7	028	29 Oct - 5 Dec 1970

Current Sampling

The velocity measurements were made with Savonius rotor current meters manufactured by the Geodyne Co., Waltham, Massachusetts. Type A-100 S.E. and model 850 current meters were used for the fall 1970 and spring 1971 measurements respectively. With either instrument, the speed is sensed by a Savonius rotor with an accuracy, as specified by the manufacturer, of three percent. The direction of flow relative to the current meter case is detected by a vane while the orientation of the case is obtained with a magnetic compass. The resolution of both the compass and vane is 2.8 degrees, resulting in a direction relative

to the earth's magnetic field to within approximately five degrees.

The two instruments differ only in their actual recording scheme. The type A-100 S.E. current meters photographically record a data pulse every two and thirty-two rotor revolutions (this ratio may be varied). The model 850 current meters record the number of rotor revolutions in every five second interval directly on magnetic tape. Both instruments record instantaneous compass and vane readings every five seconds of operation.

Preliminary data obtained by the authors in the summer of 1970 as well as the data compiled by Haight (1938) suggested that mean speed estimates in the West Passage are an order of magnitude less than the amplitude of the instantaneous tidal flow. Therefore, lengthy records were needed to try to arrive at a reliable estimate of such a relatively small mean. The records obtained in the fall of 1970 were of much longer duration. The spring 1971 measurements were only of two week duration owing to limited availability of the current meters.

Currents were sampled for 2.5 minutes every 15.0 minutes during the fall experiment and 2.5 minutes every 7.5 minutes during the spring experiment. These are the maximum sampling rates that are available for the particular current meters and record lengths used for a single mooring. Since the tidal currents in Narragansett Bay can be adequately described by the M_2 , M_4 , and the M_6 tidal harmonics (Haight (1938)), the sampling rates used were sufficient to prevent aliasing by motions at frequencies higher than Nyquist. Frequencies beyond the resolution of the sensors, such as those associated with surface gravity waves, present a different problem; this is discussed in Appendix 2.

Subsidiary Data

Wind data were obtained from the U.S. Naval Air Station, Quonset Point, Rhode Island (see Figure 1). Speed and direction are measured hourly with a three cup anemometer and an arrow vane. The instrument is located approximately 10 m above sea level.

Temperature and salinity determinations were made at various times of high and low water slack using a Beckman, model RS 5-3, in situ sali-

nometer (Beckman Instruments Inc., Cedar Grove, New Jersey). Readings were taken at two or three meter intervals and water samples were taken for independent laboratory comparison.

River runoff data were supplied by the U.S. Geological Survey, Boston, Massachusetts.

Support Equipment

Rigidly Moored Array

In order to prevent the data from being affected by mooring motion, a rigid structure was required for the near surface measurements. A telephone pole provided such a structure as shown in Figure 4. Figure 5 gives a top view of the current meter mounting scheme. Wooden booms held the instruments away from the region of streamline distortion about the pole. The booms were attached to non-magnetic stainless steel brackets on the current meter pressure case and galvanized steel studs protruding through the pole. The current meters were supported in the vertical by ropes connecting the current meters to the next higher steel stud as shown in Figure 4. All magnetic materials were sufficiently far from the current meters to avoid biasing their compasses.

A six point mooring system aided in holding the pole stable and upright. Twice during stormy conditions wave action worked the anchors loose, and divers had to readjust the mooring lines. To avoid this problem during the spring measurements the portion of the pole just above the topmost current meter was cut off. In addition, two subsurface buoys were attached to provide a more stabilizing buoyant force. Since the pole was now completely submerged two spar buoy navigation markers were set and slender bamboo poles served as a direct marker. Observation of the bamboo poles showed that the mooring remained steady.

Buoyantly Moored Array

The buoyantly moored array is shown in Figure 6. The current meters were supported by a subsurface buoy consisting of two steel spheres. A wooden vane was attached to the buoy enabling it to weather cock with the current, and form drag was opposed by a four point mooring. The current

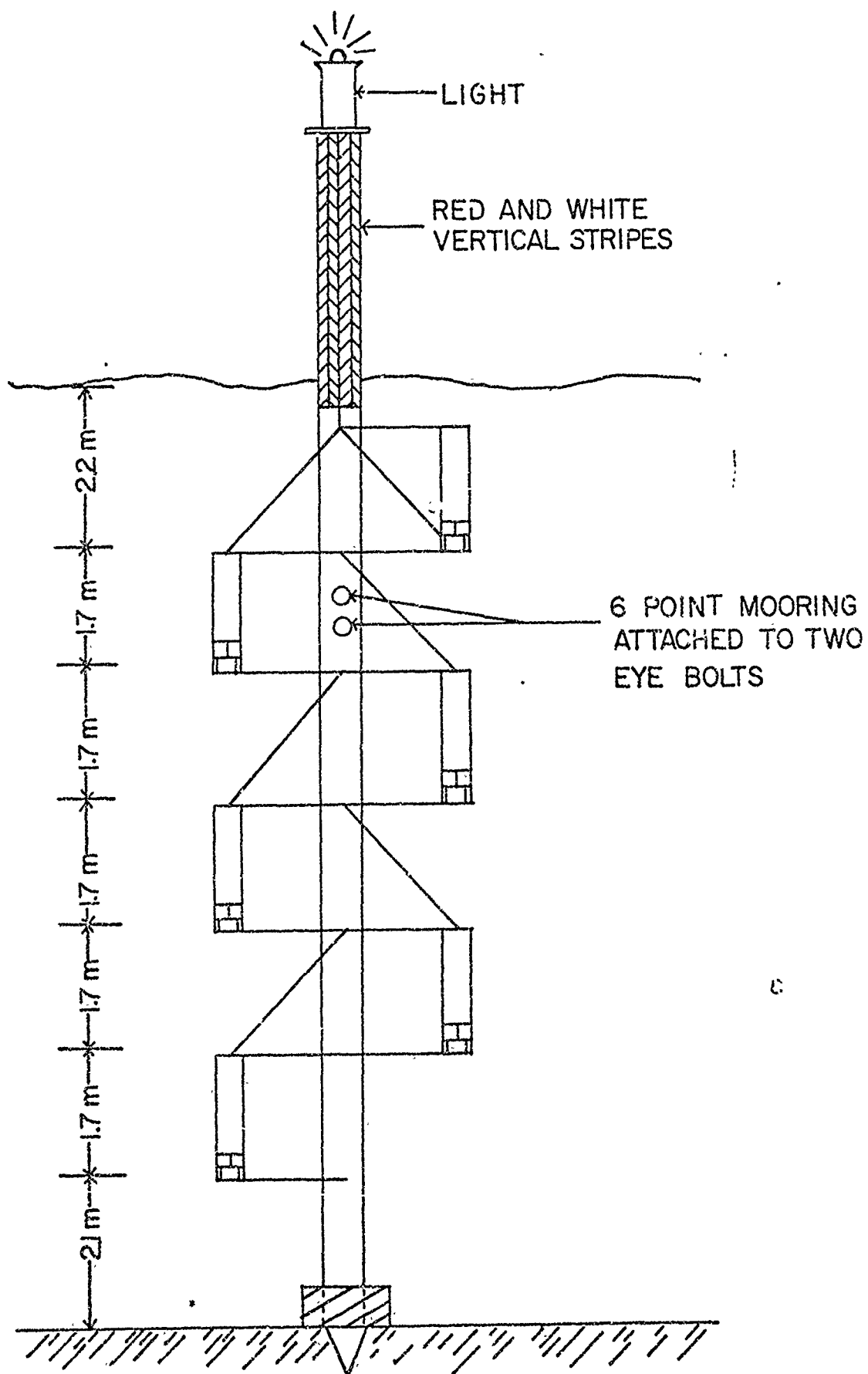


Figure 4. The rigidly moored array used at the Rome Point station.

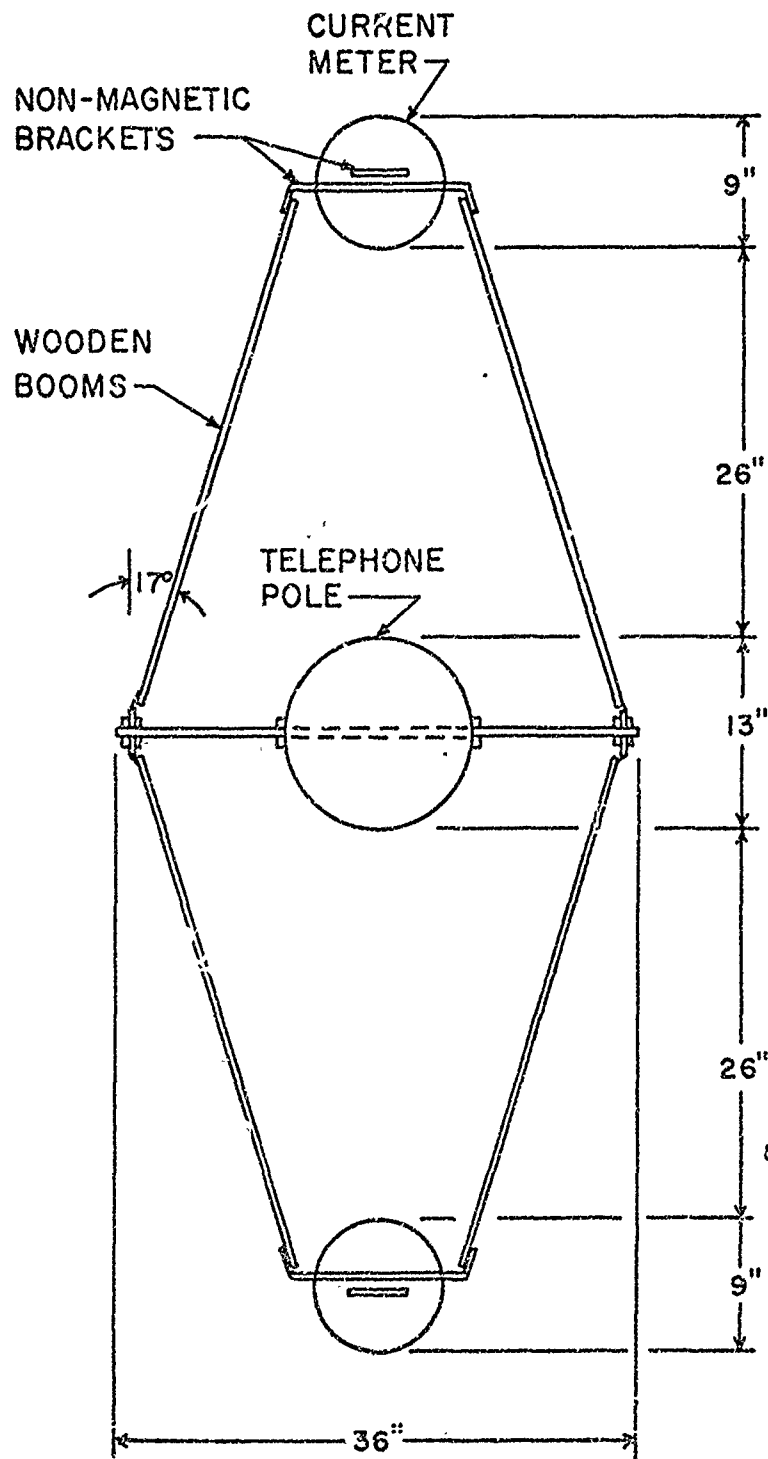


Figure 5. The rigidly moored current meter mounting scheme.

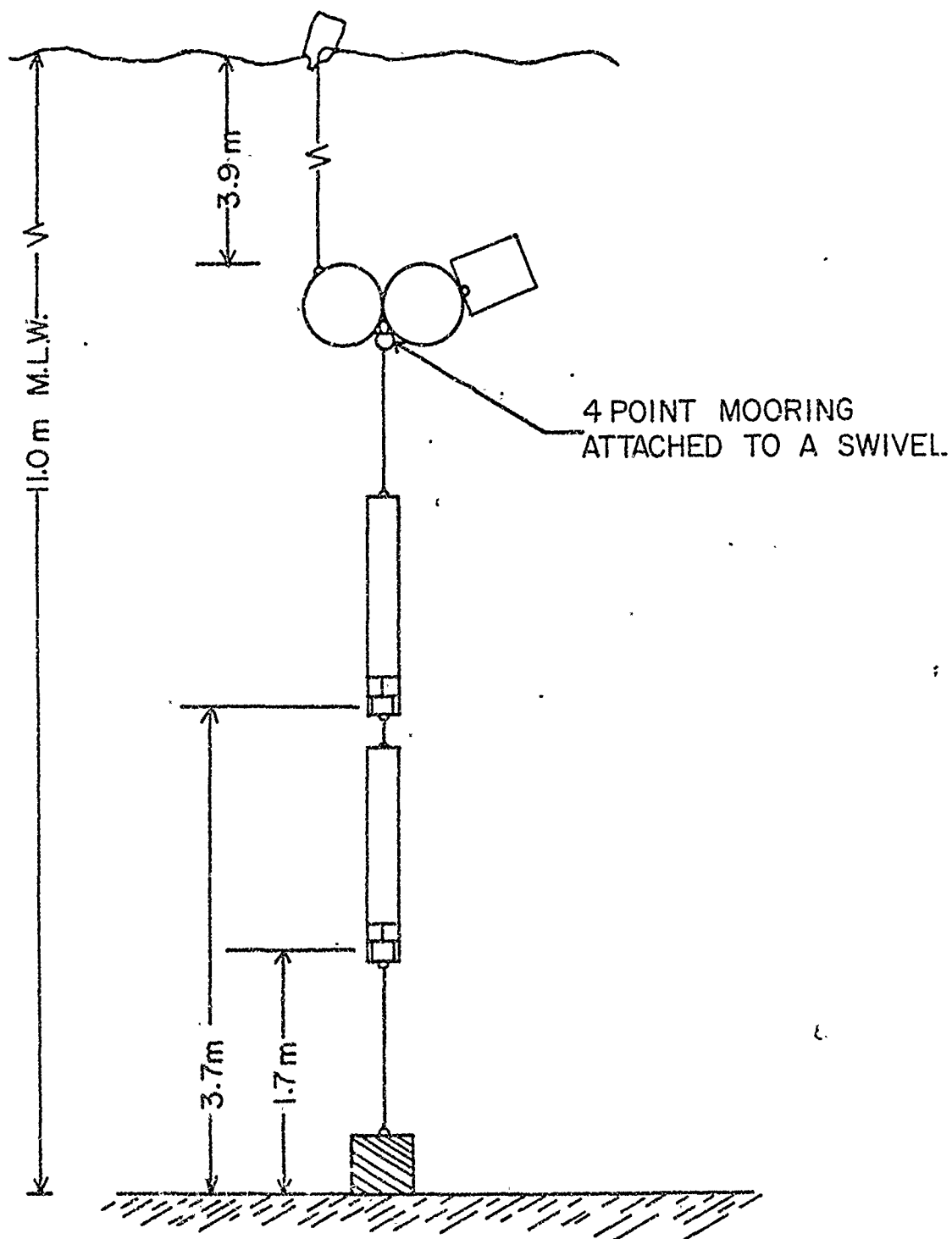


Figure 6. The buoyantly moored array used at the Bonnet Shores station.

meters had the capability to measure inclination to within five degrees but none was observed.

Field Procedures

Deployment of the fall Rome Point station began on 18 October 1970. The pole was dragged from the beach at the Narragansett Bay Campus and towed to the mooring site. There it was winched up, oriented, and dropped into position. Divers then secured the six point anchor system and bolted on the mounting hardware. The current meters were attached by divers on 19 October 1970. Throughout the course of the fall measurements weekly and sometimes biweekly visual checks of the apparatus were made. Time markings were made on three occasions by tying the vanes perpendicular to the direction of flow for one hour (four recording intervals) thus leaving obvious marks on the film records. The array was recovered on 1 December 1970. Very little fouling had occurred with only a thin film of algae perceptible.

The buoyantly moored array at the Bonnet Shores station was set on 29 October 1970. Visual diver checks and time markings were made as with the Rome Point station. This array was recovered on 8 December 1970,

The assembly of the spring Rome Point station was similar to the fall one. The pole was set on 13 March 1971. The bottom two current meters were installed on 17 March and the top two on 19 March 1971. The array was recovered on 1 April 1971.

III DATA PROCESSING AND RESULTS

The film recorded current meter data from the fall 1970 experiment were read and transferred to magnetic tape by the Geodyne Co. Initial data inspection revealed three malfunctions, all occurring at the Rome Point station. Records 021 and 024 had to be discarded in their entirety along with the latter half of record 022. Further machine processing was performed at the University of Rhode Island. The current meter data from the spring 1971 experiment were processed at the Woods Hole Oceanographic Institute. Of the four records, number two had to be discarded.

North and east components were taken of all current and wind records. The choice of component direction followed from the longitudinal axis of the West Passage being essentially north-south.

Instantaneous Currents

The north and east components of velocity from the fall and spring experiments are shown in Appendix 1. The currents are dominated by semi-diurnal tides. Current amplitude varies from neap to spring tides by roughly 25-60 cm/s.

A kinetic energy spectrum of the current measured 2.1 m below mean low water (record 026) is shown in Figure 7 (this along with other spectral computations to be mentioned later were made using the Biomedical Computer Programs, Dixon, 1970, ed., available at the U.R.I. computer lab). Thirty degrees of freedom were used and the 80% confidence interval is given in the figure. The principal energy is distributed about the semi-diurnal peak (M_2), but significant peaks also appear at the M_4 and M_6 harmonics.

In order to study the variation in harmonic structure from neap to spring tides the current records were broken into 50 hour segments whose Fourier coefficients were then computed. A partial listing of the results for currents measured 2.1 m and 7.2 m below mean low water are given in Table 3. Included are the r.m.s. values, the percentage of energy (speed squared) contained in the M_2 and M_4 harmonics, and the phase difference between the M_2 harmonic at 2.1 m and 7.2 m. The designations spring and neap refer to the 50 hour segments centered about strong or weak flows

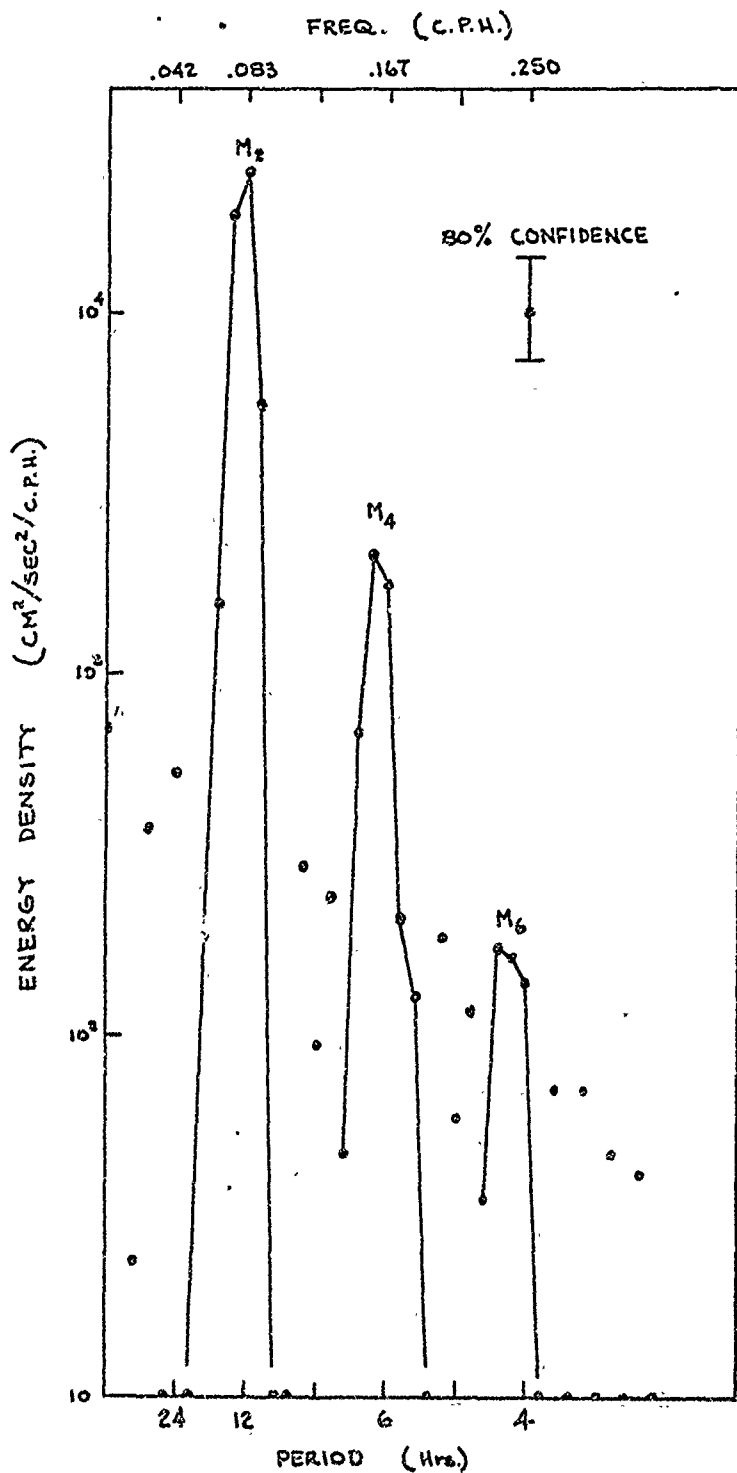


Figure 7. The kinetic energy spectrum of the near surface current (record 026) observed at the fall 1970 Rome Point station.

respectively. It should be noted that the terms M_2 and M_4 specifically refer to the periodicities of 12.5 hr. and 6.25 hr. used in our computations. Our record lengths are too short to distinguish between individual semi-diurnal tidal species, hence they have all been lumped under the heading M_2 .

Table 3. The r.m.s. current speed, percentage of energy contained in the M_2 and M_4 harmonics and the phase difference ($\Delta\phi_{M_2}$) of the M_2 harmonic for currents measured 2.1 m and 7.2 m below mean low water.

Segment start time and designation									
	0700	2230	0030	0400	1800	1300	1600	1900	
	21 Oct	23 Oct	28 Oct	2 Nov	4 Nov	11 Nov	15 Nov	19 Nov	
	NEAP	NEAP	SPRING	SPRING	NEAP	SPRING	SPRING	NEAP	
rms (cm/s)	17.9	18.3	24.8	25.4	19.2	31.4	25.7	13.7	
2.1 m % M_2	70	76	86	86	75	89	87	72	
% M_4	17	4	6	6	16	8	6	9	
rms (cm/s)	14.6	17.1	24.8	21.8	17.2	26.9	23.8	14.2	
7.2 m % M_2	70	87	86	83	77	86	83	70	
% M_4	14	4	5	7	12	6	6	10	
2.1m-7.2m $\Delta\phi_{M_2}$ (rad.)	.22	.16	.20	.18	.16	.23	.38	.20	

During spring tides as much as 89% and 97% of the energy is contained in the M_2 and $M_2 + M_4$ harmonics respectively. During neap tides, however, as little as 70% and 80% of the energy is contained in the M_2 and $M_2 + M_4$ harmonics. Hence, we see that the instantaneous current structure is more complicated during neap tides with the higher tidal harmonics playing a proportionately larger role than during spring tides.

Figure 8 presents the north component of velocity at the depth of 2.1 m and 7.2 m superimposed on the same graph. A conspicuous feature is the phase difference between the two records. The deeper current leads the near surface current throughout the record. This phase advance with depth appears to depend on lunar phase, varying from 1-3 hours during neap and intermediate range tides to near zero during spring tides. A discussion

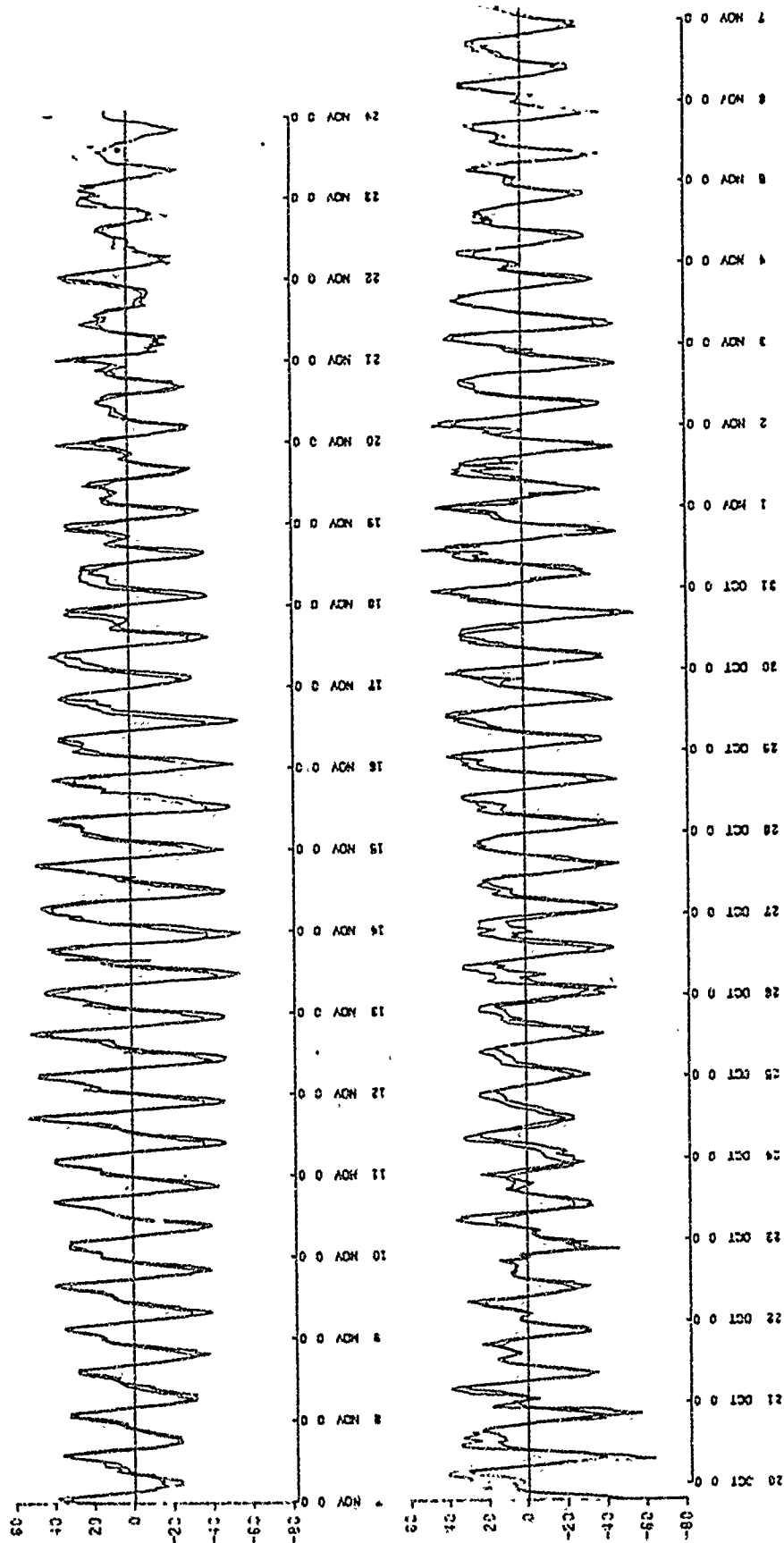


Figure 8. The north component of currents measured 2.1 m and 7.2 m below mean low water (records 026 and 023 respectively). The deeper current leads the near surface current.

of this phase advance will be given in a later section.

The north component of instantaneous motion is again represented in Figure 9. Here speed is plotted as a function of depth for various stages of a tidal cycle midway between neap and spring tides. Due to the phase advance, the instantaneous motion is not constant with depth. Note that about low water slack it is possible to measure a seaward flow near the surface with a corresponding landward flow near the bottom. Such an observation is due to vertical differences in the phase of the instantaneous motion and should not be confused with the gravitational convection scheme of net estuarine circulation.

Net Currents (Fall 1970)

Averaging Technique

The primary interest of this study was the analysis of the time-averaged currents from which the net transport can be estimated. Therefore, it was desired to average out the tidal motion. The basic tidal period is semi-diurnal (12.42 hours); however several factors such as diurnal inequality, variability of the basic tidal period due to other tidal harmonics, and independent disturbances of unknown period complicate the choice of a suitable averaging interval. Simple unweighted averages over every two tidal cycles were first formed. Although not presented here, these showed considerable variability which seemed to be correlated with the wind.

Further pursuit of this apparent correlation required an averaging technique that would filter out the high frequency fluctuations (tides) without significantly affecting the magnitude and phase of the lower frequency constituents (net currents). A Gaussian shaped numerical filter was chosen (see, for example, the discussion by Holloway 1958). The weights for a Gaussian filter sum to unity and they are evenly distributed about a principal value. Hence, neither the mean of a time series nor the phase of its individual frequency constituents are affected by the filtering. Figure 10 shows the frequency response function for the Gaussian filter. The cut-off frequency, i.e., the frequency at which the response of the filter drops to a negligible value, is determined

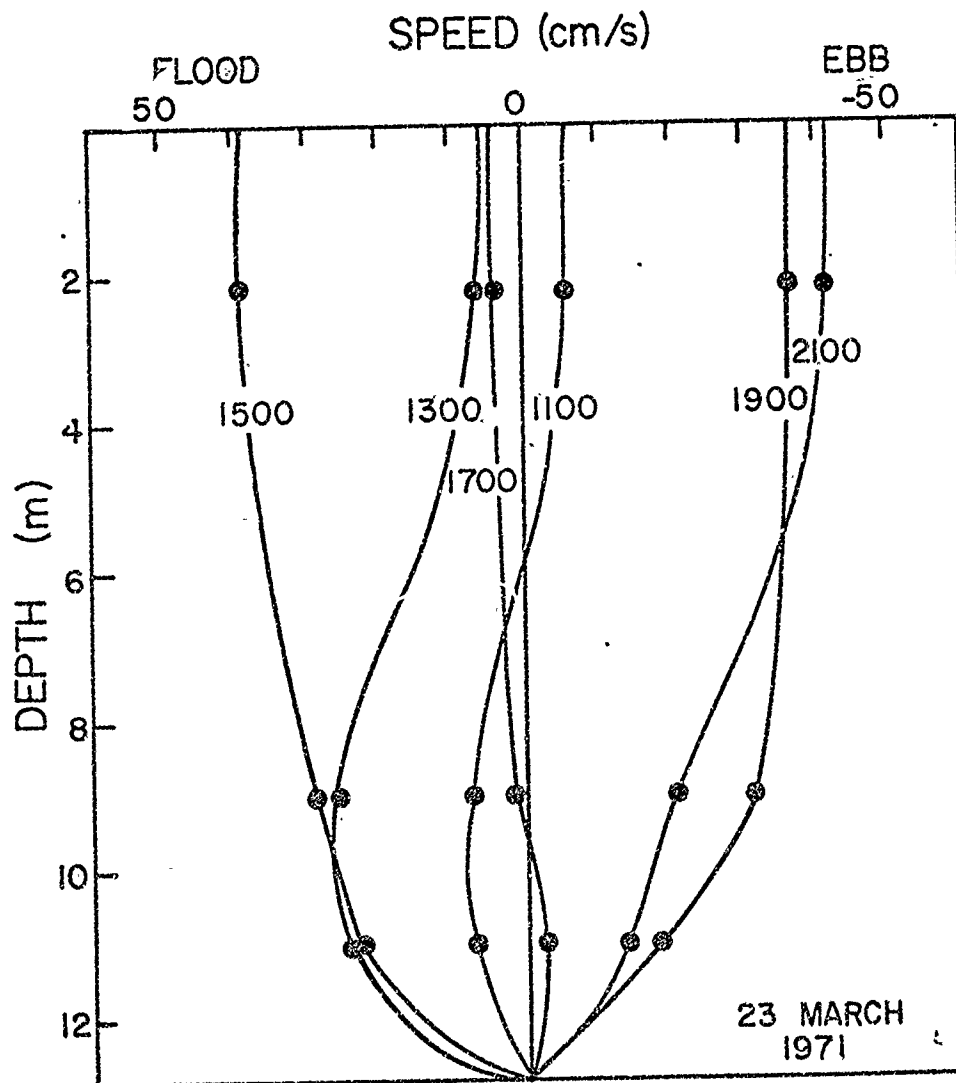


Figure 9. The north component of instantaneous current at the Rome Point station as a function of depth for different stages of a tidal cycle.

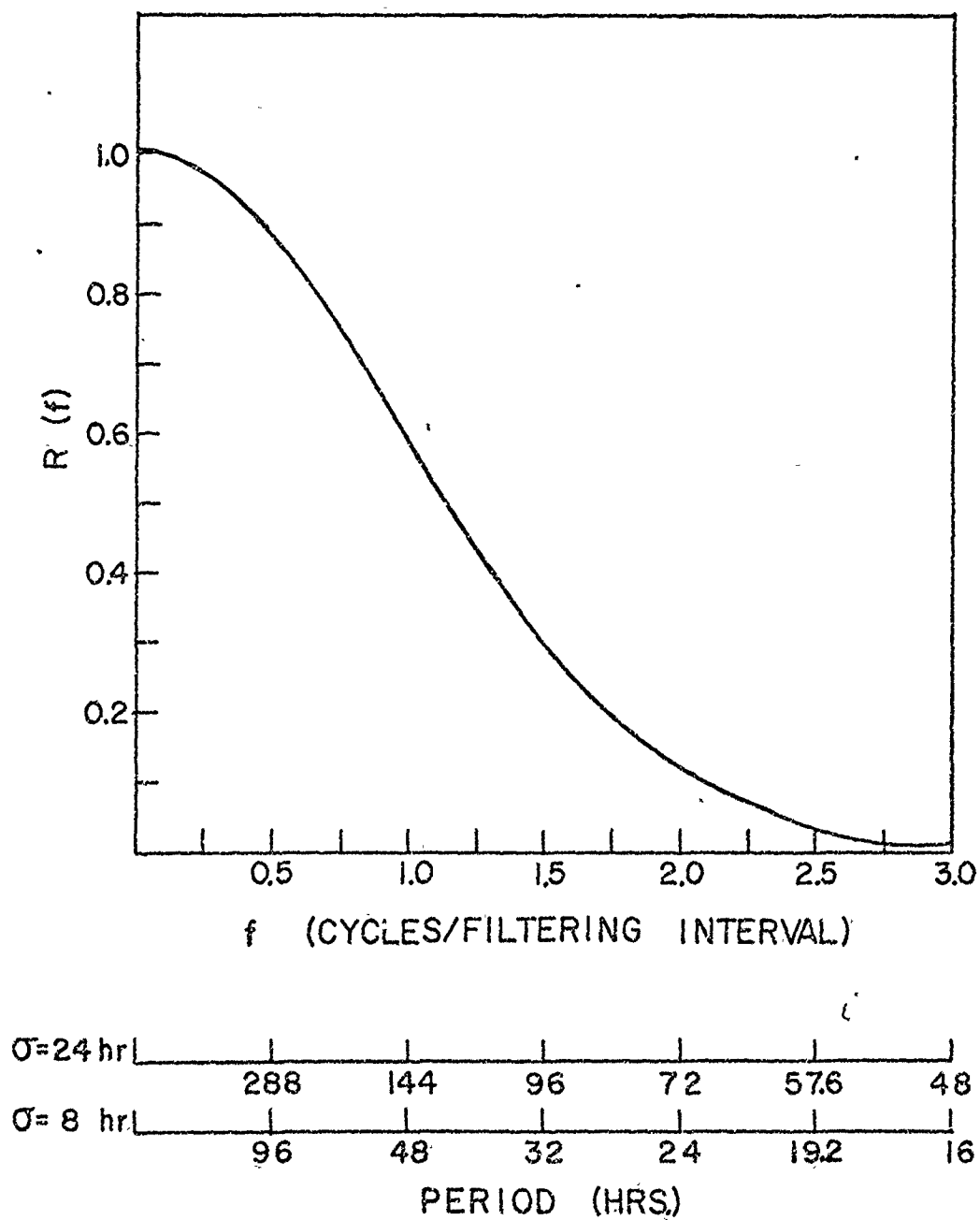


Figure 10. The frequency response function of a Gaussian filter.

by the standard deviation of the filter σ . $\sigma = 8$ hours was determined to be the smallest standard deviation that would effectively remove both the semi-diurnal and the diurnal tidal periodicities in the West Passage.

The components of the wind and current data were put in the form of hourly time series by taking unweighted averages of every four 15 minute current data points. The origins of all the hourly time series were then synchronized. Next, running weighted averages were taken using a Gaussian filter with a standard deviation of $\sigma = 8$ hours. The filtering interval, or length, was 48 hours (6σ). The filter was stepped ahead every 8 hours, except for the near surface record (026) and the wind, for which it was stepped ahead each hour. An 8 hour step was sufficient because the frequency response function yields negligible values for frequencies greater than 3 cycles per filtering interval, i.e. periods less than 2σ in length. A 1 hour step was used for record 026 and the wind since hourly values were needed for subsequent correlation analysis.

Results of the Filtering

Figures 11 a, b, and c show the net current and wind time series which resulted from the filtering operation just discussed. The top two curves are the east (+) and north (+) components of the wind. The sign convention used is the reverse of the usual meteorological one, i.e., here it is meant that a northward wind blows toward the north. The other curves are the north (+) component time series of the net currents. The net current values comprising the time series are spaced eight hours apart and represent a weighted average taken over one filtering interval (48 hrs). Note the presence of dashed lines rather than data points on October 27-28, November 2-3, and November 12-13. These particular data are unreliable: we suspect wind-wave biasing which is impossible to correct (see Appendix 2). Our error analysis suggests that the other net current values are accurate to within ± 0.5 cm/s (also see Appendix 2).

The mean values averaged over the entire record length are given in Table 4 together with the root mean square deviations of the filtered and unfiltered north component time series about their mean values (standard deviations). Two features are evident from the table: (1) the filtering reduced the standard deviations by an order of magnitude because the tidal

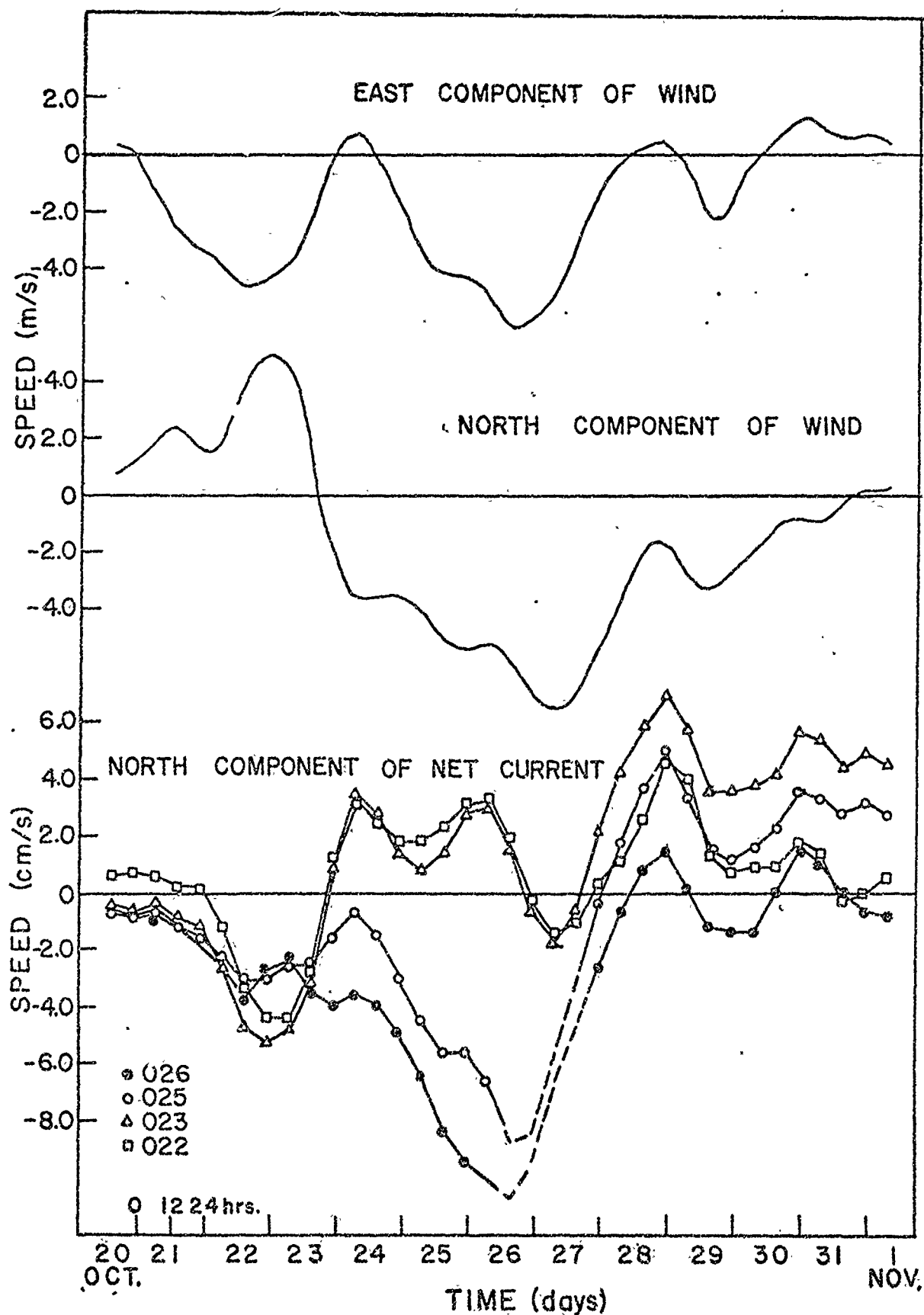


Figure 11a. The net current and smoothed wind time series obtained during the fall of 1970.

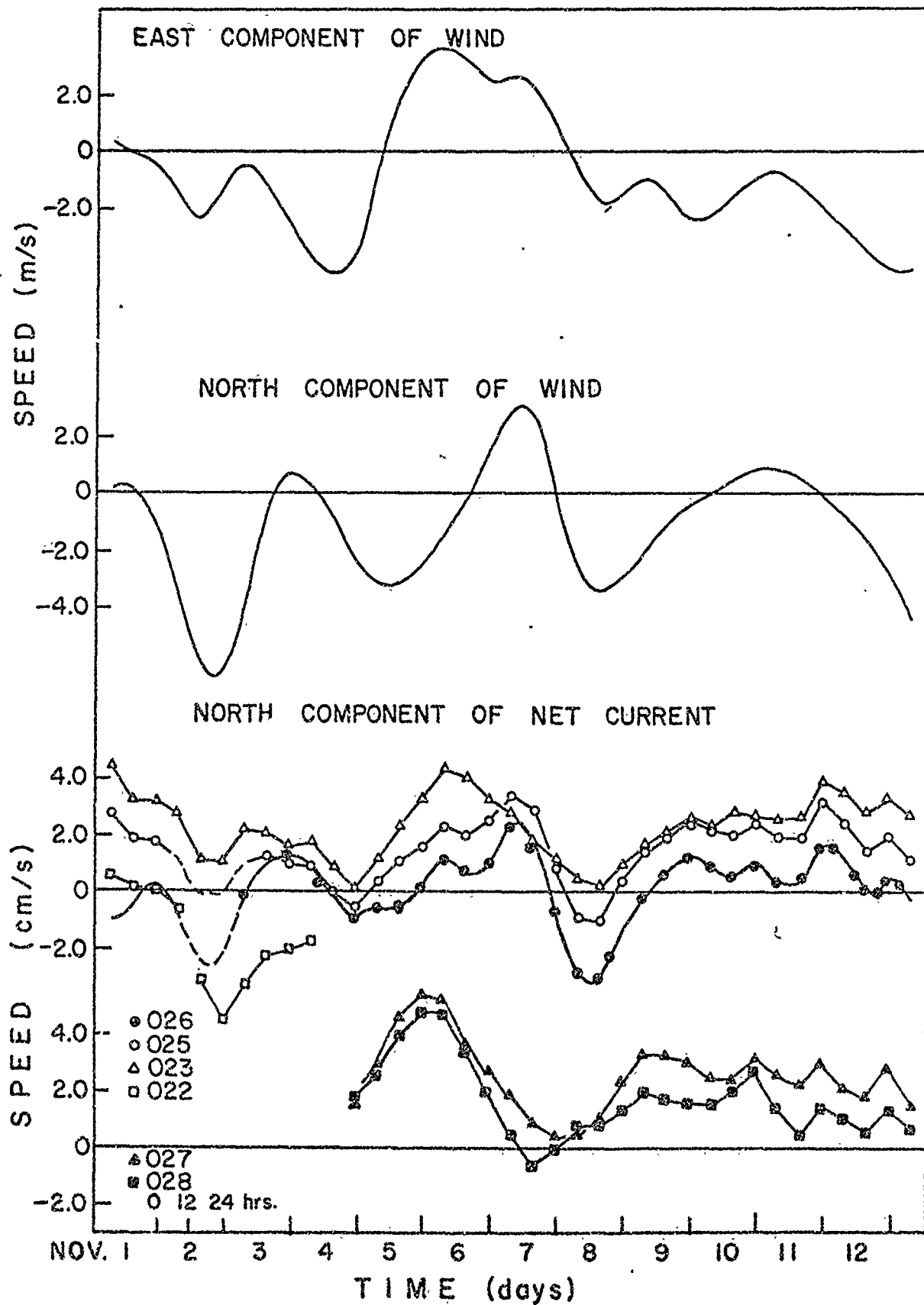


Figure 11 b. The net current and smoothed wind time series obtained during the fall of 1970.

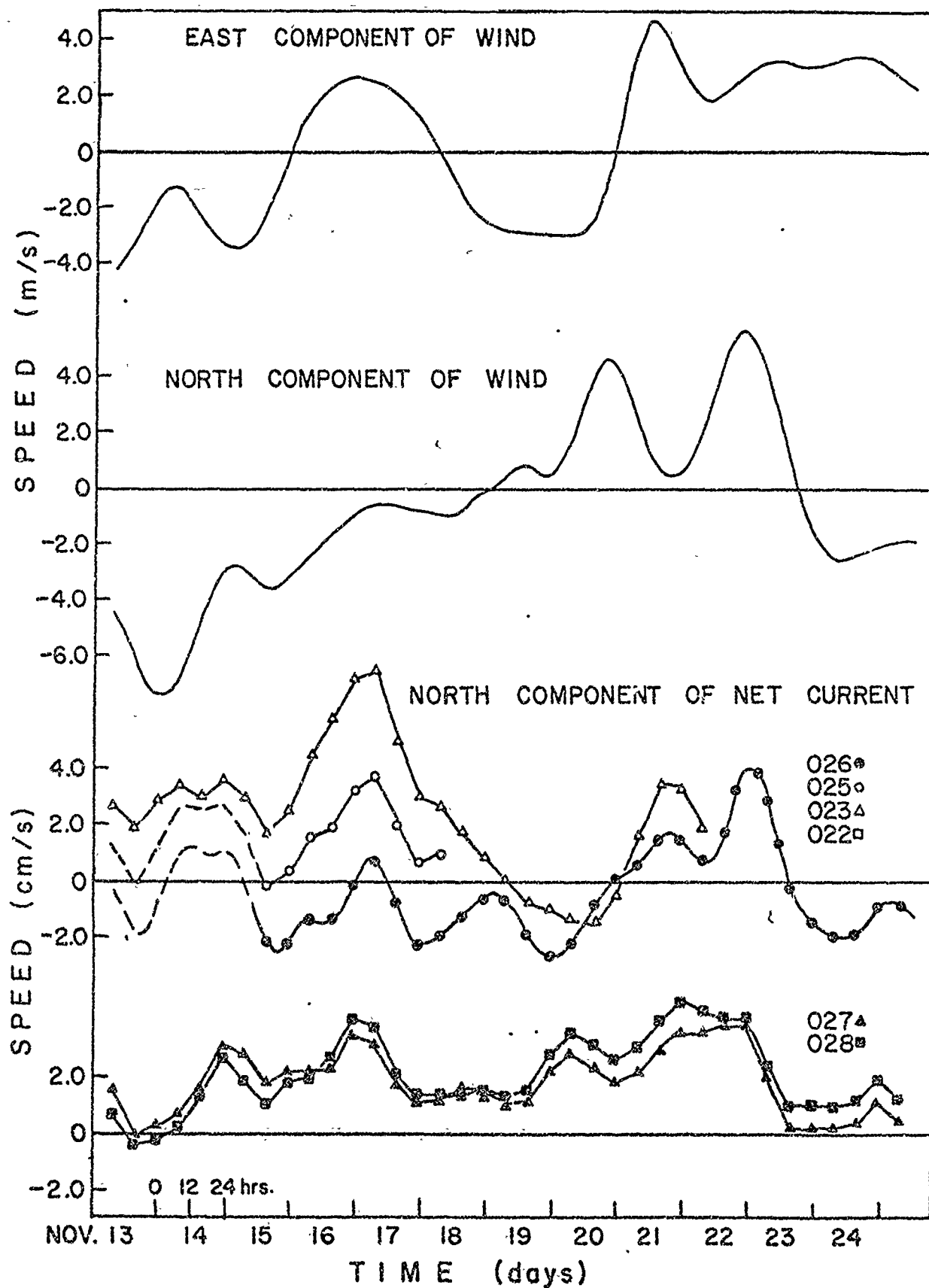


Figure 11 c. The net current and smoothed wind time series obtained during the fall of 1970.

motion was removed, (2) record 022, being only half the length of the others, had a mean value much smaller than expected if one assumed two layered mean estuarine flow. The first observation implies that the net circulation in the West Passage is an order of magnitude less than the amplitude of the instantaneous motion. This is clearly evident from Figure 12. The second observation raises a question of major importance! We know that the circulation in an estuary may vary with wind, river runoff, tidal strength, etc., but it has been customary to associate averages over a few tidal cycles with the gravitational convection scheme of estuarine circulation. How long then must a current meter record in an estuary be so that its mean value is truly representative of the gravitationally convected flow?

Table 4. The mean values and the root mean square deviations about the mean for the Gaussian filtered ($\tau = 8$ hr) and the unfiltered north component time series obtained from the fall 1970 Rome Point station. Positive denotes flow to the north.

North component time series Record#	Height (m) off Bottom	Mean (cm/s)	Standard Deviation cm/s	
			filtered	unfiltered
026	10.6	-1.1	2.6	22.0
025	8.9	0.4	2.7	22.8
023	5.5	2.1	2.4	21.2
022	3.8	0.1	2.2	17.0
Wind		-1.2 m/s	3.2 m/s	3.6 m/s

Digression on Estimating the Uncertainty of the Mean Values

The observed mean values based on our records are, of course, only estimates of the "true" mean values that could be computed from indefinitely long records. We refer here to an observed mean value as a mean estimate μ . The standard error ϵ of the mean estimate is given by,

$$\epsilon = \sqrt{\text{var } \mu}$$

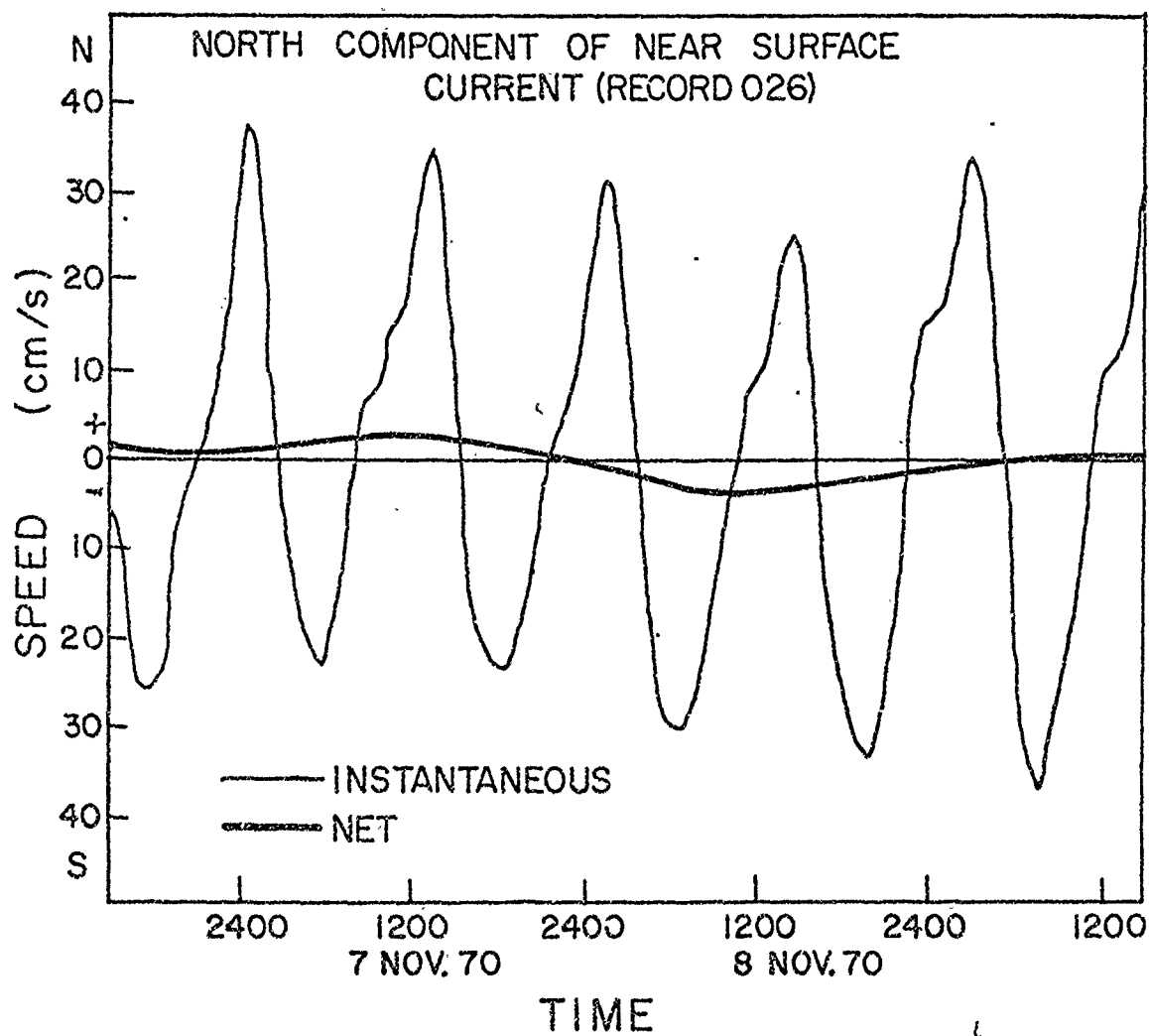


Figure 12. A comparison of the instantaneous and net near surface current (record 026) at the Rome Point station.

where $\text{var } \mu$ is the variance of the mean estimate. For the familiar case of Gaussian distributed white noise with standard deviation Σ ,

$$\text{var } \mu = \frac{\Sigma^2}{N}$$

where N is the number of samples. Most oceanographic measurements have a more complex correlation structure which is unknown a priori. The variance of the mean estimate is related to this correlation structure by,

$$\text{var } \mu = \frac{1}{T} \int_{-\infty}^{\infty} C(\tau) d\tau$$

where $C(\tau)$ is the autocovariance function at time lag τ (after the purely periodic motions have been filtered out) and T is the record length, e.g., see Bendat and Piersol (1966, p. 185).

The autocovariance function for the north component of net near surface current (record 026) is shown in Figure 13. From this the standard error of the mean estimate was calculated to be 0.8 cm/s. Hence, the mean value of record 026 may be written as -1.2 ± 1.6 cm/s (to within the 95 percent confidence interval or two standard errors). The point to be made here is that even with a record length of approximately one month, the variance of the mean estimate is appreciable in comparison to the small mean estimate itself. In other words: if we had a different month-long record (with the same autocovariance function) and we computed its mean value, we would arrive at an answer anywhere within the specified limits 95 percent of the time.

Results of Filtering (continued)

In light of the above discussion, although the mean values averaged over a month are an interesting result (implying a two layered circulation) they are not significantly different from zero. Therefore, when viewing Figures 11 a, b, and c, concern should be focused on the variability of the net currents and their seeming correlation with the wind. Neither of these features are prevalent in the published estuarine literature for two reasons. First, sufficiently long records do not seem to have been taken

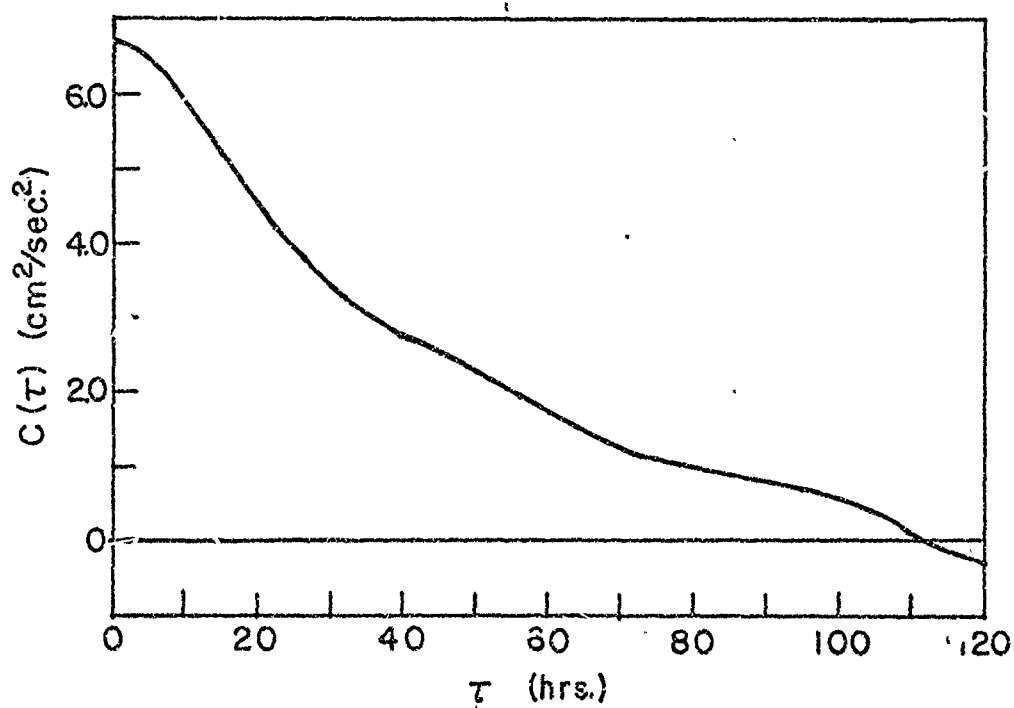


Figure 13. The autocovariance function of the net near surface current (record 026) at the Rome Point station.

in estuaries and second, the averaging techniques employed have not been suited for discerning these features.

The correlation appears to be strongest between the north components of wind and net near surface current (record 026); however throughout most of the records, the coherence between the net currents as a function of depth is quite obvious. The net currents are also coherent longitudinally between the Rome Point and Bonnet Shores stations. In particular note the relation between records 023 at the Rome Point station and 027 at the Bonnet Shores station both of which were taken at approximately the same depth (7.3 m).

Qualitative Correlation Analysis

Figure 14 is a scatter plot of the north component of net near surface current (record 026) as a function of the smoothed north component of wind. The data points were taken at eight hour intervals from Figure 11 a, b, and c. This figure is instructive because a qualitative explanation can be afforded each quadrant.

Quadrants one and three (the upper right and lower left) represent a positive correlation between the north components of wind and net near surface current; that is northward winds tend to produce northerly net currents and vice versa. If the net near surface flow in the West Passage was typical of two layered estuarine circulation, we would expect it to be southerly in the absence of wind.

The points in quadrant four (lower right) are the result of winds blowing towards the north-west. This direction is perpendicular to the area joining the East and West Passages between Conanicut and Prudence Islands (see Figure 1). Therefore, fourth quadrant points are representative of wind induced flow from the East to West Passage. The resulting flow in the West Passage is south by continuity.

Most of the second quadrant points occurred after the sudden arrest of a strong southward wind. When a wind blows over a confined body of water it causes the surface to slope, thus balancing the stress of the wind. Upon removal of this wind stress the water flows in the opposite direction to remove the slope. Hence, second quadrant points represent

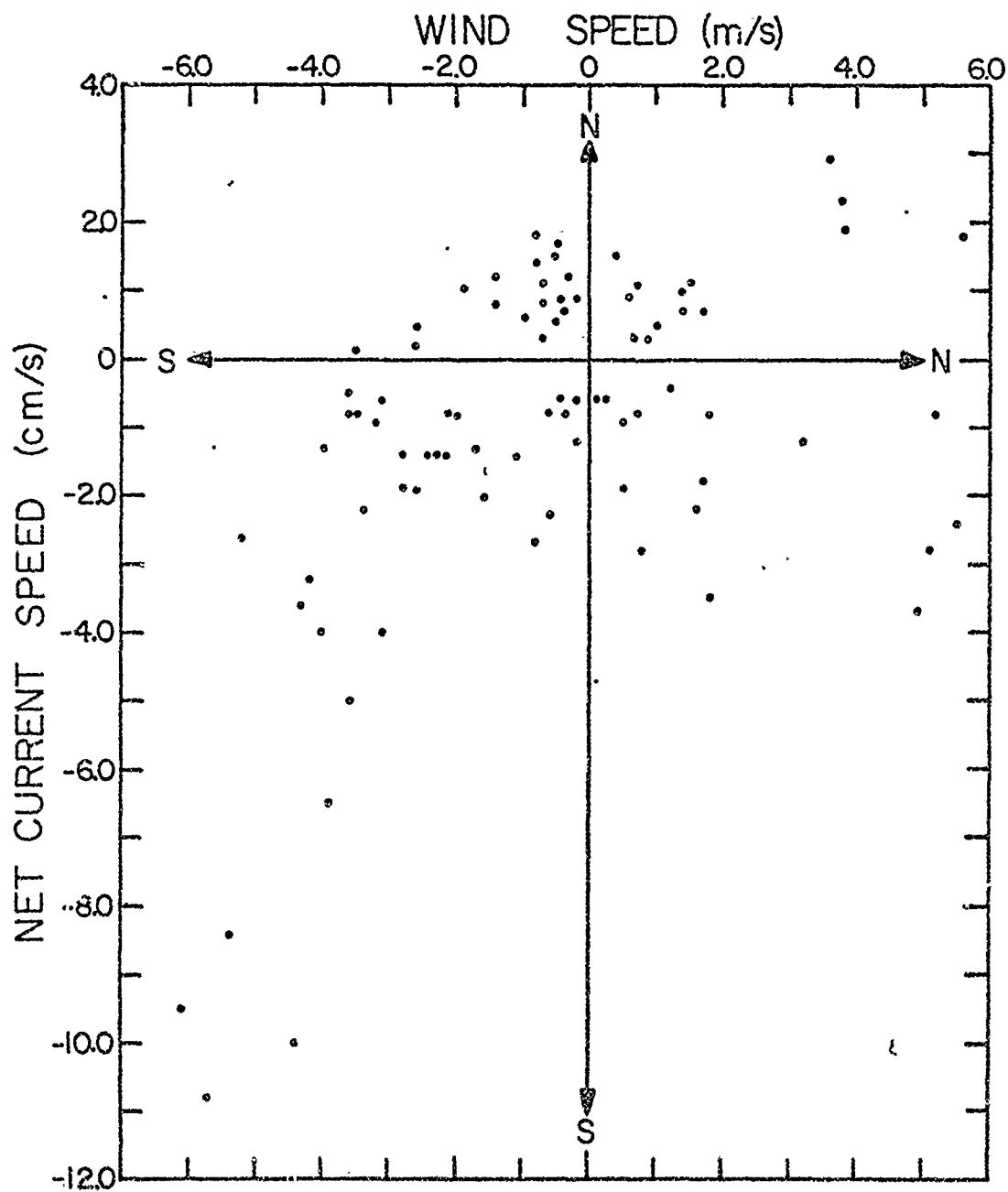


Figure 14. A scatter plot of the north components of net near surface current (record 026) and wind.

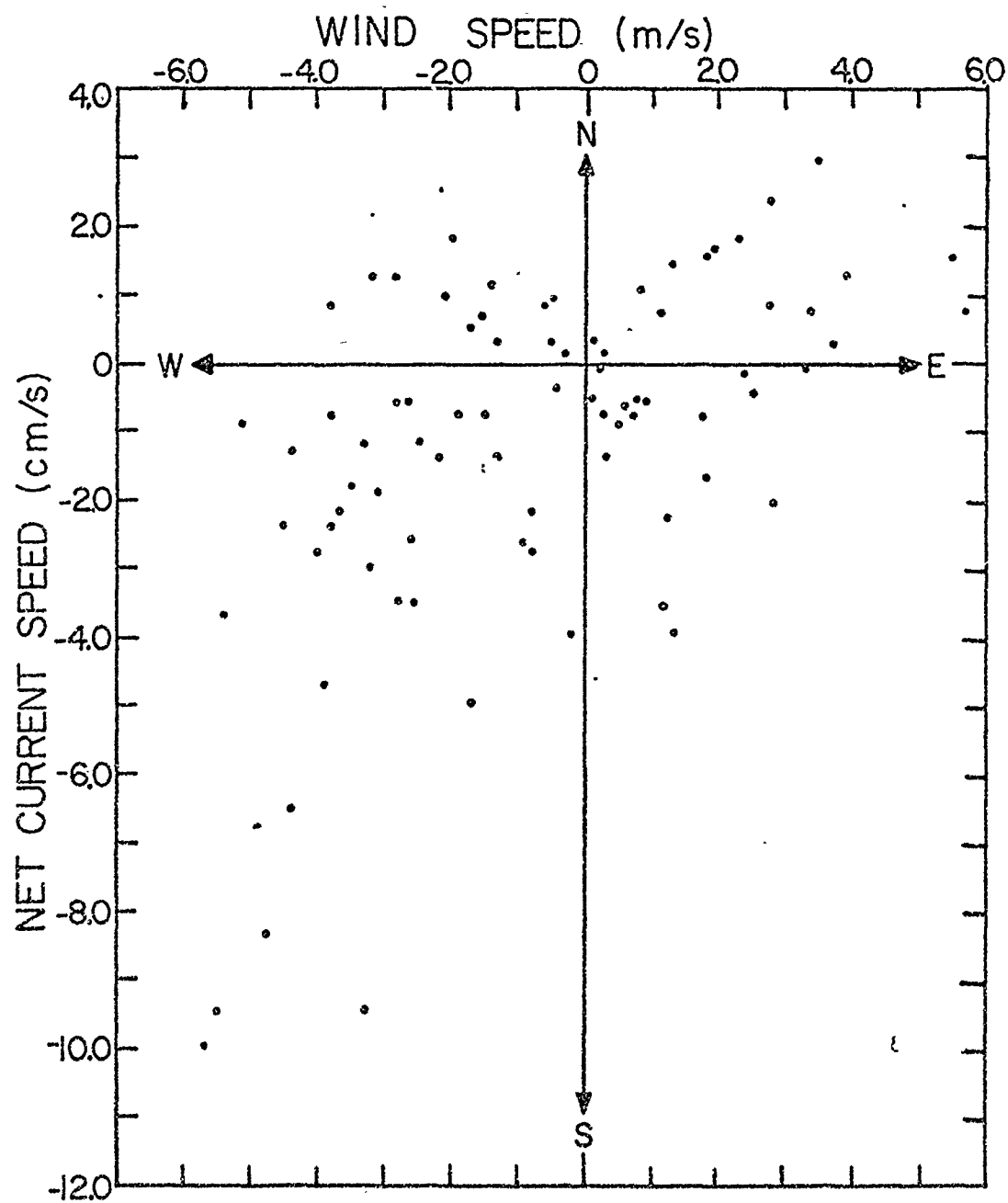


Figure 15. A scatter plot of the north component of net near surface current (record 026) and the east component of wind.

a northward flux of water after the subsidence of a strong southward wind. This phenomena will be referred to as a rebound.

Figure 15 is a scatter plot of the north component of net near surface current (record 026) as a function of the smoothed east component of wind. The points were plotted as in Figure 14. Although disperse they show a general positive correlation whereby winds blowing west tend to be associated with net currents flowing toward the south and vice versa. This is consistent with the idea of wind induced transport between the East and West Passages.

Vertical Distributions of the Net North Velocity Component at the Rome Point Station

Vertical distributions of the net north velocity component for different situations are shown in Figures 16-19. The distributions were drawn from the Rome Point station data as given in Figures 11 a, b, and c.

The vertical distribution of the net current time series averaged over their entire record length of one month is shown in Figure 16. Two pair of uncertainty bounds are also given. The first, and narrower, band (± 1.6 cm/s) is the uncertainty of the mean estimate as discussed previously. The mean estimates suggest a two layered flow with inflow at depth and outflow near the surface, but we are forced to recognize that the numerical values are not significantly different from zero. This awkward result does not derive from measurement error, rather from the large variability of the signal itself. The second band (± 2.6 cm/s) indicates the large variability of the signal. It is one standard deviation of the net current time series about their mean values. This is the day-to-day variability that should be expected due to the vagaries of the weather. It is clear from Figure 16 and 11 a, b, and c that the net flow may be either seaward or landward throughout the water column for durations of up to 2-3 days.

Figure 17 shows two contrasting cases, one for strong winds toward the southwest, and one for strong winds toward the northwest. The former case results in two layered flow with the upper layer speeds greatly enhanced. The latter case, as previously mentioned, results in a transport of water from the East to the West Passage. Note that the flow near the

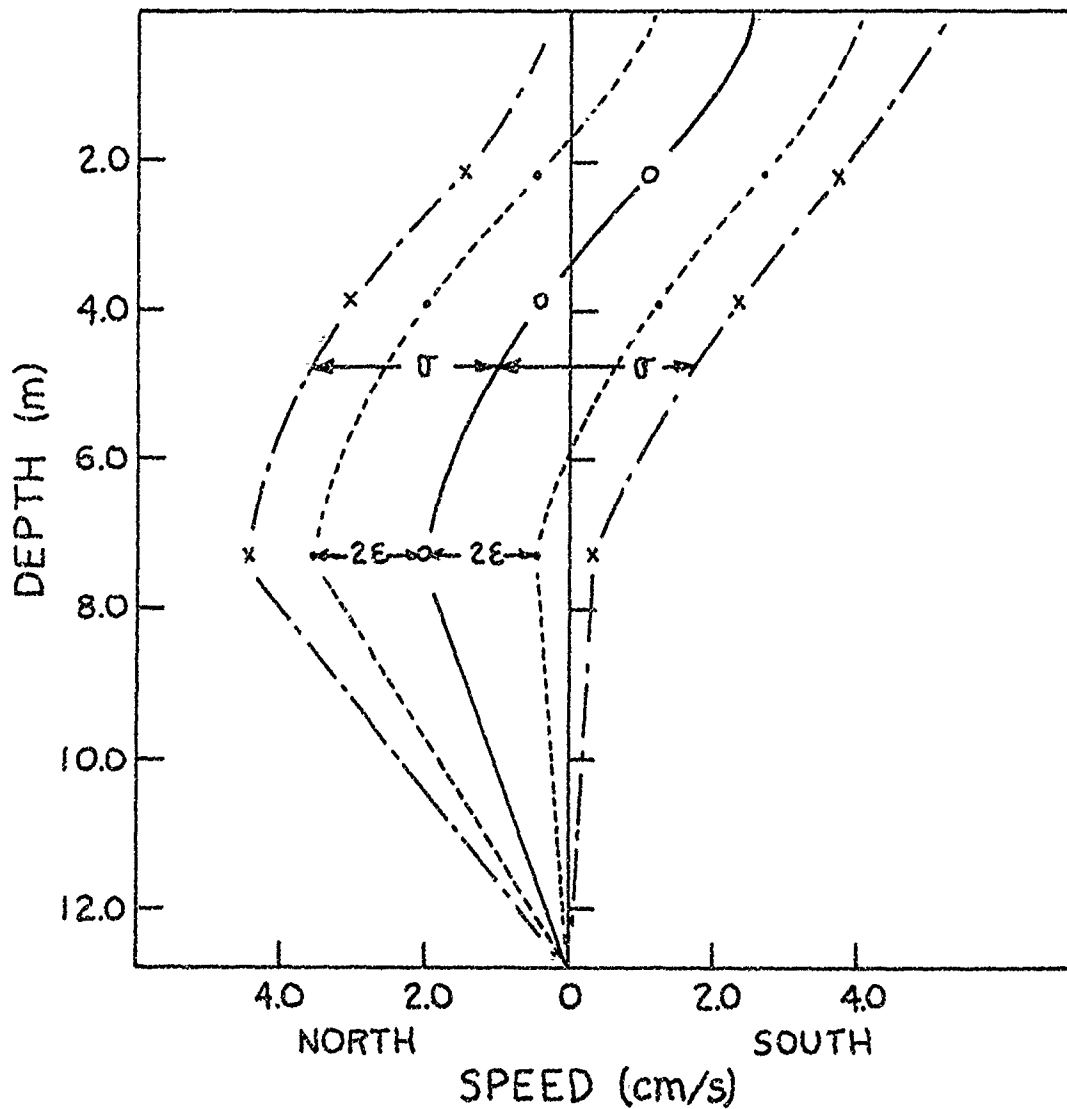


Figure 16. A vertical distribution of the net north component of velocity at the Rome Point station. Included are: the mean values averaged over the entire record length of one month (center curve), the mean values plus and minus two standard errors of the mean (2ϵ), and the mean values plus and minus one standard deviation of the signal (σ).

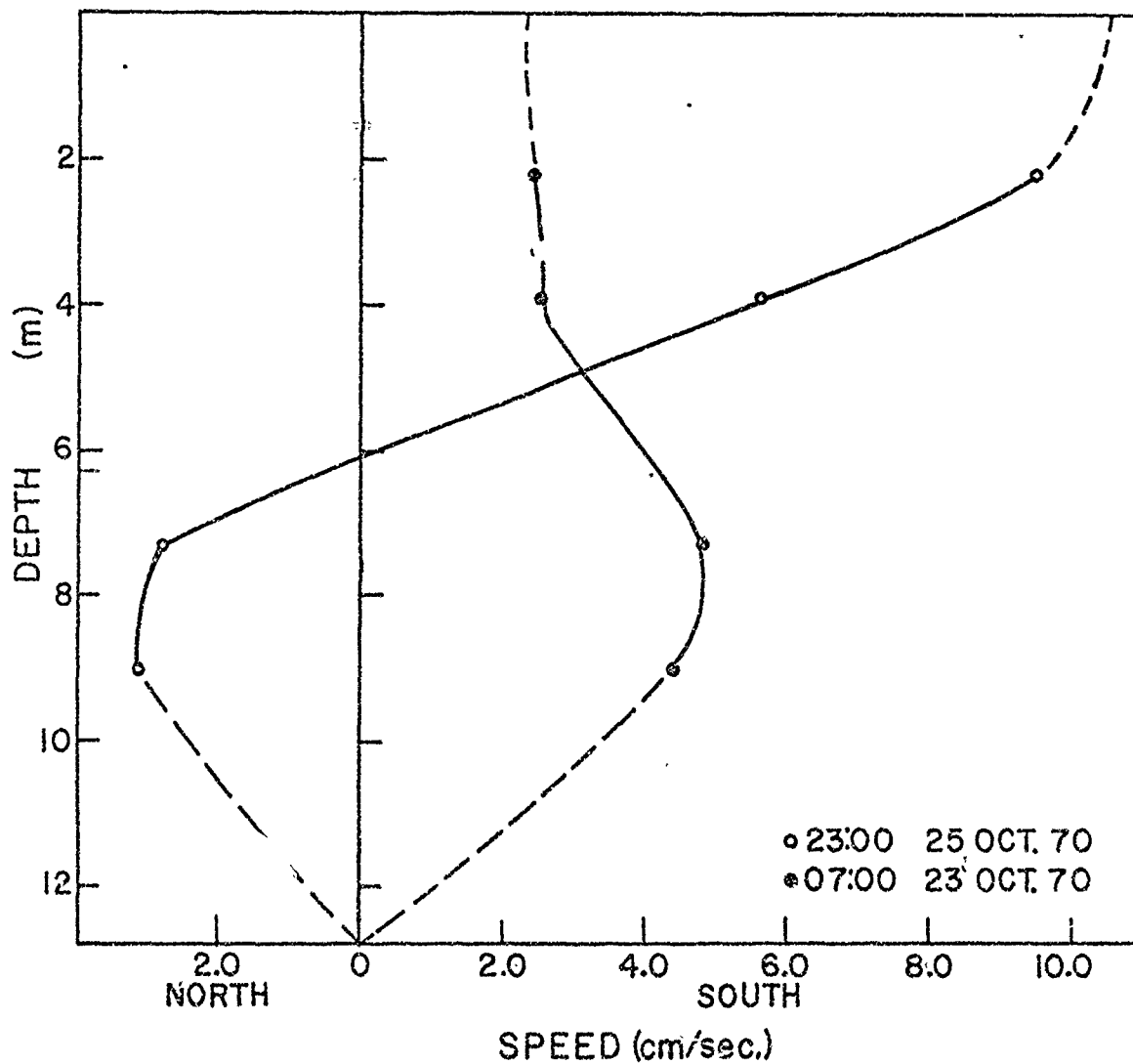


Figure 17. The vertical distribution of the net north component of velocity at the Rome Point station comparing winds blowing toward the northwest and southwest.

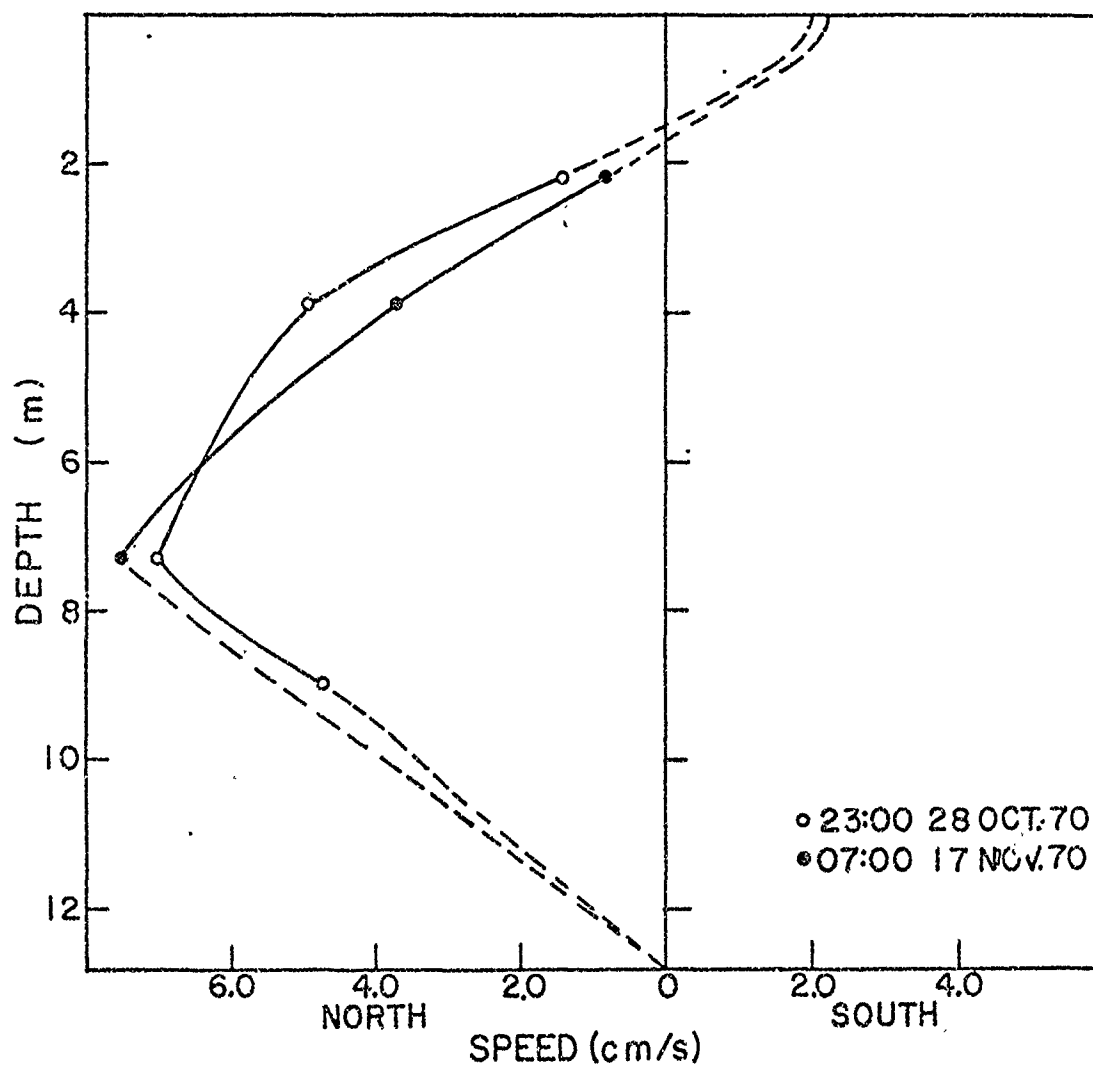


Figure 18. The vertical distribution of the net north component of velocity at the Rome Point station for two independent rebound events.

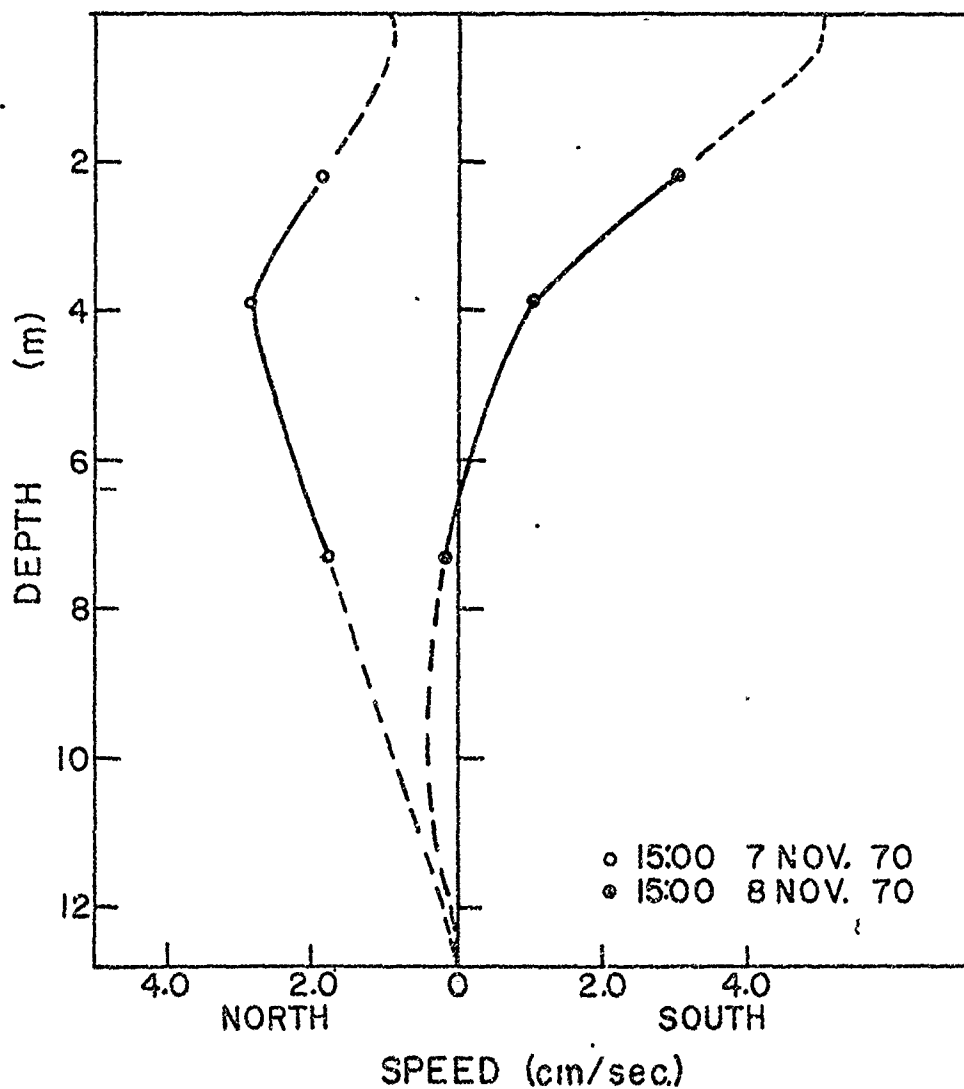


Figure 19. The vertical distribution of the net north component of velocity at the Rome Point station showing the response of the West Passage to a quick reversal in wind direction.

surface, although south, is impeded by the wind relative to the larger speeds in the deeper waters.

Figure 18 shows two independent rebound events. Prior to both events the wind blew strongly toward the south thus driving water out of the West Passage. Rapid abatement of the wind resulted in a lower layer influx of water to re-establish equilibrium. Although they occurred about three weeks apart, the two events are almost identical.

Figure 19 shows how quickly the West Passage responds to a change in wind direction. Within a day the entire distribution is seen to shift from northerly flow to southerly flow in response to the wind.

Net Transport

The net transport of water through the West Passage, at the Rome Point station, was estimated for the flow situations just discussed. The speeds were taken from Figures 16-19 and the cross sectional areas were obtained from Figure 2. It was assumed that at any given depth the net north component of velocity does not vary laterally across the section. This assumption was substantiated by Kowalski et al., (1971). They found the flow to be uniform to within approximately 20%.

The results are shown in Table 5. Three values are given for the transports. The upper and lower layer values refer to flow above and below the zero speed point and the total is the sum of the upper and lower layers. Since the zero speed point is variable so are the extents of the upper and lower layers. In some situations layering does not exist, i.e., flow is entirely north or south, so only the total transport value is given. Also shown in the table is the corresponding fresh water input to the West Passage (see Appendix 3).

The error bounds on the net transport estimates were calculated from the error bounds on the net speeds (± 0.5 cm/s, as shown in Appendix 2). Since the Rome Point station was situated near the deepest part of the channel it is believed that any lateral variability would tend to decrease the net transport. Hence, the transport estimates given in Table 5 may be considered as upper limits to the actual net transport.

Table 5. The net transport of water through the West Passage as computed from the fall 1970 Rome Point station data. Estimates are given for the mean plus or minus two standard errors, the mean plus or minus one standard deviation (s.d.) and for various wind conditions. The river input rate (see Appendix 3) is also included for comparison. An asterisk indicates values that are not statistically different from zero.

Condition Time	Transport ($m^3/s.$)		Total
	Upper Layer	Lower Layer	
Mean \pm two standard errors of the mean	-150*	110*	- 40* \pm 340
Mean + one s.d. of the signal			-540
Mean - one s.d. of the signal			460
Strong wind from S-E 07:00 23 Oct. 70			- 60 \pm 100
Strong wind from N-E 15:00 26 Oct. 70	-1160 \pm 80	90 \pm 20	-1050 \pm 100
Rebound 23:00 28 Oct. 70	-50 \pm 20	660 \pm 80	610 \pm 100
07:00 17 Nov. 70	-50 \pm 20	580 \pm 80	530 \pm 100
Reversal 15:00 7 Nov. 70			390 \pm 100
15:00 8 Nov. 70	-400 \pm 80	10 \pm 10	-390 \pm 100
Fresh water input			-5

Correlation Analysis between the North Component of Wind and Net Near Surface Current

The net current structure in the West Passage arises in a complex manner with the magnitude, direction, and rate of change of the wind overshadowing the gravitational convection scheme of estuarine circulation. Qualitative interpretations have been given in the previous sections concerning the east component and the rate of change of the wind. Since both quantitatively and dynamically, the most important factor seems to be the north component of the wind, its relation to the net circulation will now be studied in more detail.

Two measures of the linear correlation between the time series $x(t)$ and $y(t)$ are the correlation coefficient and the squared coherence function (a discussion of the statistical parameters used in this section may be found in Bendat and Piersol 1966). The correlation coefficient $\rho_{xy}(\tau)$, gives the average linear correlation between the two series in their entirety as a function of their relative time displacement, or lag, τ . It is calculated from,

$$\rho_{xy}(\tau) = \frac{C_{xy}(\tau)}{C_x(0) C_y(0)}$$

where $C_x(0)$ and $C_y(0)$ are the variances and $C_{xy}(\tau)$ is the cross-covariance of the two time series. A more detailed display of the correlation structure is given by the squared coherence function and phase, $\gamma_{xy}^2(f)$ and $\theta_{xy}(f)$, at frequency f , i.e., both the magnitude of the correlation and the relative phase is given for all frequency bands constituting the data. $\gamma_{xy}^2(f)$ is computed from,

$$\gamma_{xy}^2(f) = \frac{|G_{xy}(f)|^2}{G_x(f) G_y(f)}$$

where $G_x(f)$ and $G_y(f)$ are the autospectral density estimates and $|G_{xy}(f)|$ is the magnitude of the cross spectral density estimate at frequency f .

$\theta_{xy}(f)$ is computed from,

$$\theta_{xy}(f) = \tan^{-1} \left[\frac{Q_{xy}(f)}{C_{xy}(f)} \right]$$

where $Q_{xy}(f)$ and $C_{xy}(f)$ are the quadrature and co-spectral estimates at frequency f .

Another statistical description of $x(t)$ and $y(t)$ is the transfer function $H_{xy}(f)$ which may be expressed in polar form as,

$$H_{xy}(f) = |H_{xy}(f)| \exp(-i \theta_{xy}(f))$$

The magnitude of the transfer function equals the ratio of a given frequency constituent in series $y(t)$ to that of series $x(t)$ and is calculated from,

$$|H_{xy}(f)| = \frac{|G_{xy}(f)|}{G_x(f)}$$

It was desired to compute these statistics between the north components of wind and net near surface current (record 026) shown in Figure 11 a, b, and c. This was complicated by the non-stationary nature of the two time series. Inspection suggests that the non-stationarity is primarily associated with the lower frequencies; periods greater than 4 days. Hence, the two time series were bandpass filtered to exclude both the tidal frequencies and the low frequencies causing non-stationarity problems. This was accomplished by three steps: (1) the high frequencies were filtered with a $\sigma = 8$ hr Gaussian filter as described earlier, (2) both intermediate and high frequencies were filtered with a $\sigma = 24$ hr Gaussian filter thus leaving only the low frequencies (refer to Figure 10 for the frequency response), and (3) the results of step (2) were subtracted from those of step (1) thus leaving only the intermediate frequencies. The frequency response function for the end product equals the frequency response of the $\sigma = 8$ hr filter minus that of $\sigma = 24$ hr filter.

The results of the bandpass filtering may be seen in Figures 20 a, b, and c along with the low frequencies that were excluded. The sum of the low and bandpass time series equals their respective series given in Figures 11 a, b, and c.

The bandpass filtered time series of the north component of wind $x(t)$ and the near surface current $y(t)$ were spectrally analysed for the compu-

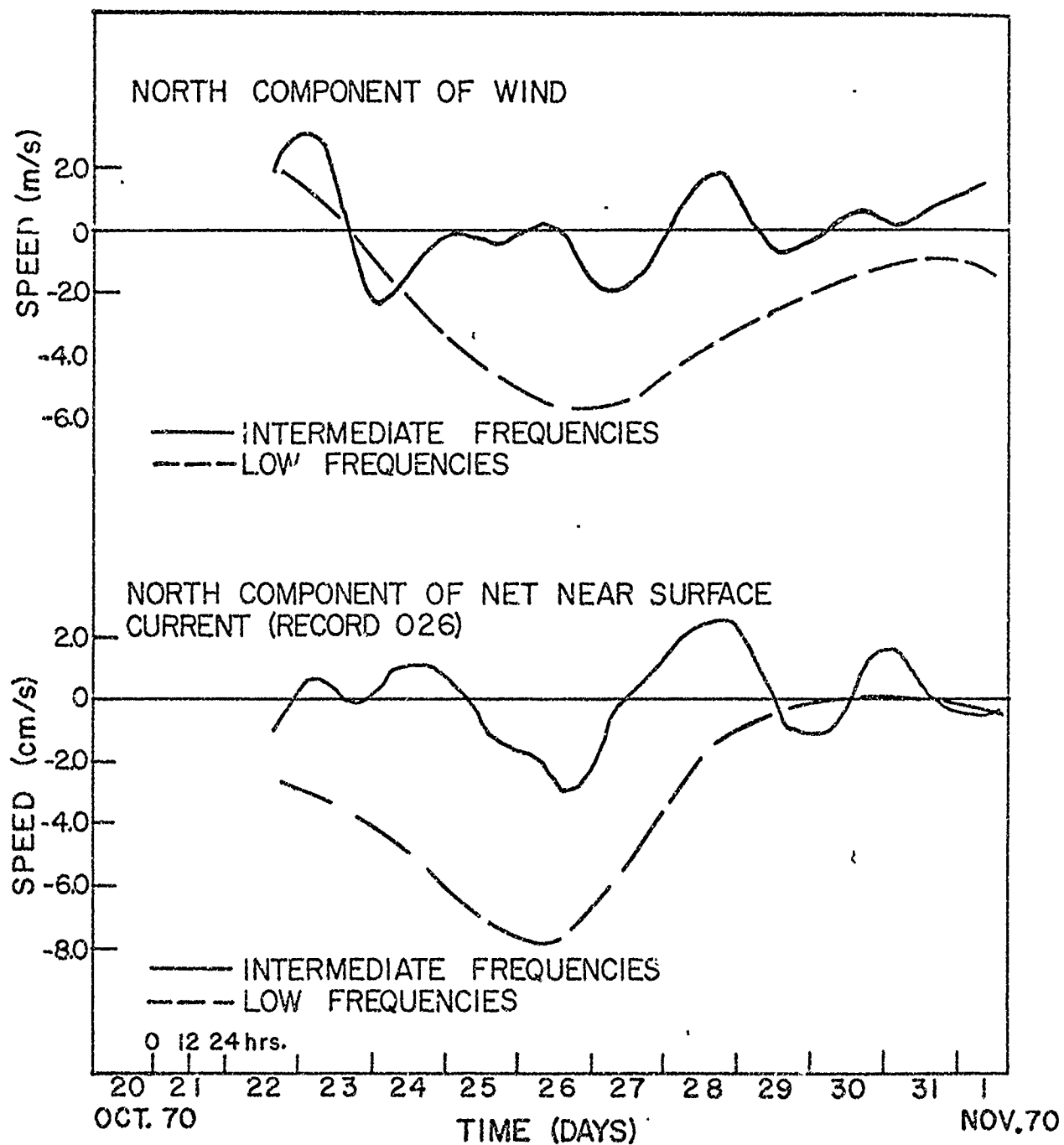


Figure 20 a. The bandpass filtered time series of the north components of wind and near surface current (record 026) at the Pome Point station.

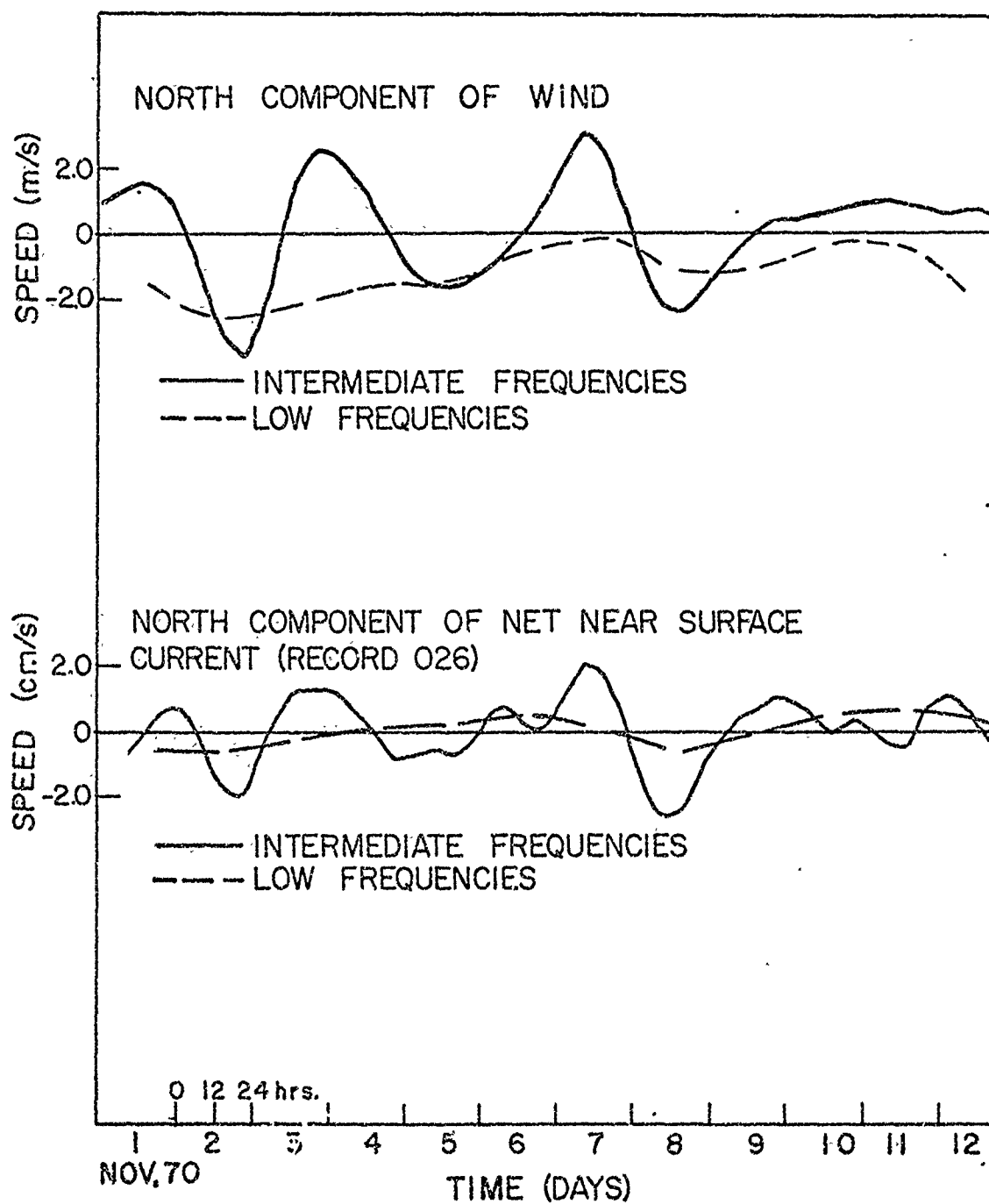


Figure 20 b. The bandpass filtered time series of the north components of wind and near surface current (record 026) at the Rome Point station.

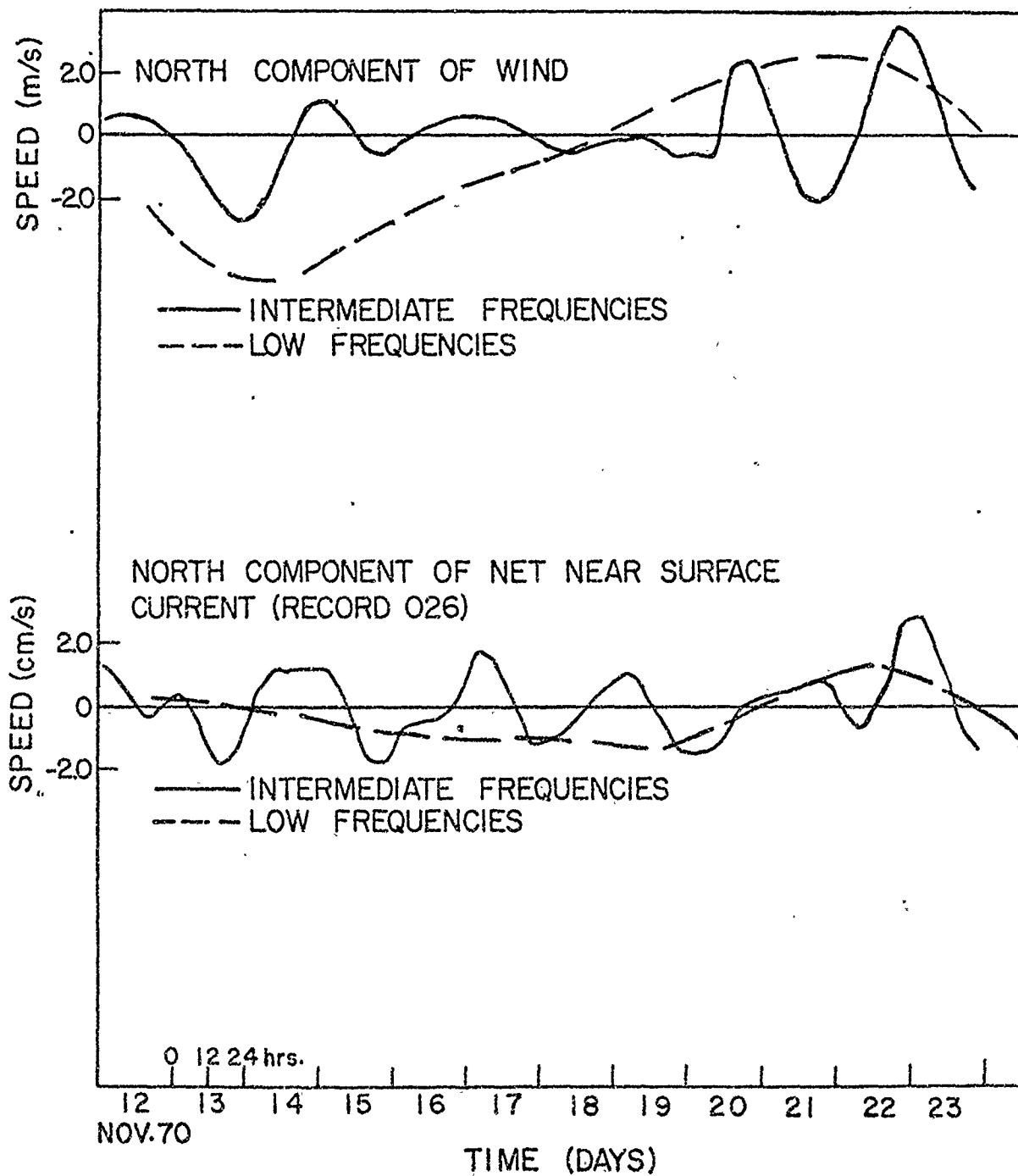


Figure 20 c. The bandpass filtered time series of the north components of wind and near surface current (record 026) at the Rome Point station.

tation of $\rho_{xy}(\tau)$, $\gamma_{xy}^2(f)$, $\theta_{xy}(f)$, and $H_{xy}(f)$. The results now follow.

The maximum value of the correlation coefficient between the wind and net near surface current occurs at zero lag and equals 0.62. Table 6 gives the other pertinent statistics. Only those frequency bands for which the response of the bandpass filter was greater than 0.5 are included. Since a rather narrow frequency range fell within this category it was necessary to highly resolve the spectra. 12 degrees of freedom were used for the calculation so with a 5% significance level, the null hypothesis is rejected with 90% confidence for squared coherences greater than 0.4 (see Amos and Koopmans, 1963, p. 41). In other words, with perhaps the exception of 0.0167 c/hr, all squared coherences given in Table 5 represent real wind-net current correlations and are not just a product of noise interaction.

Table 6. Squared coherence, phase, and transfer function for the bandpass filtered north component time series of wind and net near surface current (record 026). The data were obtained from the fall 1970 Rome Point station. A negative value of phase indicates that the net current lags the wind.

Frequency (c/hr)	Period (hr)	Squared Coherence	Phase (hr)	Transfer Function Magnitude
0.0125	80	0.63	+8.0	0.49×10^{-2}
0.0167	60	0.41	+2.0	0.48×10^{-2}
0.0208	48	0.65	-3.0	0.73×10^{-2}
0.0250	40	0.68	-2.4	0.72×10^{-2}

The coherence is largest at the frequency bands centered on 0.025 and 0.021 cycles per hour (encompassing periods of 1.5-2.5 days). Also, the net current lags the wind. Hence, it appears that the water column responds well to the wind as a causal mechanism of net currents.

The phase lag between variations of wind and the water response can be readily explained since the input of momentum to the water by wind requires a finite amount of time. An order of magnitude estimate of

this time may be obtained from the appropriate terms in the momentum conservation equations,

$$\rho_w \frac{du}{dt} = \frac{\delta \mathcal{T}}{\delta z}$$

where ρ_w is the water density, u is the water speed, \mathcal{T} is the wind stress, t is time, and z is depth. Neglecting bottom stress and integrating vertically results in,

$$\rho_w \frac{du}{dt} h = \mathcal{T}$$

where h is the total depth. Assuming a constant wind stress, the time required for the water to reach a given speed u is now,

$$t = \frac{\rho_w u h}{\mathcal{T}}$$

The wind stress may be calculated from,

$$\mathcal{T} = \rho_a C_d w^2$$

where ρ_a is the air density, C_d is the drag coefficient, and w is the wind speed. Thus, the response time is

$$t = \frac{\rho_w}{\rho_a} \cdot \frac{h}{C_d w} \cdot \frac{u}{w}$$

The above quantities are either known or may be calculated. The ratio u/w was found to be stable at 0.7×10^{-2} for periods about 2 days (Table 6). For an r.m.s. wind speed of 3.6 m/s the drag coefficient C_d is 1×10^{-3} (see Wu 1967, p. 17). The average depth at the Rome Point section (Figure 2) is 6.7 m. Using these values in the preceding equation we arrive at a response time of 3.6 hrs. This calculated response time agrees fairly well with the observed phase lag of approximately 3 hours for wind fluctuations of period about 2 days. The point to be made from this simple calculation is that the phase lag of the waters response to wind fluctuations can be adequately accounted for by the water's inertia; frictional coupling with the bottom need not be involved.

Considerable past work has been performed to determine the ratio of current speed to wind speed ("wind factor") in the open ocean. These investigations are summarized in Defant (1961 p. 418) with the general result being 0.01 - 0.02, or roughly twice that as obtained here. The value obtained here is expected to be less because in coastal waters, the effects of stratification and especially limited fetch tend to decrease the wind induced motion.

At lower frequencies the coherence decreases, as noted from Table 5 and inspection of Figures 20 a, b, and c, and the phase reverses, i.e. the current leads the wind. The latter is not consistent with a physically reasonable cause (wind) and effect (net current) mechanism, but it does not preclude one. It simply points to the complicated nature of the system whereby mechanisms other than the north component of wind (such as the east component of wind, the rate of change of wind, as well as gravitational convection) are important in driving the net circulation in the West Passage.

Net Currents (Spring 1971)

The results of the spring net current determinations are similar to those of the fall. Unweighted averages of the north components of current were formed over every two tidal cycles and the wind time series were smoothed with a $\sigma = 8$ hour Gaussian filter. The results are given in Figure 21. Since the second instrument from the surface failed no data is available from the middle of the water column.

Unfortunately the wind conditions during the spring measurements were more severe than during the fall, and a larger percentage of the current data points may be biased as designated by the dashed lines in Figure 21. Table 7 gives the mean values and root mean square deviations about the mean for the north component time series of net current.

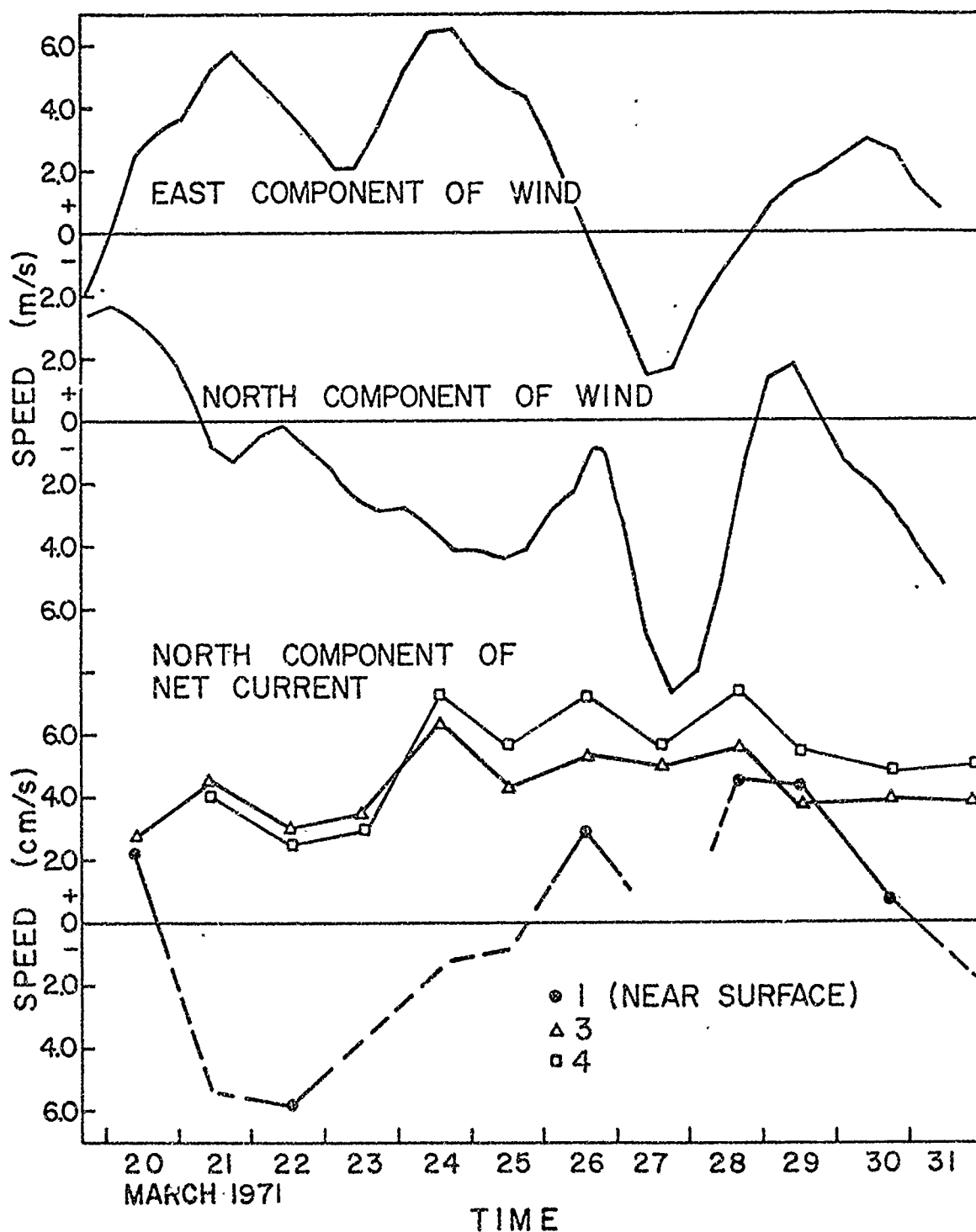


Figure 21. The net current and smoothed wind time series obtained during the spring of 1971.

Table 7. The mean values and root mean square deviations about the mean for the net currents obtained from the spring 1971 Rome Point station. Positive denotes flow toward the north.

Record	Height (m) measured from the Bottom	Mean (cm/s)	Standard Deviation (cm/s)
1	10.6	-0.1	3.4
2	8.9	4.6	1.3
4	2.1	5.0	1.6

No significance can be given to the mean of record 1 due to the predominance of possibly biased data. However, certain features of the spring 1971 net currents are noteworthy. The deep net currents are slightly greater and less variable than those for the fall and are directed landward. This may be attributed to the increase in stratification as shown in Appendix 4. An apparent rebound seems to have occurred on 28 and 29 March. We find the net water flow to be northward at all depths upon the subsidence of a strong southward component of wind. This observation is in agreement with similar observations during the fall 1970 experiment. Also of interest are the relatively large southerly net near surface current values about 22 March. This corresponds to a period of maximum river input as shown in Appendix 3.

IV DISCUSSION

Wind Induced Transport

The net water transport through the West Passage rarely, if ever, equals its river input. Rather, the net transport may be directed seaward or landward over the entire water column in response to the wind. This section will discuss some features of wind induced currents as they apply to the West Passage.

The direction and variation with depth of wind generated currents was studied in detail by Ekman (1905). Graphical solutions for wind induced currents near a coastal boundary are given in Figure 22. Included are various examples for different ratios of water depth to the so-called depth of frictional influence, or Ekman depth, and wind direction relative to the coastal boundary.

The depth of frictional influence depends on the eddy transfer of momentum through the water column. In the absence of abrupt density changes, the Ekman depth in a stratified fluid is similar to that for a homogeneous fluid and it is calculated to be of order 50-100 m assuming a constant eddy viscosity coefficient (see Neumann and Pierson, 1966, pp. 195-197 and 210). Some observations suggest that the Ekman depth is less since the eddy viscosity coefficient associated with wind induced motions is not constant but rather decreases with depth (e.g., see Sverdrup et al. 1942 p. 496). We conclude, however, that the Ekman depth is larger than the depth of the West Passage and a situation similar to examples 7 and 8 of Figure 22 should apply to a wind blowing parallel to the West Passage. The resulting current vector lies approximately in the direction of the wind throughout the water column and decreases to zero at the bottom. This agrees with the present observations (see Figure 19).

The wind induced water transport in an enclosed basin results in a surface slope whose associated pressure gradient balances the wind stress on the sea surface. Neglecting stratification, this slope θ is given by,

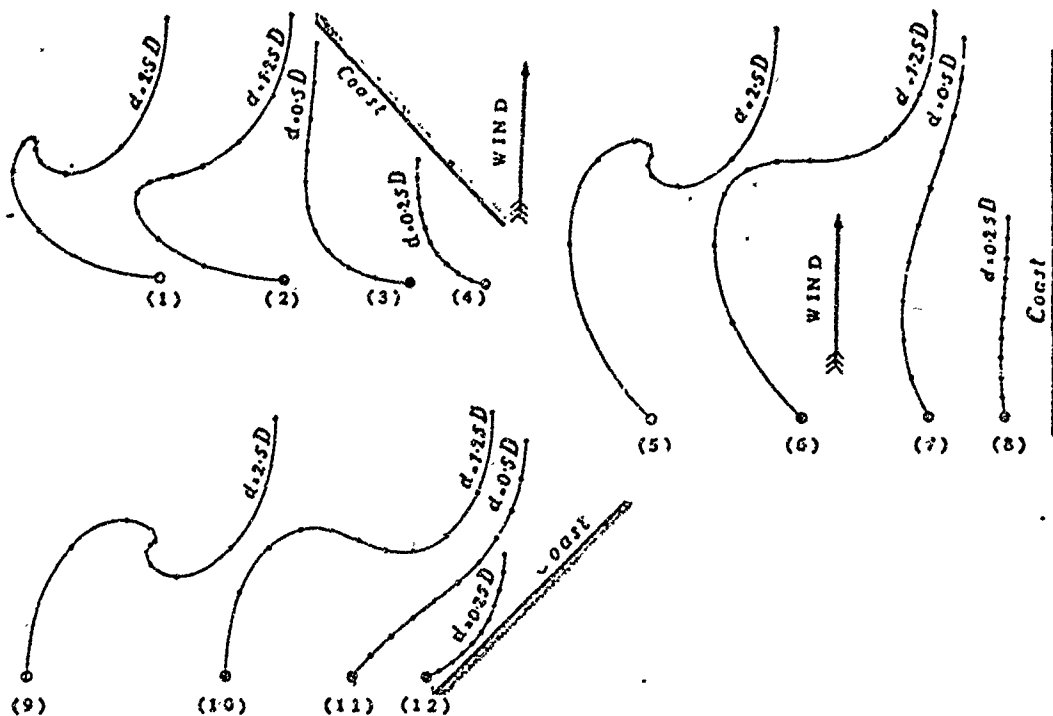


Figure 22. The vertical distribution of Ekman's elementary current system projected on a horizontal plane. Examples 7 or 8 apply to a wind blowing parallel to the axis of the West Passage (from Ekman (1905)).

$$\beta = \frac{3}{2} \frac{\tau}{\rho_w g d}$$

where τ is the wind stress, d and ρ_w are the water depth and density and g is the acceleration of gravity (e.g. see Defant 1961, p. 419). The effect of stratification is to increase the slope; however for durations of a few days the above equation is a good approximation (e.g. see Defant 1961 pp. 545-547).

For a rectangular basin of length x the characteristic time t to set up the required slope is,

$$t = \frac{\beta x^2}{2 v d}$$

where v is the average velocity over the water column. Putting in the appropriate numbers for the West Passage it is estimated that, once the water column has been set in motion, it takes less than an hour to re-distribute enough water to balance the stress of a 5-10 m/s northward wind. In other words, we might expect there to be a net transport over the entire water column for a few hours of sufficient volume to establish a new water level. However, the observed velocities show that net inflows or outflows may occur for a few days. We conclude, that under these conditions, there must be a net transport of water from West Passage to East Passage or vice versa.

The flow from the West Passage to the East Passage under the influence of a northward wind may easily be explained by the difference in the depths of the two passages. West Passage is only about two thirds as deep as the East Passage. Since the surface slope is inversely proportional to depth, the water in the West Passage is raised somewhat higher than in the East Passage, resulting in a west to east driving force. Table 8 offers a sample calculation showing that under the influence of a 10 m/s northward wind a hydrostatic pressure head of about 2 cm results at the northern tip of Conanicutt Island. The adequacy of this pressure differential as a driving mechanism may be shown in either of two ways: (1) by calculating the resulting pressure gradient force between the West and East Passages or (2) by calculating the resulting potential exit velocity V using Torricelli's theorem,

$$V = \sqrt{2g\Delta H}$$

The former calculation suggests that the west to east pressure gradient calculated over a distance of 2 km is the same order of magnitude as the tidal forcing function. The latter yields a potential exit velocity of around 60 cm/s. In either case it is concluded that the mechanism just described is a physically reasonable means of driving water from the West to East Passage under a moderate northward wind.

Table 8. A sample calculation showing the surface elevation at the northern tip of Conanicut Island under the influence of a 10 m/s northward wind.

	West Passage	East Passage
Wind Speed,	10 m/s	10 m/s
Wind Stress,	3.5 dynes/cm ²	3.5 dynes/cm ²
Fetch	10 km	10 km
Average depth, d	10 m	15 m
Wind induced elevation, H	5 cm	3 cm

$$(1) \quad \tau = 2.6 \times 10^{-3} \rho_w w^2$$

$$(2) \quad H = (\text{slope}) (\text{fetch}); \text{ slope} = \frac{3}{2} \frac{\tau}{\rho_w g d}$$

Phase Advance of the Instantaneous Motion with Depth

The phase advance of the instantaneous motion with depth may arise as an effect of bottom friction. Consider a simplified two-dimensional model of a harmonically driven current $U(z,t)$ moving over a flat bottom. Let x denote the longitudinal axis and z the vertical axis (directed upward from the bottom). Assuming a homogeneous fluid with constant eddy

viscosity coefficient A, the linearized longitudinal equation of motion becomes,

$$\frac{\partial U}{\partial t} - A \frac{\partial^2 U}{\partial z^2} = F \exp(i\omega t)$$

where $F \exp(i\omega t)$ is a harmonically varying pressure gradient force per unit mass. Using the hydrostatic assumption for a homogeneous fluid, it can be shown that the pressure gradient force is constant with depth and equal to $\rho g \frac{\partial h}{\partial x}$, where h is the height of the sea surface.

An intuitive explanation of the phase advance may now be given. A tidal current reaches its maximum absolute value when $\frac{\partial U}{\partial t} = 0$. In the present model, this occurs when the pressure gradient force is balanced by friction. The former is constant with depth while the latter arises from the bottom and decreases upwards. Hence, $\frac{\partial U}{\partial t} = 0$, first occurs near the bottom and then occurs progressively later toward the surface. It follows that the near bottom currents lead the surface currents.

Lamb (1932, pp. 622-623) gives an exact solution to the preceding equation of motion subject to the boundary conditions,

$$\begin{aligned} U &= 0 \text{ at } z = 0; \text{ no slip} \\ \frac{\partial U}{\partial z} &= 0 \text{ at } z = h; \text{ no shear stress at the surface.} \end{aligned}$$

The solution is

$$U(z, t) = \frac{F}{\omega} \sin \omega t - \frac{F}{\omega} \exp(-\beta z) \sin(\omega t - \beta z)$$

where $\beta = \sqrt{\frac{\omega}{2A}}$. The particular part, $F/\omega \sin \omega t$, is purely oscillatory; analogous to an irrotational wave. The complimentary part, $-F/\omega \exp(-\beta z) \sin(\omega t - \beta z)$, has rotation and characterizes the disturbance due to bottom friction. The vertical extent of this frictional disturbance may be chosen as the point where $e^{-\beta z} = e^{-\pi}$ or at $z = \pi/\beta$. Hence, the vertical extent depends on the frequency of the motion and the eddy exchange of momentum. Two numerical examples are given in Table 9, one for molecular viscosity and one for a value of the eddy viscosity coefficient obtained for the James River estuary by Rattray and Hansen (1962). It is

seen that bottom frictional effects may permeate most of the water column in a shallow estuary.

Table 9. Sample calculations showing the vertical extent of bottom frictional effects.

	Molecular Viscosity (after Lamb (1932))	Eddy Viscosity
	$A = 0.0178 \text{ cm}^2/\text{s}$	$A = 4 \text{ cm}^2/\text{s}$
ω	$2\pi / 12.42 \text{ radians/hr}$	$2\pi / 12.42 \text{ radians/hr}$
$\beta = \sqrt{\omega/2A}$	6.3 m^{-1}	0.42 m^{-1}
Vertical extent = π/β	0.5 m	7.5 m

Lamb's solution may be put in the simpler form of

$$U(z,t) = B(z) \sin (\omega t - \alpha(z))$$

where

$$B(z) = U_0 \left[1 - 2 \exp (-\beta z) \cos \beta z + \exp (-2 \beta z) \right]$$

and

$$\alpha(z) = \text{TAN}^{-1} \left[\frac{-\sin \beta z}{\exp \beta z - \cos \beta z} \right]$$

from which the limit of $\alpha(z)$ as z approaches zero is 45 degrees. Figures 23a and b show the amplitude $B(z)$ and the phase $\alpha(z)$ for a semi-diurnal oscillation using various eddy viscosity coefficients. Three sets of semi-diurnal component data points are included in the figure. One set was computed over four tidal cycles in the Pawtuxent River estuary by Cannon (1969). The other two sets are averages formed over the four neap and spring conditions given in Table 3. The agreement between the observations and theory is pleasingly good. Note that our data shifts from neap to spring tides toward a larger value of eddy viscosity, as would be expected for an increase in current speed.

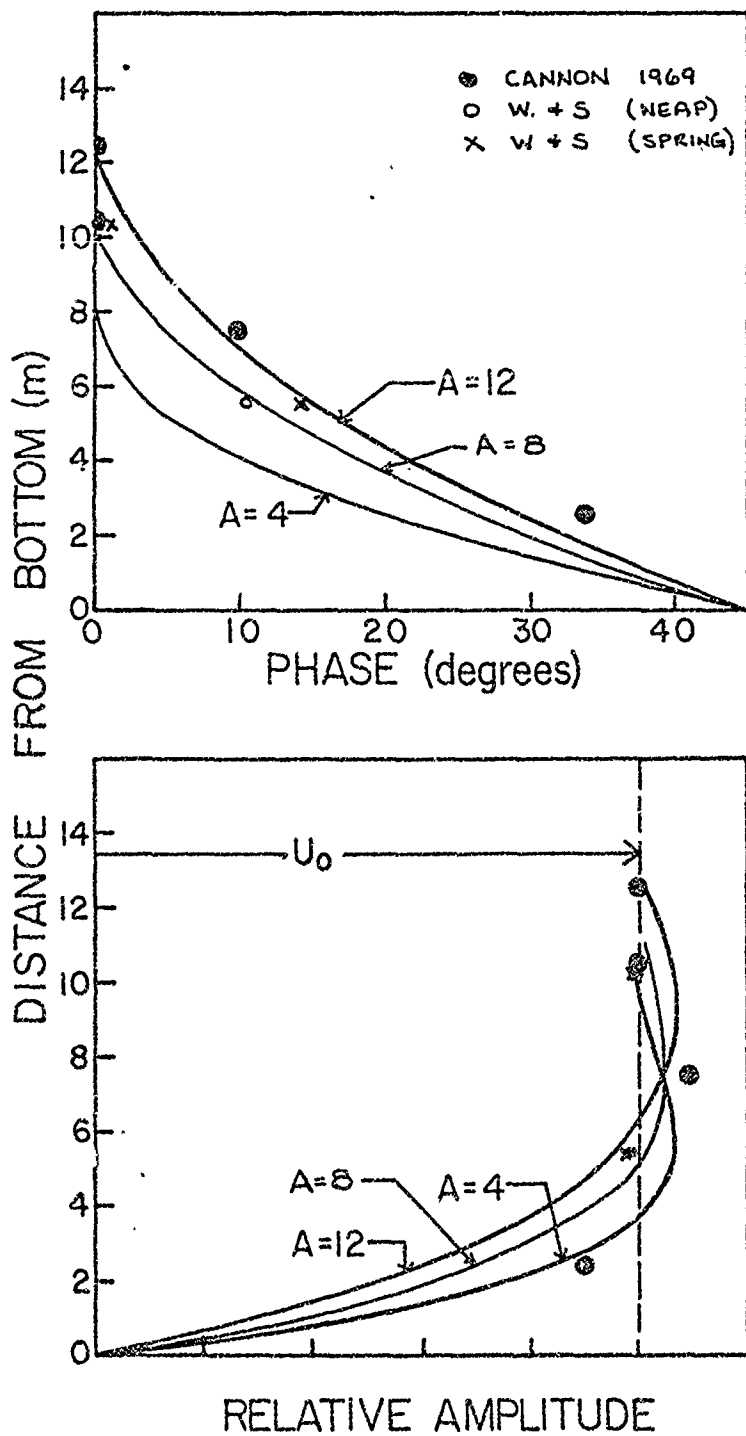


Figure 23 a, b. The depth distribution for the relative amplitude and phase of a simple harmonic oscillation over a flat plate. Curves are given for three different values of the eddy viscosity coefficient. The comparative data points are from Cannon (1969) and the present study.

As nice as this simple frictional model appears, it does not fully explain the observations shown in Figure 8, i.e., the phase advance in the West Passage varies with lunar phase and is asymmetric about a tidal cycle. The phase advance is most visible to the eye at the times when the speed passes through zero. As interpreted from these zero crossings, the phase advance ranges from about 1-3 hours for neap and intermediate range tides to near zero for spring tides. This result is puzzling: we would expect the phase advance to be larger during spring tides if it indeed originates from bottom frictional drag. The paradox is resolved by referring back to the Fourier decomposition of the signal given in Table 3. Looking at the M_2 component alone, we see that the average phase shifts between currents measured at depths of 2.1 m and 7.2 m are 0.18 radians for neap tides and 0.25 radians for spring tides (as in Figure 23). Therefore, although the phase advance of the signal as a whole (as determined from zero crossings) decreases upon the approach of spring tides, the phase advance of the M_2 component does, in fact, increase.

The cause for the larger zero crossing discrepancies during neap tides resides with the higher tidal harmonics which are relatively more important about neaps. Small changes in the amplitude ratio or phase between the M_4 and M_2 harmonics markedly affect the zero crossings (for example, see the U.S.C. & G.S. Sp. Pub. # 260, p. 36).

In summary, bottom frictional drag appears to be an underlying factor in the observed phase advance with depth of the instantaneous tidal currents but it is not the only important factor. Higher tidal harmonics modify and complicate the waveform, particularly about neap tides, thus accounting for real time surface to bottom phase shifts of as much as 3 hours.

V SUMMARY AND CONCLUSIONS

The primary interest of this study was the analysis of the net motion, i.e., the motion exclusive of the periodic tides. Net current time series were obtained by filtering the diurnal and higher tidal frequencies out of the instantaneous current meter records. The resulting net currents during the fall of 1970 were found to be an order of magnitude less than the instantaneous motion and well correlated with the prevailing 2-10 m/s winds. The correlation was strongest between the north components (parallel to the axis of the West Passage) of wind and net near surface current. For periodicities about two days the squared coherence and phase between the north component time series of wind and net near surface current were 0.7 and 3 hrs. The north component of net current also exhibited coherence vertically at both stations, as well as longitudinally between them. Hence, the West Passage seems to respond well to the north component of wind as a causal mechanism of fluctuating net currents.

Net transport calculations were made for various wind conditions. It was found that the net transport of water through the West Passage may be directed either seaward or landward over the entire water column in response to the wind, for durations of up to a few days. We conclude that a corresponding water transport occurs between the East Passage and West Passage. Typical wind induced variations in the net water transport through the West Passage are roughly $\pm 500 \text{ m}^3/\text{s}$ (one standard deviation of the net current signal).

In order to investigate the gravitationally convected circulation apart from wind effects, the net current time series were averaged over their entire length of one month. The resulting mean estimates exhibited a two layered structure with a seaward flow in the upper layer and a landward flow in the lower layer. However, due to the large variance and non-stationary nature of the net current time series, the mean estimates were not significantly different from zero. Furthermore, it is doubtful whether the gravitationally convected circulation in the West Passage can be extracted from current observations, irrespective of record length. In a single channel estuary the net transport must equal the river input. In that case, a mean flow estimate can be representative of the gravitationally

convected circulation, but, only if the averaging interval is sufficiently larger than the periods of local wind fluctuations, even if the winds are light. This is an important result. It warns estuarine investigators --at least in Narragansett Bay-- not to put much confidence in mean values computed from data taken over only a few tidal cycles.

In conclusion: the West Passage of Narragansett Bay does not behave as a typical two-layered estuary for two reasons. First, the day to day net water transport through the West Passage does not equal its river input. Second, gravitational convection, although of underlying importance, is eclipsed by wind as the dominant mechanism driving the net circulation. Hence, the net circulation in the West Passage should be viewed as a stochastic process. It is suggested that the next step in its study be the development of a predictive model, whereby the net circulation could be estimated from such parameters as wind speed and direction, river runoff, and atmospheric pressure.

ACKNOWLEDGEMENTS

The authors have enjoyed the enthusiastic support of many people. Mr. Roger Smith participated in all aspects of the field program. Messrs. James Allan and Al Davis provided the necessary underwater assistance. The field work was simplified by the able boat handling of Mr. Stanley Spink; captain of the R/V Billie II, and Mr. John Miller; captain of the R/V Islander. Miss Susan Tarbell and Mr. George Tupper of the Woods Hole Oceanographic Institute offered their assistance for the spring experiment. The final typing and proofreading was expedited with the thoughtful aid of Mrs. Leonore Allen. Special thanks go to Mr. William Kramer for his help with all of the computer related data processing.

BIBLIOGRAPHY

Bendat, J.S. and A.G. Piérsol

1966. Measurement and Analysis of Random Data. Wiley, New York, 390 pp.

Cameron, W.M. and D.W. Pritchard

1963. Estuaries. In: The Sea, Vol. 2, M.N. Hill, ed., Wiley, New York, pp. 306-324.

Cannon, G.A.

1969. Observations of Motion at Intermediate and Large Scales in a Coastal Plain Estuary. Chesapeake Bay Institute, Technical Report #52.

Defant, A.

1961. Physical Oceanography. Vol. 1, Pergamon Press, Oxford, 729 pp.

Dixon, W.D., ed.

1970. Biomedical Computer Programs. University of California Publications in Automatic Computation #2, University of California Press, Berkeley.

Ekman, V.W.

1905. On the Influence of the Earth's Rotation on Ocean Currents. Royal Swedish Academy of Science, Stockholm, 52 pp.

Fofonoff, N.P. and Y. Ercan

1967. Response Characteristics of a Savonius Rotor Current Meter. Woods Hole Oceanographic Institute, Technical Report #67-33.

Haight, F.J.

1938. Currents of Narragansett Bay, Buzzards Bay, and Vineyard Sound. U.S. Coast and Geodetic Survey, Special Publication #208.

Hansen, D.V. and M. Rattray

1965. Gravitational Convection in Straits and Estuaries. J. Mar. Res., 23: 104-122.

Hansen, D.V. and M. Rattray

1966. New Dimensions in Estuary Classification. Limnol. Oceanogr., 11: 319-326.

Hicks, S.D.

1959. The Physical Oceanography of Narragansett Bay. Limnol. Oceanogr., 4: 316-327.

Hicks, S.D.

1963. Physical Oceanographic Studies of Narragansett Bay. U.S. Fish and Wildlife Service, Special Science Report, Fisheries #457.

Holloway, J.L.

1958. Smoothing and Filtering of Time Series and Space Fields. Advances in Geophysics, 4: 351-389.

Kowalski, T., et al.

1971. Drifting Drogue Studies in the Vicinity of Rome Point. In: Rome Point Circulation Study. University of Rhode Island Technical Report #98-20-7057.

Lamb, H.

1932. Hydrodynamics. Dover, New York, 738 pp.

Neumann, G. and W.J. Pierson, Jr.

1966. Principles of Physical Oceanography. Prentice-Hall Englewood Cliffs, New Jersey, 54 pp.

Pickard, G.L. and K. Rodgers

1959. Current Measurements in Knight Inlet, British Columbia. J. Fish. Res. Bd. Canada, 16: 635-684.

Pritchard, D.W. and R.E. Kent

1956. A Method for Determining Mean Longitudinal Velocities in a Coastal Plain Estuary. J. Mar. Res. 15: 81-91.

Rattray, M. and D.V. Hansen

1962. A Similarity Solution for Circulation in an Estuary. J. Mar. Res. 20: 121-133.

Sturges, W. and R.H. Weisberg

1971. Non-Tidal Transport, West Passage of Narragansett Bay Near Rome Point. In: Rome Point Circulation Study, University of Rhode Island Technical Report #98-20-7057.

Sverdrup, H.U., M.W. Johnson, and R.H. Fleming

1942. The Oceans. Prentice-Hall, Englewood Cliffs, New Jersey, 1087 pp.

Sverdrup, H.U. and W. Munk

1947. Wind, Sea, and Swell: Theory of Relations and Forecasting. U.S. Naval Oceanographic Office, Special Publication #601.

U.S. Dept. of Commerce, Coast and Geodetic Survey.

1952. Manual of Harmonic Constant Reductions, Special Publication #260,
U.S. Government Printing Office, Washington 25, D.C.

Weigel, R.L.

1964. Oceanographical Engineering. Prentice-Hall, Englewood Cliffs,
New Jersey, 532 pp.

Wu, J.

1967. Wind Stress and Surface Roughness at Air-Sea Interface.
Hydronautics; Incorporated, Technical Report #231-18.

APPENDIX 1

Instantaneous Motion

The north and east components of current observed during the fall 1970 and spring 1971 experiments are shown in Figures A 1.1 through A 1.9. The figures were drawn using one hour averages.

These data are available at the Graduate School of Oceanography, University of Rhode Island.

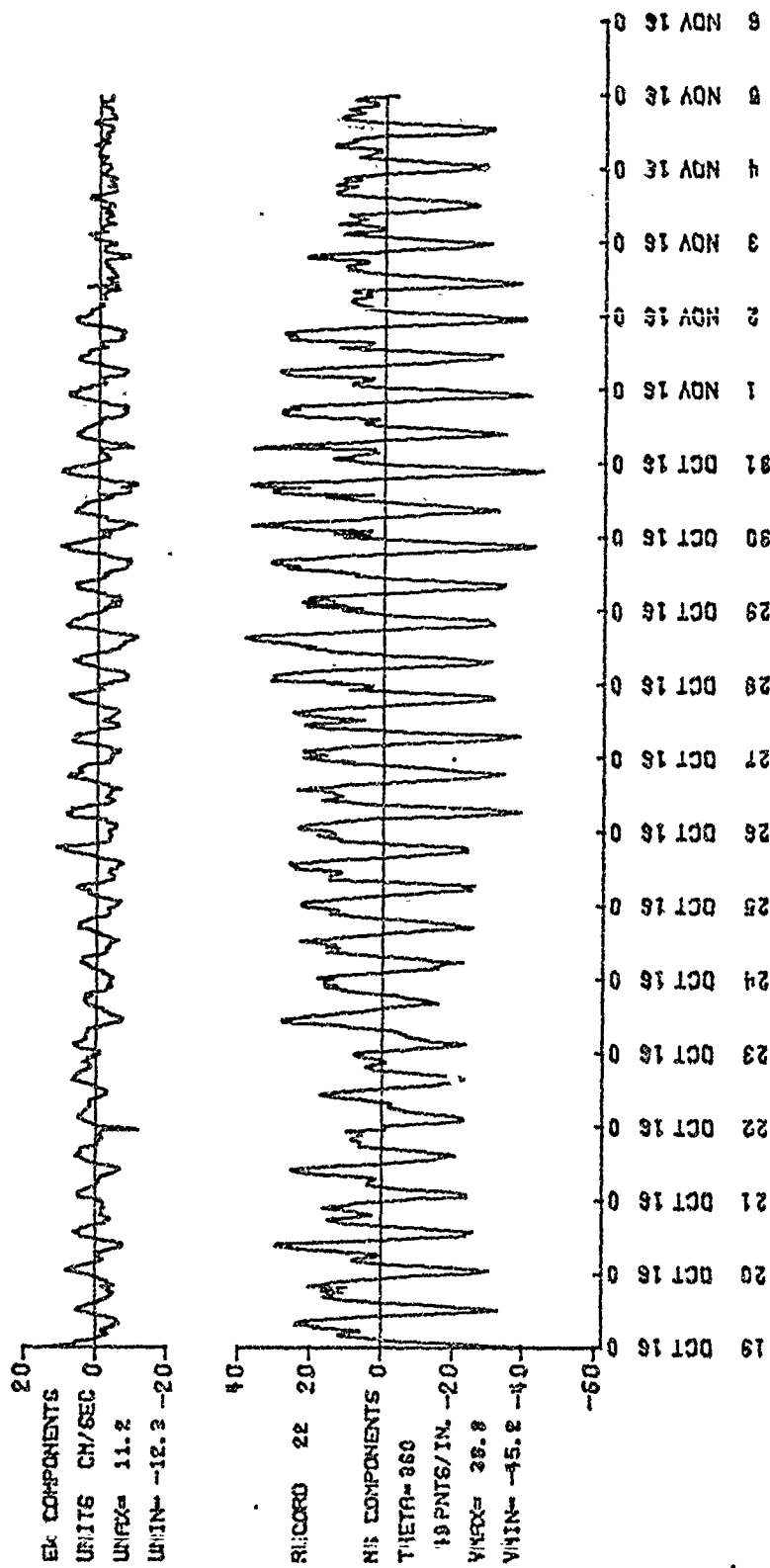


Figure A 1.1 Record 022; Position: Rome Point Station, 3.8 m from the bottom.

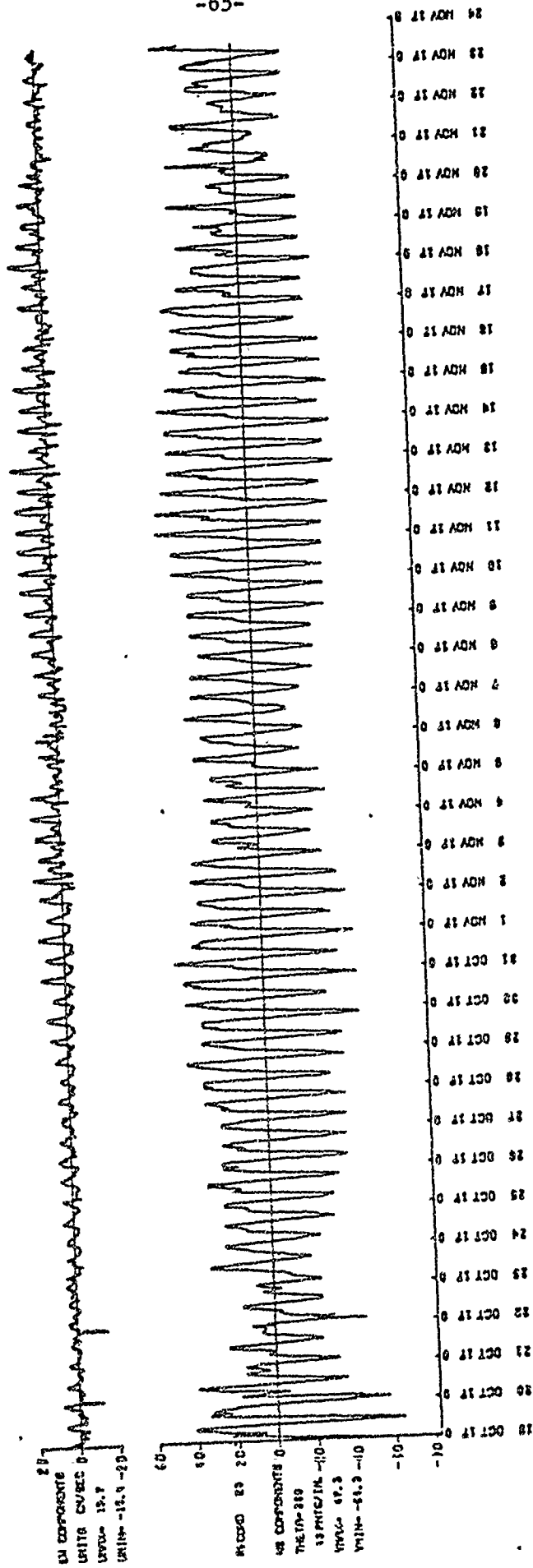


Figure A 1.2 Record 023; Position: Rome Point Station, 5.5 m from the bottom.

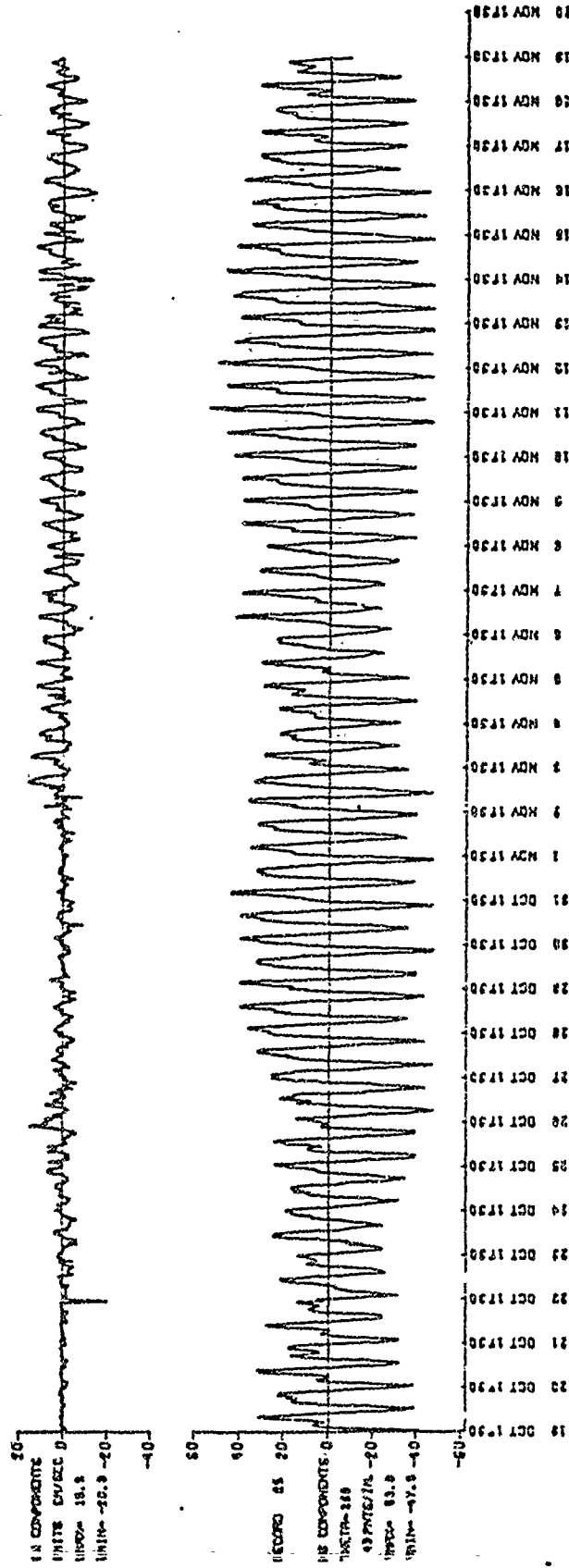


Figure A 1.3 Record 025; Position: Rome Point Station, 8.9 m from the bottom.

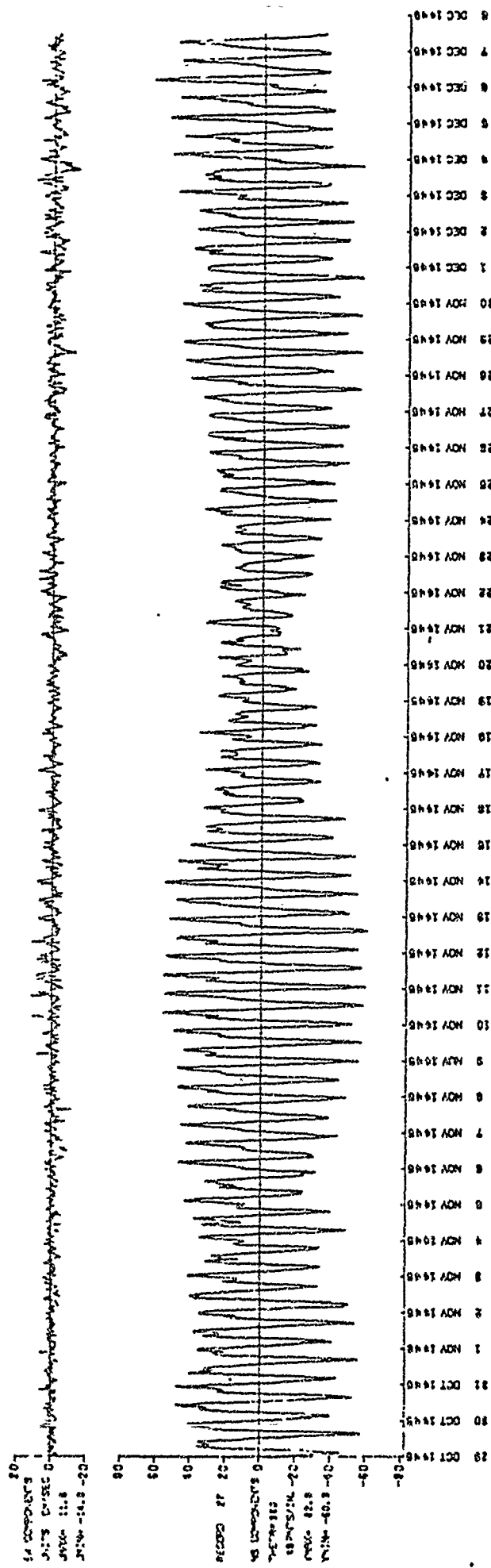
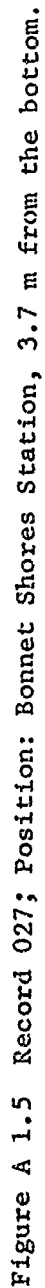


Figure A 1.5 Record 027; Position: Bonnet Shores Station, 3.7 m from the bottom.



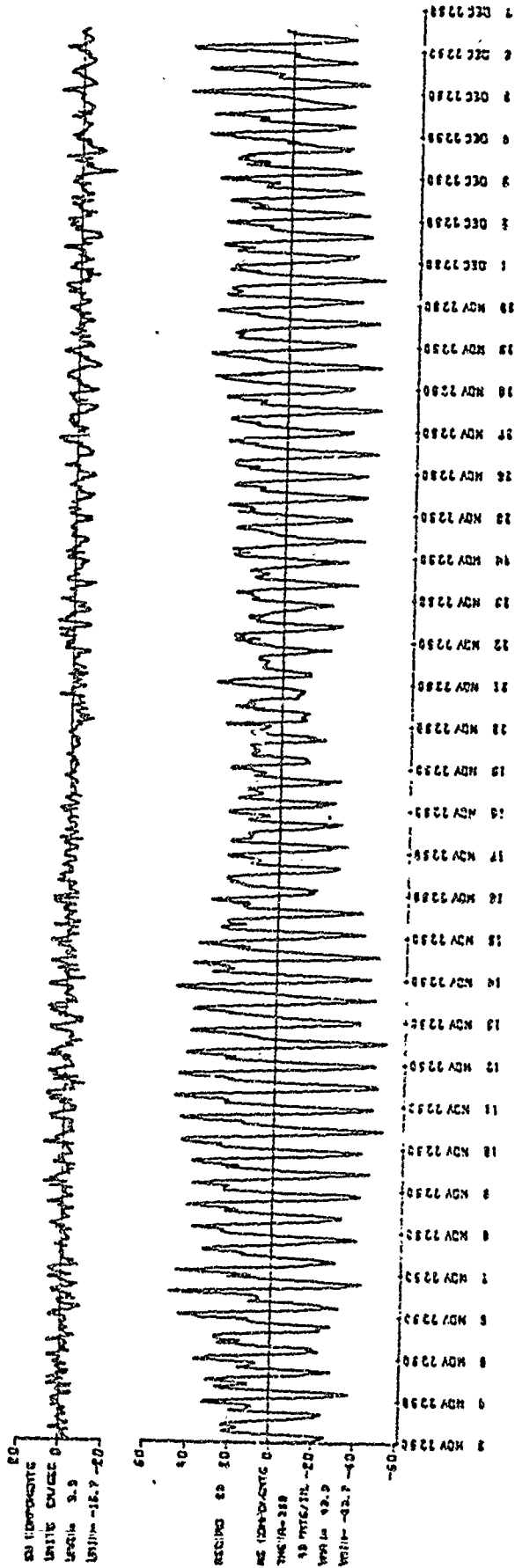


Figure A 1.6 Record 028; Position: Bonnet Shores Station, 1.7 m from the bottom.

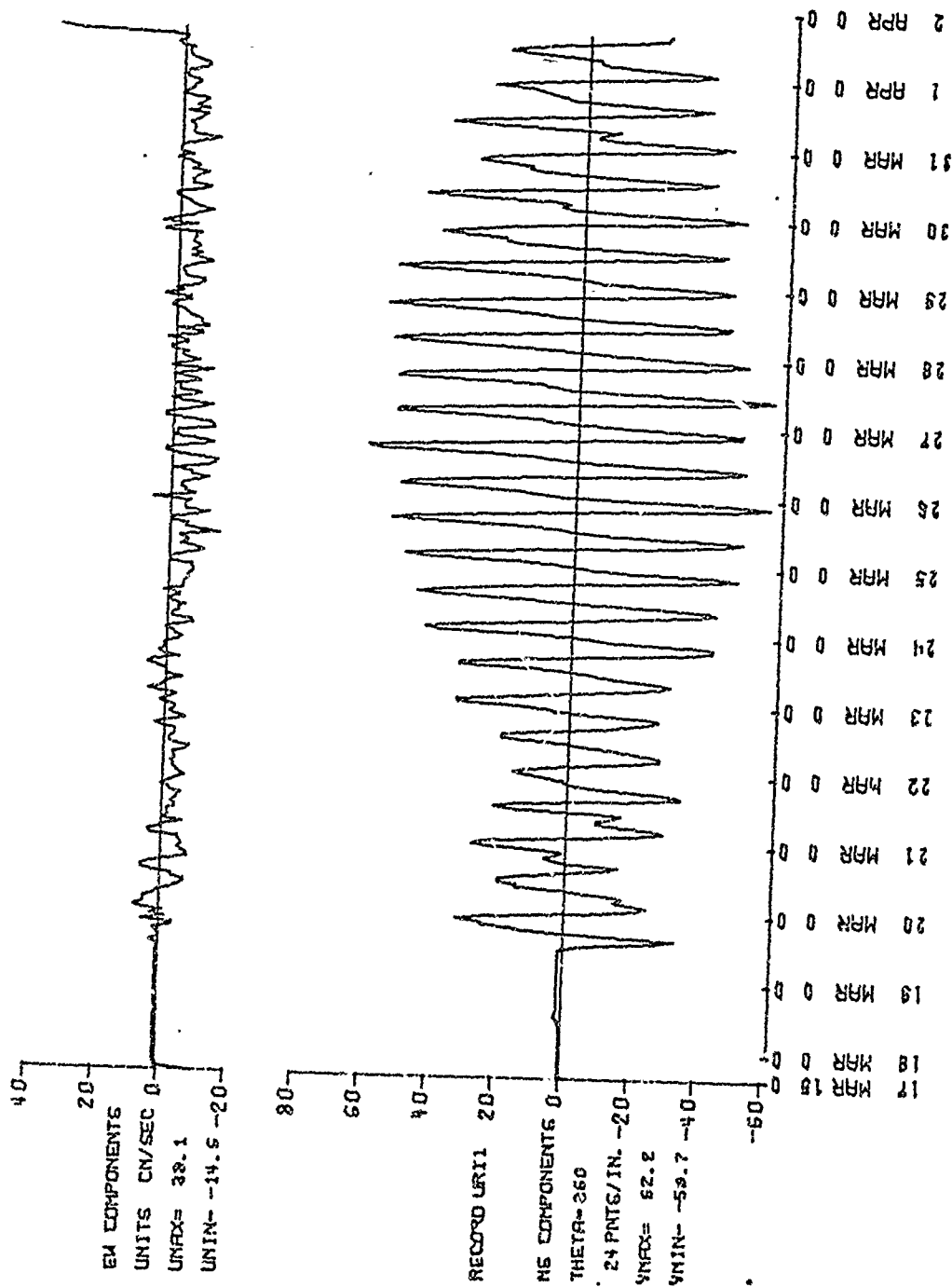


Figure A 1.7 Record 1; Position: Rome Point Station, 10.6 m from the bottom.

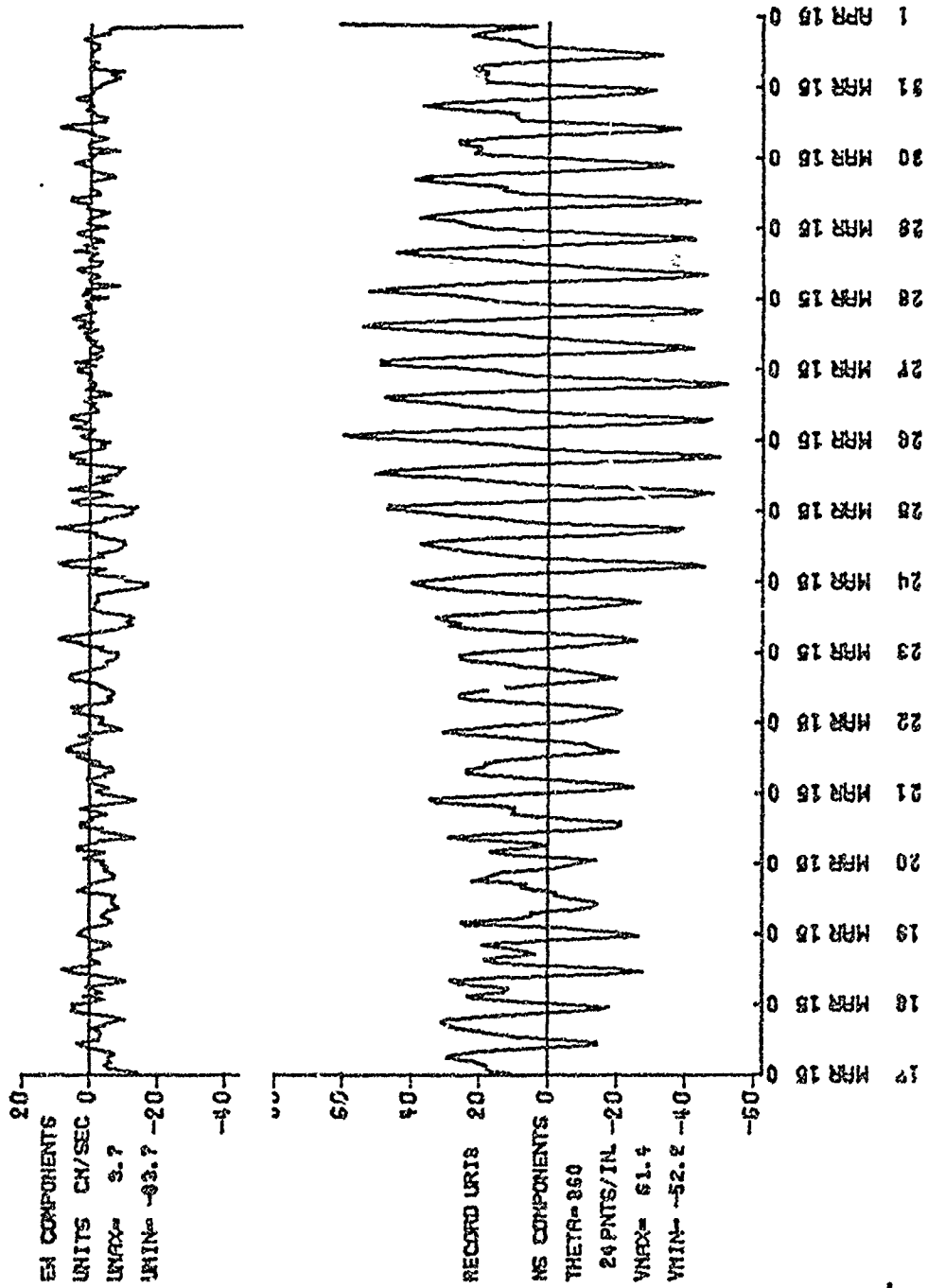


Figure A 1 2 Record 3; Position: Rome Point Station, 3.8 m from the bottom.

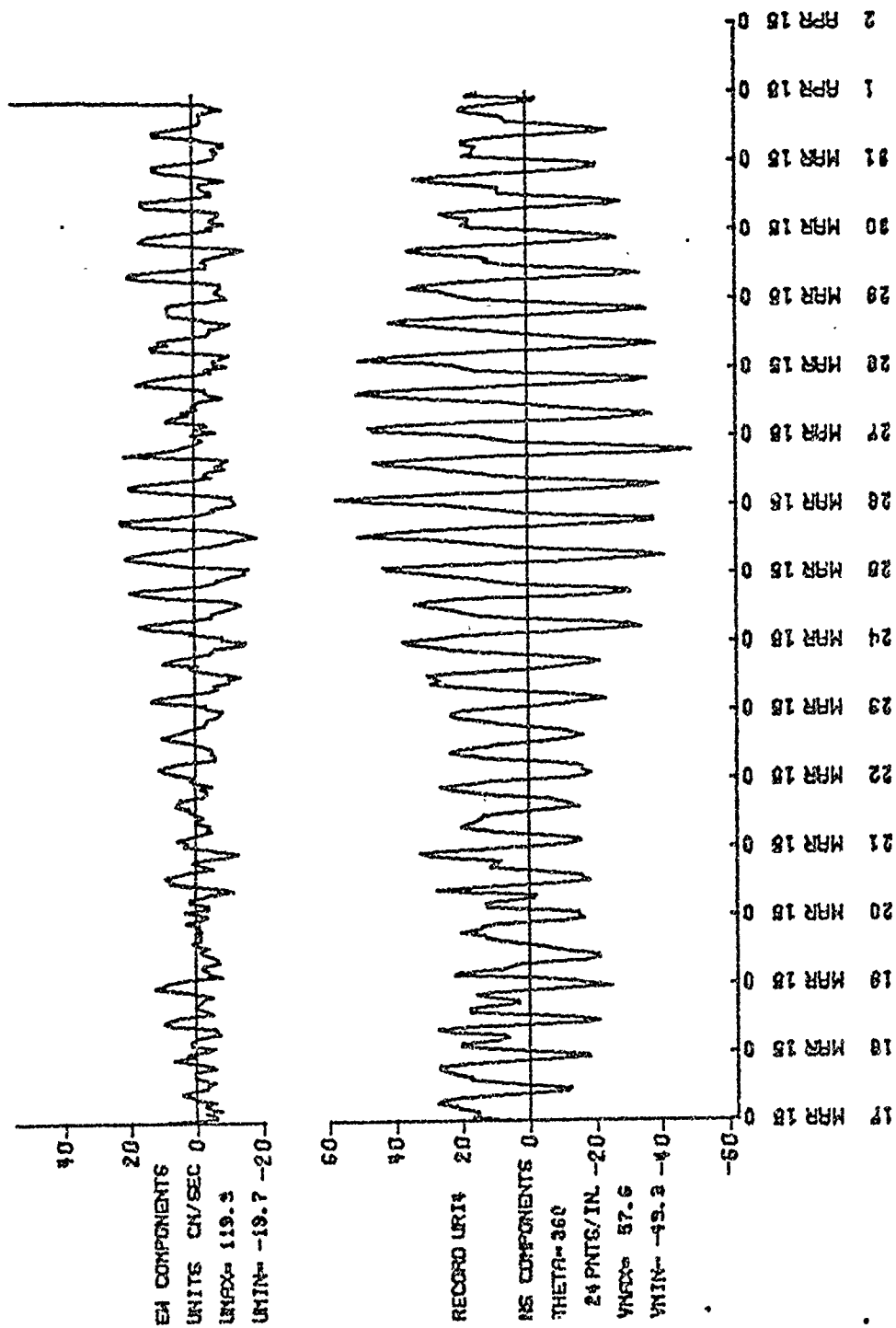


Figure A 1.9 Record 4; Position: Rome Point Station, 2.1 m from the bottom.

APPENDIX 2

Error Analysis

The high frequency resolution of a Savonius rotor current meter is limited by the recording scheme (previously discussed) and the response characteristics of the rotor and vane. Inadequate resolution itself would not be problematic here, excepting the non-linear behavior of the rotor to rectify motions above a critical frequency (different than the Nyquist frequency of 0.1 cycles per second). This section will discuss rectification of motions due to surface waves in order to obtain an estimate of their biasing impact on the data.

Consider a steady current V_0 upon which a sinusoidal disturbance $V_d \sin \omega t$ is superimposed. If $V_d < V_0$ the direction vane would remain stationary while the rotor would speed up and slow down with the same frequency as the disturbance. Any rectification of this periodic rotor response would appear as a fraudulent increase in current speed; biasing subsequent computations. If $V_d > V_0$, as may be the case during slack water, the vane would also respond to the disturbance. Therefore, at slack water, either abnormally high speed recordings or variable directions may indicate the presence of wave biasing.

The response of a Savonius rotor to the situation just described has been studied by Fofonoff and Ercan (1967). The response decreases with increasing frequency with the attenuation being large for "effective wavelengths" less than the critical value $L_c = 164$ cm. This critical "effective wavelength" is related to the steady current by,

$$L_c = V_0 T$$

where T is the period of the disturbance. L_c also represents the scale of motion below which the rotor response becomes non-linear. For "effective wavelengths" less than 164 cm, they gave the ratio of apparent rectified current δV to the steady current as,

$$\delta V / V_0 = 0.337 (V_{rms} / V_0)^2$$

where V_{rms} is the root mean square of the disturbance V_d . For $V_{rms}/V_0 = 0.24$ the ratio $\{V/V_0$ approaches 0.02. Unfortunately the above equation isn't applicable for rms fluctuations approaching the magnitude of the steady current. Hence, it can not be used during times of slack water.

If $V_0 > 10$ cm/s ($V_0 < 10$ cm/s only occurs in the West Passage about slack water) the above analysis suggests insignificant rectification for $V_d < 4$ cm/s. Similarly for 4 cm/s $< V_d < 8$ cm/s rectification may contribute ± 1 cm/s to the true current speed. Application will now be made to waves in the West Passage.

Under the influence of a deep water wave, a water particle follows a nearly circular path whose radius decreases exponentially with depth z . The horizontal component of the motion U is described by,

$$U = \frac{H\pi}{T} \exp\left(\frac{2\pi z}{L}\right) \sin \frac{2\pi t}{T}$$

$$= V_d \sin \frac{2\pi t}{T}$$

where H , L , and T are the wave height, length, and period. In order to estimate V_d it was first necessary to estimate H , L , and T using wave forecasting techniques Wiegell (1964) and Sverdrup and Munk (1947) .

The growth of waves in the West Passage is fetch limited. Figure A 2.1 shows the region of interest broken into eight segments, each with a given fetch. Wave height and wave age (the ratio of phase speed to wind speed) were obtained as a function of wind speed and fetch from Figure A 2.2. Figure A 2.3 was then used to calculate the corresponding wavelengths. The results, given in Tables A 2.1 a, b, and c are consistent with common experience. Since the calculated wave periods are all less than 3 sec, the scale of the wave motion relative to the tidal current is less than the critical "effective wavelength" L_c ; hence some rectification is expected.

Table A 2.2 gives the magnitude of V_d at a depth of 2 m (depth of the near surface current meter). These values are overestimates since no consideration has been given to the width of the wind generation field, a factor which also limits the growth of waves, e.g., see Wiegell (1967) p. 230. The dashed line demarks the limit after which wave biasing may be troublesome. All wind speed and fetch combinations to the left of

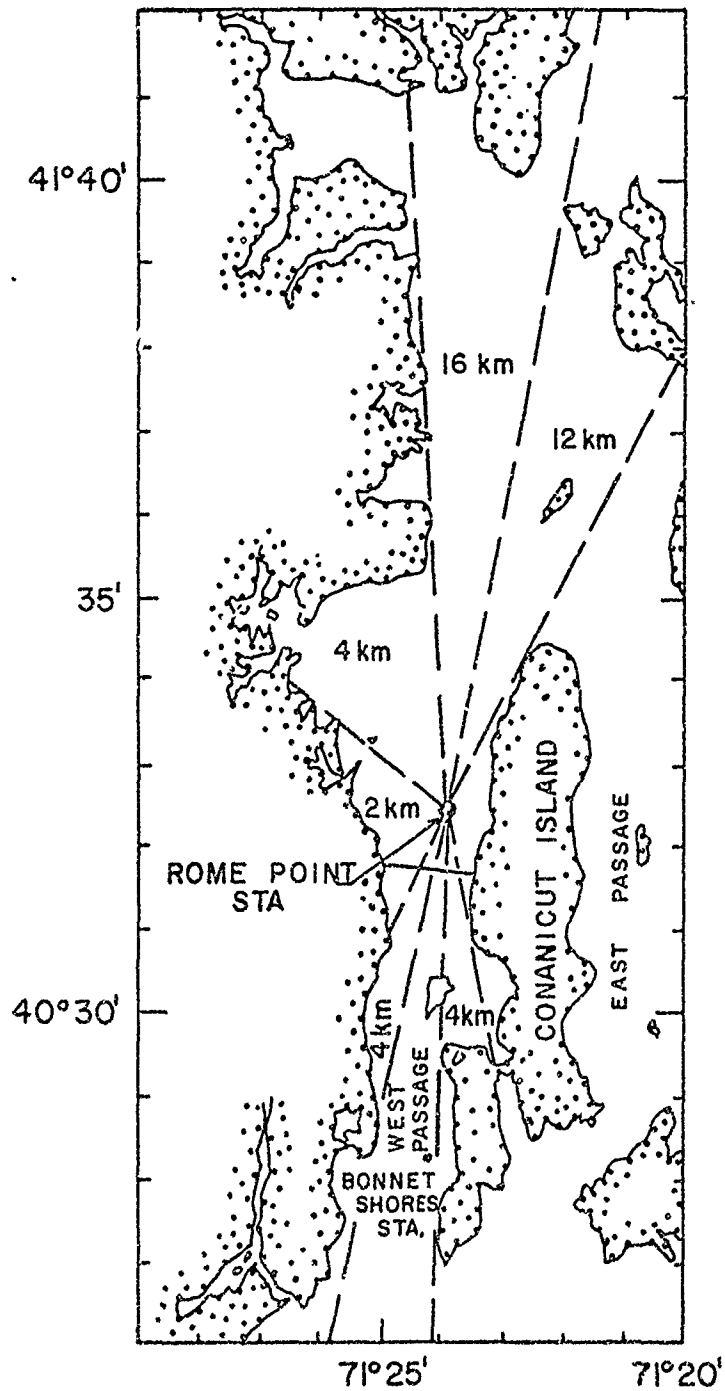


Figure A 2.1 The West Passage broken into eight regions, each with a characteristic fetch.

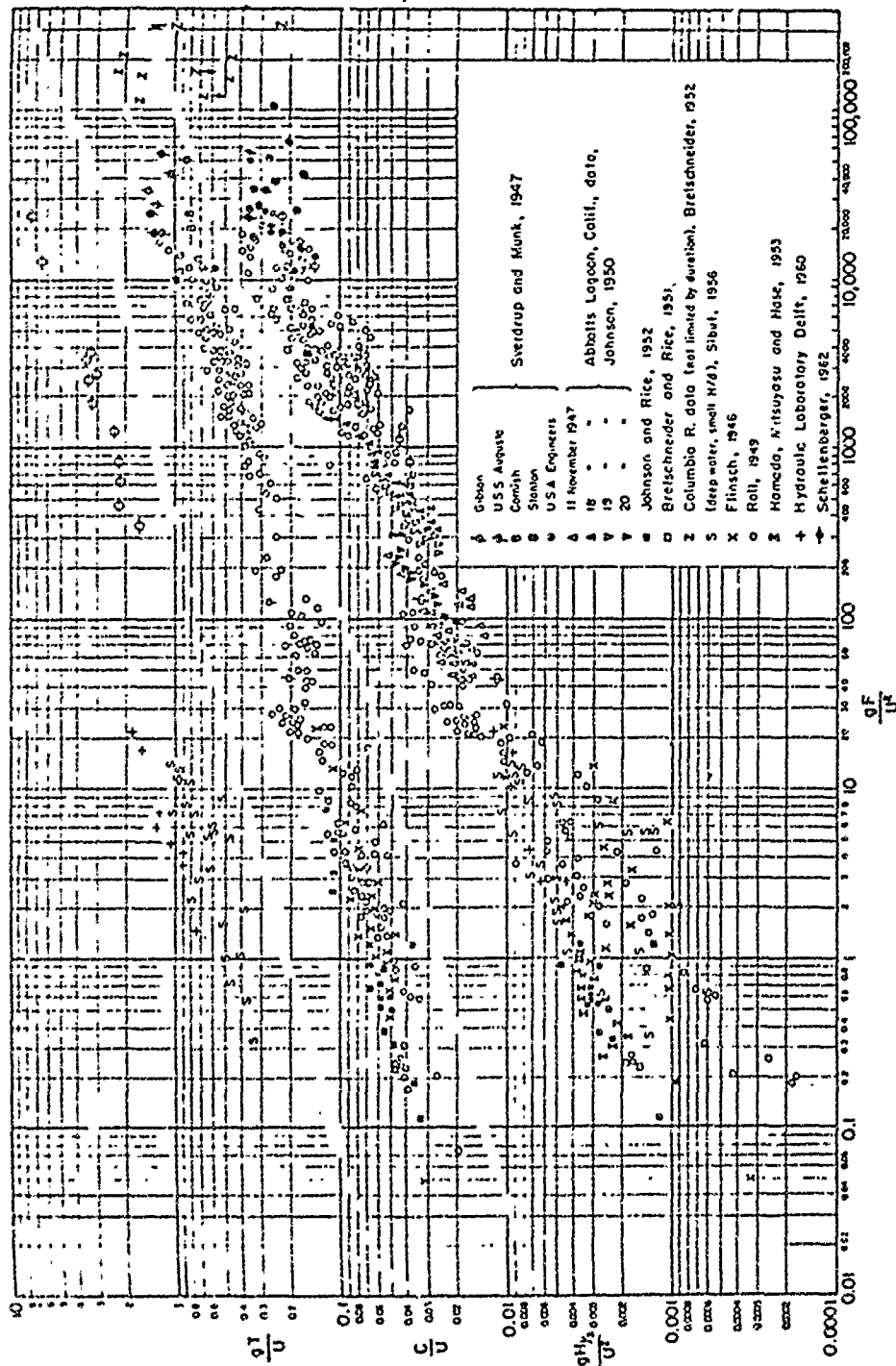


Figure A 2.2 Wave height, age, and period as a function of wind speed and fetch
(from Weigel 1964).

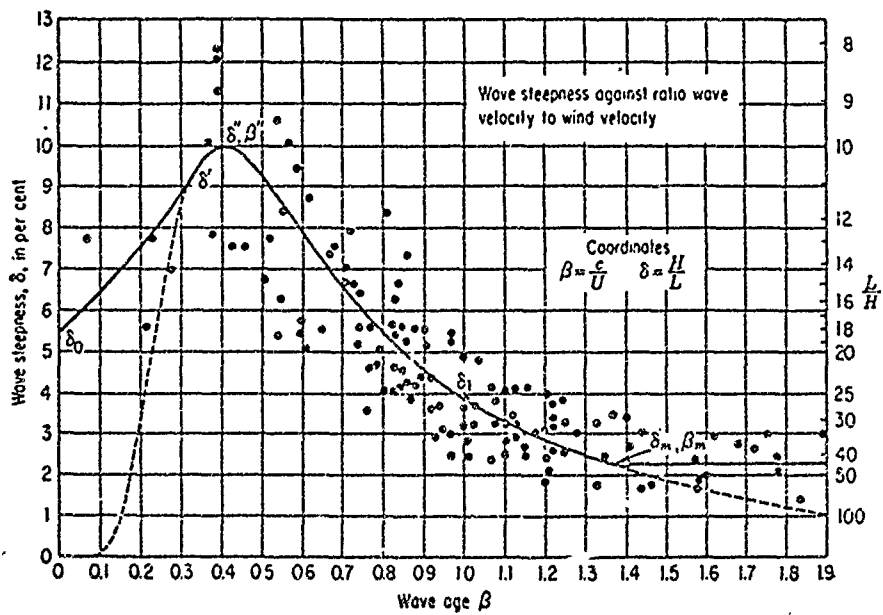


Figure A 2.3 Wave steepness as a function of wave age (after Sverdrup & Munk 1947).

Table A2.1a. Calculated wave heights (cm) as a function of wind speed and fetch.

	Wind Speed (m/s)					
	2	4	6	8	10	12
Fetch (km)						
2	6	15	22	29	35	40
4	8	21	33	43	52	61
8	9	28	48	61	75	93
12	10	29	55	80	97	116
16	10	33	63	93	112	134

Table A2.1b. Calculated wave lengths (m) as a function of wind speed and fetch.

	Wind Speed (m/s)					
	2	4	6	8	10	12
Fetch (km)						
2	0.7	1.5	2.4	3.3	4.1	5.1
4	1.2	2.1	3.3	4.7	5.8	6.9
8	1.8	3.3	4.9	6.1	7.7	9.9
12	2.2	3.8	6.0	8.2	9.7	12.0
16	2.6	5.0	7.4	9.9	11.2	13.4

Table A2.1c. Calculated wave periods (sec) as a function of wind speed and fetch.

	Wind Speed (m/s)					
	2	4	6	8	10	12
Fetch (km)						
2	0.6	0.9	1.3	1.5	1.6	1.8
4	0.9	1.2	1.4	1.8	1.9	2.0
8	1.1	1.4	1.8	1.9	2.2	2.5
12	1.2	1.5	2.0	2.3	2.4	2.9
16	1.3	1.8	2.2	2.6	2.7	2.9

Table A2.2. The magnitude V_d (cm/s) of the wave induced water motions at a depth of 2 m (depth of the near surface current meter). The dashed line demarks the limit after which wave biasing may be troublesome.

	WIND SPEED (m/s)					
	2	4	6	8	10	12
2	0	0	0	1	3	6
4	0	0	2	5	9	15
8	0	1	6	13	20	21
12	0	2	11	24	34	47
16	0	4	16	30	43	55

that line should have less than a ± 1 cm/s effect upon the instantaneous current measurements.

Figure A 2.4 is a progressive vector diagram of the wind during the fall measurement program. Comparison with Figure A 2.1 and Table A 2.2 shows that the wind conditions, for the most part, were below the limit to cause wave biasing. Only on three occasions; October 27-28, November 2-3, and November 12-15, was biasing imminent. Indeed, careful inspection of slack water current speeds and directions confirmed that those were the only times when biasing seemed apparent. It is interesting to note that the latter two occasions are also the only times that the calculated net currents lacked a strong correlation with the wind.

Figure A 2.5 is a similar progressive vector diagram for the spring program. The winds were generally stronger than during the fall and biasing may be expected during 21, 24-25, 27-28, and 31 March. This increased proportion of biased record may account for the decrease in correlation between the wind and net near surface current during the spring program.

No corrective measures can be taken when biasing is suspected. Therefore, the data during the forementioned times must be viewed with skepticism and probably discarded. For the rest of the measurements, however, the errors attributed to wave biasing are less than ± 1 cm/s. The contribution of these errors to the net current determinations is negligible to the extent that they are symmetrically distributed about a tidal cycle. Since 93% of the energy in the wind fluctuations occurred at periods greater than 12 hours the biasing errors should indeed be negligible. The worst situation is one in which the biasing errors are present only during ebb or flood tide. In this case the error introduced to the net currents would be ± 0.5 cm/s. Hence, except for the specifically designated points in Figure 11 a, b, and c, the biasing of individual net current estimates due to waves is less than ± 0.5 cm/s.

Presumably, these errors are randomly distributed over the entire sampling duration so their effect upon the means of the net current times series is very small. Therefore, the uncertainty of the means is that due to the variability of the time series as discussed in the text.

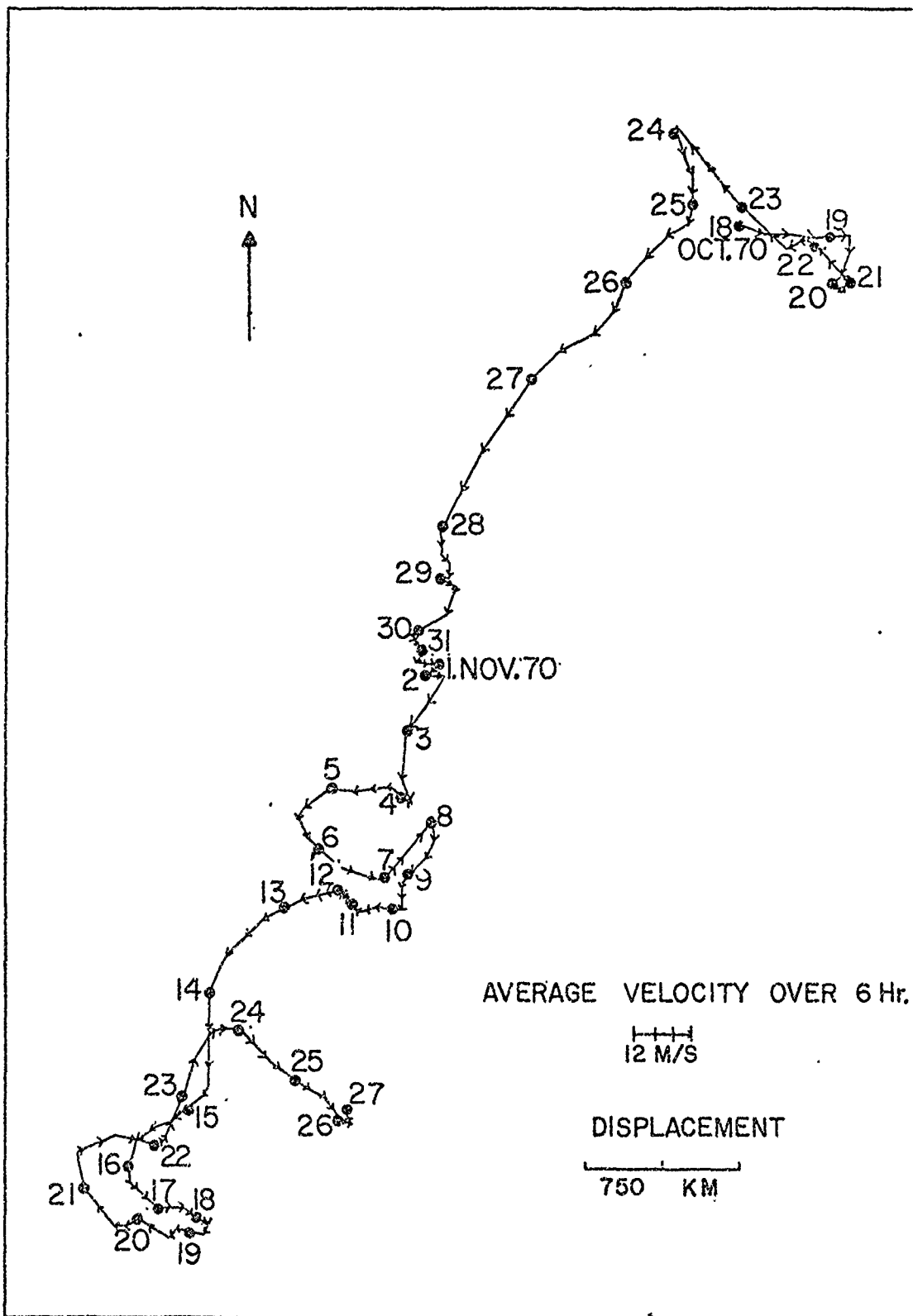


Figure A 2.4 Progressive vector diagram of the wind during the fall 1970 experiment.

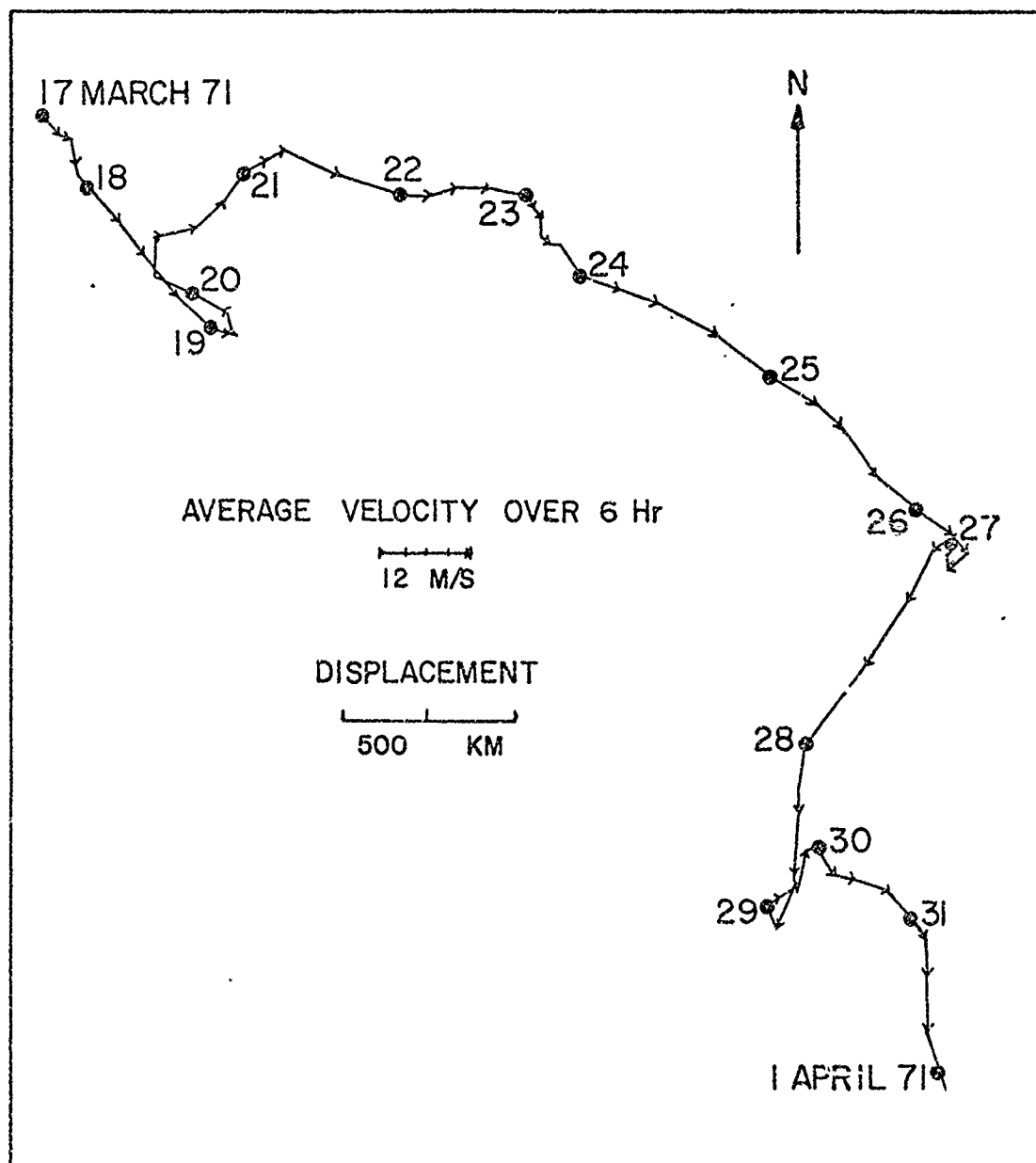


Figure A 2.5 Progressive vector diagram of the wind during the spring 1971 experiment.

Another source of error is the ± 3 percent calibration uncertainty of the Savonius rotor. This results in only a ± 3 percent error in the net currents which is negligible.

Canron (1969) measured net currents at a depth of 3 m using both Savonius rotor current meters and current meters that had been specifically designed to resolve high frequencies. He found very good agreement between the two, thus substantiating this discussion.

APPENDIX 3

Fresh Water Input

There are four rivers feeding the western side of Narragansett Bay. These are the Blackstone, Woonasquatucket, Pawtuxet, and Potowomut rivers, the location of which are shown in Figure 1. Gauging station data obtained from the U.S. Geological Survey is presented in Figures A 3.1 and A 3.2. No corrections have been made for the drainage areas downstream of each gauging station or that of Narragansett Bay itself; however an excellent view of the relative fresh water inputs to the western side of Narragansett Bay is still afforded. Beginning in February, the rate of fresh water input increases by as much as an order of magnitude over the fall values.

In accordance with Hicks (1959) the volume flow rate of fresh water into the West Passage may be approximated in terms of the volume flow rates of the above rivers by,

$$\begin{aligned} \text{Fresh water volume} &= 1/4 (\text{Blackstone} + \text{Pawtuxet} + \text{Woonasquatucket}) \\ \text{flow rate} &\quad + 1/2 (\text{Potowomut}) \end{aligned}$$

Table A 3 gives the average uncorrected volume flow rate for each river and the corresponding fresh water input to the West Passage during the fall and spring measurement programs.

Table A3. The average uncorrected volume flow rate for the rivers feeding the western side of Narragansett Bay and the corresponding fresh water input to the West Passage during the fall and spring measurement programs.

	Volume Flow Rate (m ³ /s)	
	Fall	Spring
Blackstone	10.7	52.5
Woonasquatucket	0.6	4.8
Pawtucket	6.6	11.8
Potowomut	1.0	3.5
to West Passage	5.0	19.0

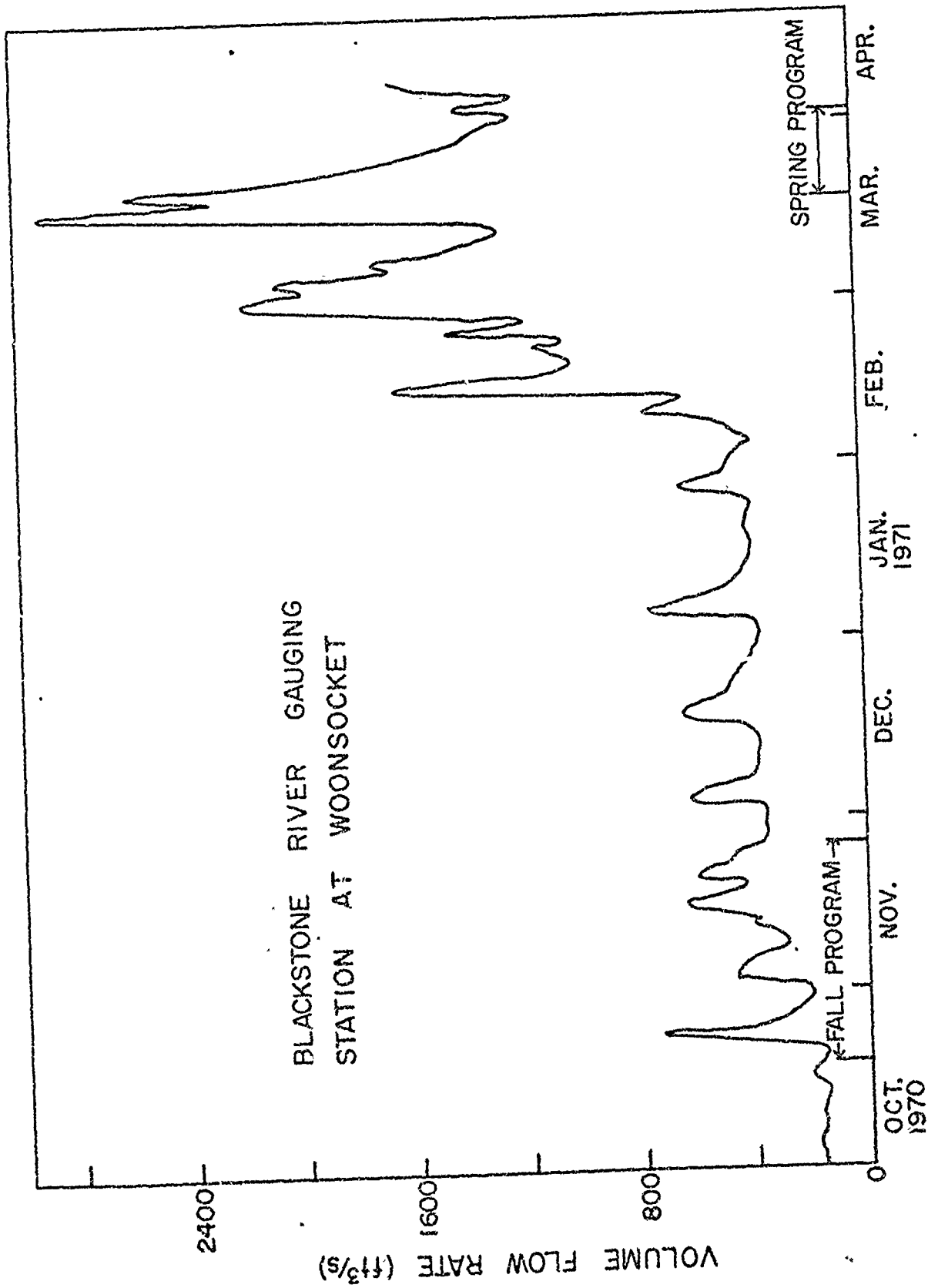


Figure A 3.1 River input data from a gauging station on the Blackstone River.

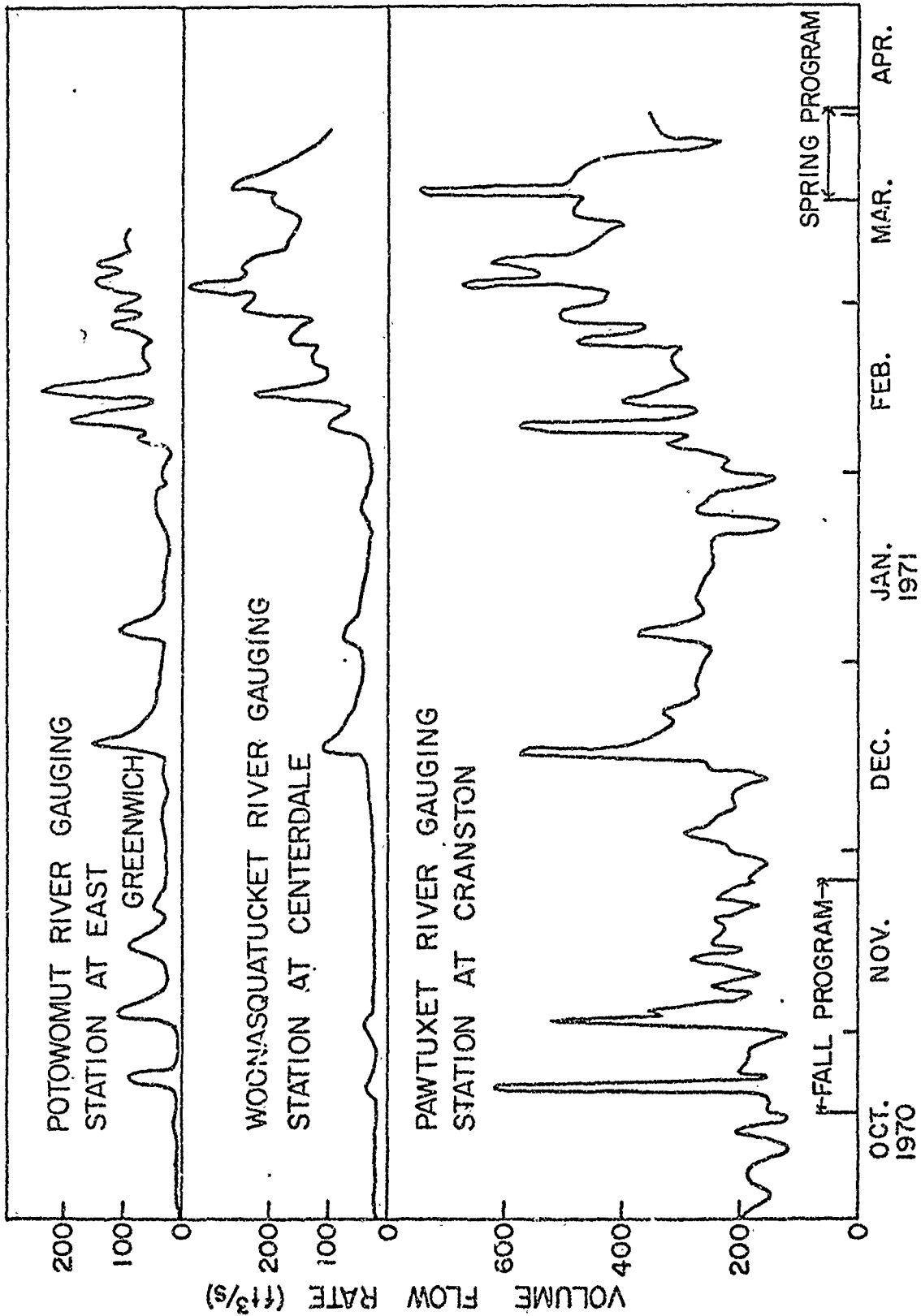


Figure A 3.2 River input data from gauging stations on the Potowomut, Woonasquatucket and Pawtuxet Rivers.

APPENDIX 4

Stratification

Temperature, salinity, and sigma-t values found in conjunction with the current measurements are given in Tables A 4.1 - A 4.4. The data during the fall is sparse due to instrument malfunctions. Figures A 4.1 and A 4.2 are representative graphs of sigma-t as a function of depth at both stations during the fall and spring. Typical order of magnitude estimates of the vertical and longitudinal density gradients were calculated from these. The results are shown in Table A 4.5.

Table A 4.5. Typical vertical and longitudinal density gradients in the West Passage during the fall and spring measurement programs.

	Vertical $\frac{1}{\rho} \frac{\Delta \rho}{\Delta z} (cm^{-1})$	Longitudinal $\frac{1}{\rho} \frac{\Delta \rho}{\Delta x} (cm^{-1})$
Fall Measurements	$2-4 \times 10^{-7}$	$\sim 7 \times 10^{-10}$
Spring Measurements	$5-6 \times 10^{-7}$	$\sim 12 \times 10^{-10}$

Both the vertical and longitudinal density gradients in the West Passage appear to increase by a factor of two from fall to spring. This increase is consistent with a previous data report by Hicks (1963) and is attributed to the increased river runoff during the spring.

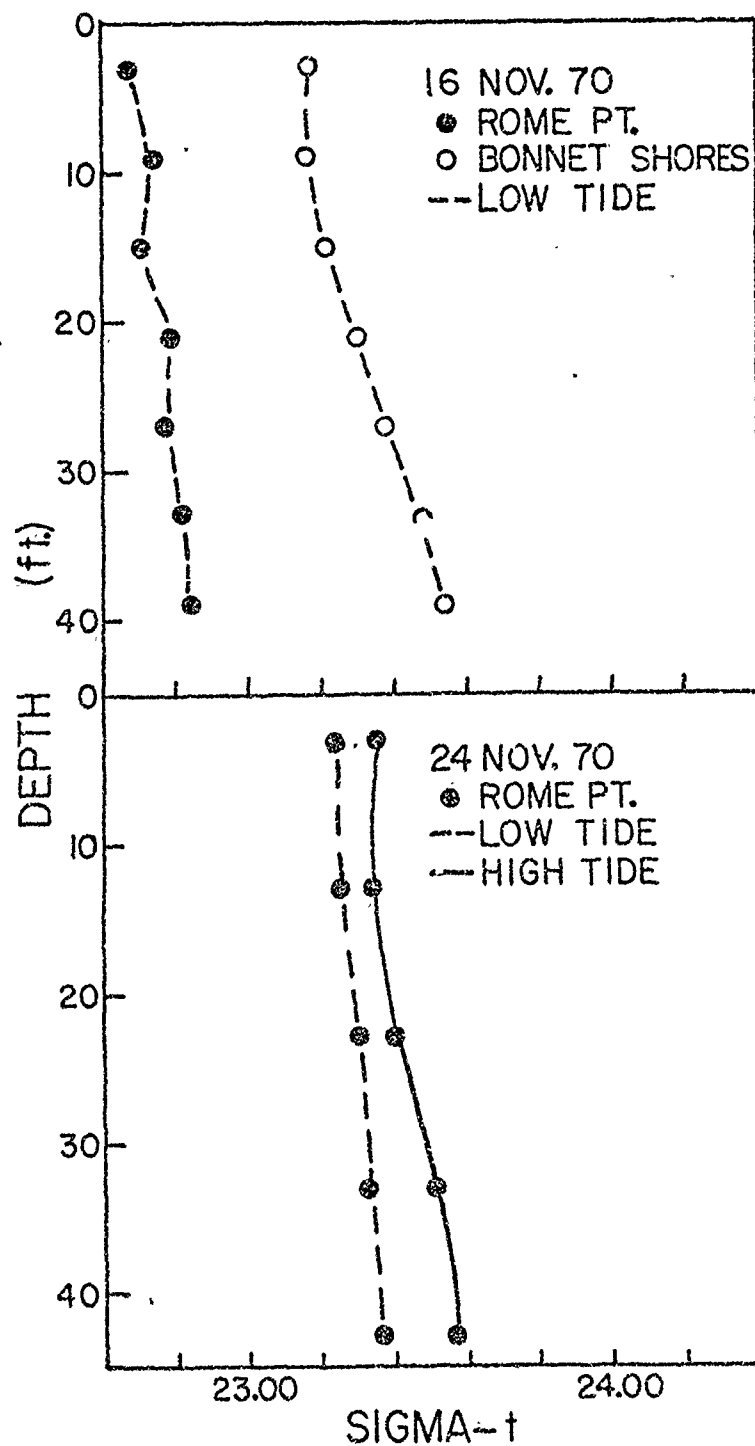


Figure A 4.1 Examples of sigma- τ as a function of depth during the fall 1970 experiment..

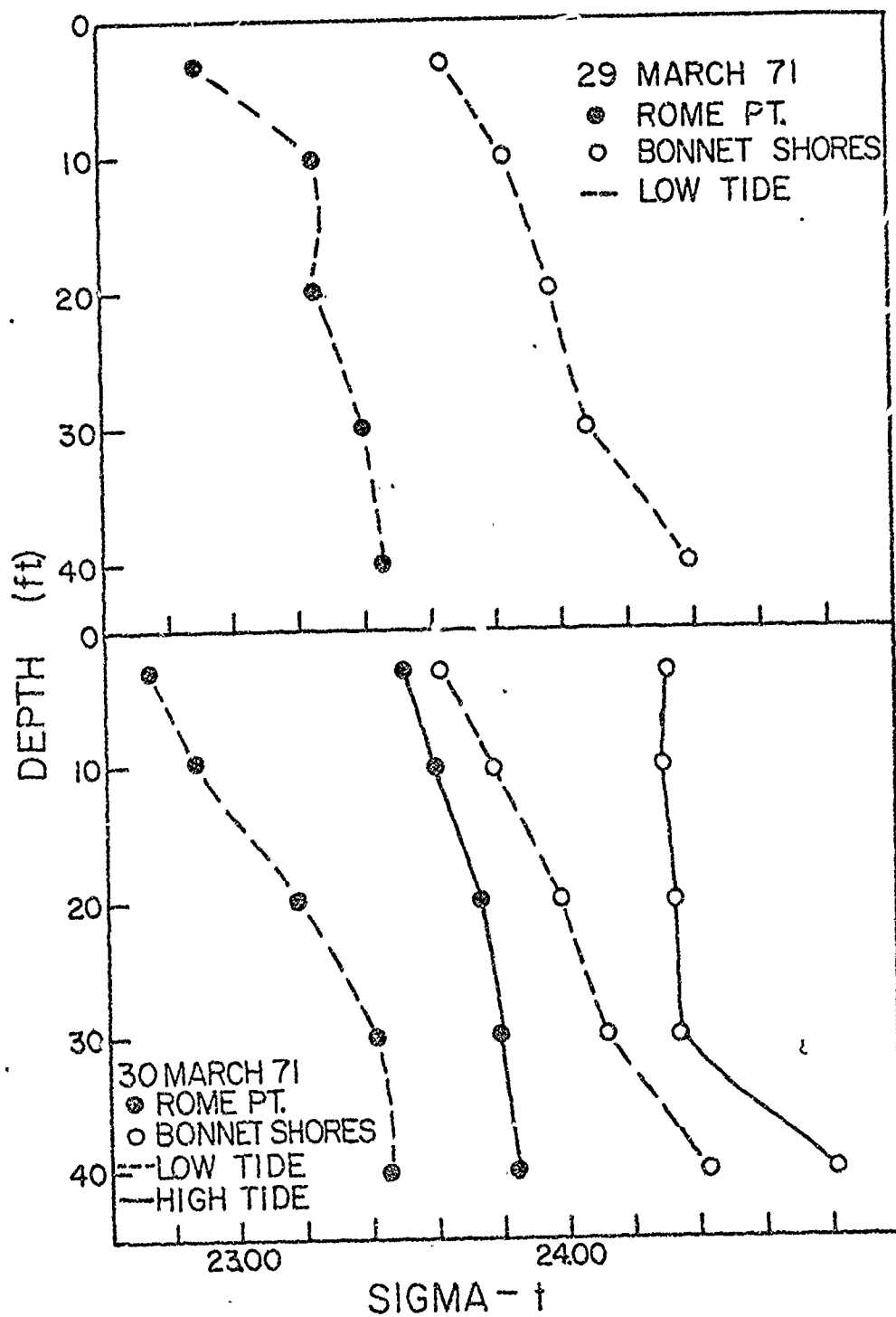


Figure A 4.2 Examples of sigma-t as a function of depth during the spring 1971 experiment.

Table A4.1. Temperature, salinity, and σ_t at the Rome Point station during the fall 1970 measurement program.

Time (EST)	Depth (ft)	Temp ($^{\circ}$ C)	Salinity ($^{\circ}$ /oo)	σ_t
16 November 1970 (low tide)				
1618	3	10.11	29.45	22.65
1619	9	10.25	29.58	22.73
1620	15	10.20	29.57	22.71
1621	21	10.35	29.68	22.78
1622	27	10.47	29.68	22.77
1623	33	10.44	29.75	22.82
1624	39	10.50	29.76	22.81
24 November 1970 (high tide)				
1629	3	9.41	30.24	23.36
1634	13	9.44	30.22	23.34
1640	23	9.46	30.31	23.41
1644	33	9.72	30.51	23.52
1647	43	9.71	30.56	23.57
1650	3	9.42	30.27	23.38
24 November 1970 (low tide)				
2203	3	9.15	30.04	23.24
2208	13	9.18	30.07	23.26
2211	23	9.20	30.14	23.31
2214	33	9.22	30.17	23.33
2217	43	9.24	30.20	23.37
2220	3		30.13	

Table A4.2. Temperature, salinity, and σ_t at the Bonnet Shores station during the fall program.

Time (EST)	Depth (ft)	Temp ($^{\circ}$ C)	Salinity ($^{\circ}$ /oo)	σ_t
16 November 1970 (low tide)				
1522	3	10.67	30.26	23.17
1523	9	10.75	30.26	23.16
1525	15	10.89	30.37	23.22
1626	21	10.99	30.49	23.30
1527	27	10.99	30.58	23.37
1528	33	11.15	30.76	23.47
1529	39	11.18	30.84	23.53

Table A4.3. Temperature, salinity, and σ_t at the Rome Point station during the spring program.

Time (EST)	Depth (ft)	Temp ($^{\circ}$ C)	Salinity ($^{\circ}$ /oo)	σ_t
20 March 1971 (low tide)				
1602	0	2.94	28.70	22.90
1604	10	2.71	28.81	23.25
1606	20	2.65	29.14	23.27
1608	30	2.64	29.31	23.40
1610	40	2.59	29.39	23.46
1613	0	2.91	28.75	22.98
30 March 1971 (high tide)				
1052	0	2.84	29.47	23.52
1054	10	2.81	29.59	23.61
1056	20	2.67	29.73	23.74
1058	30	2.60	29.82	23.80
1100	40	2.60	29.88	23.85
1103	0	2.83	29.65	23.66
30 March 1971 (low tide)				
1600	0	3.17	28.50	22.74
1603	10	3.16	28.67	22.87
1605	20	2.90	29.06	23.19
1607	30	2.90	29.10	23.23
1609	40	2.88	29.14	23.25
1611	0	3.18	28.75	22.91

Table A 4.3 continued

Time (EST)	Depth (ft)	Temp ($^{\circ}\text{C}$)	Salinity ($^{\circ}/\text{oo}$)	σ_t
5 April 1971 (low tide)				
1109	0	4.84	29.09	23.05
1111	10	4.63	29.06	23.04
1113	20	4.57	29.00	22.99
1115	30	4.06	29.43	23.36
1117	40	3.93	29.88	23.77
1119	0	4.72	29.03	23.01
13 April 1971 (high tide)				
0935	0	5.90	28.53	22.56
0937	10	5.51	29.09	22.99
0930	20	5.51	29.14	23.02
0941	30	5.31	29.18	23.07
0950	40	4.81	29.64	23.47
0952	0	6.12	28.32	22.29
15 April 1971 (high tide)				
1020	0	5.00	29.15	23.42
1022	10	4.95	29.20	23.41
1024	20	5.03	29.20	23.45
1026	30	4.90	29.20	23.55
1030	40	4.80	29.19	23.57
1034	0	4.99	29.19	23.35

Table A4.4. Temperature, salinity, and σ_t at the Bonnet Shores station during the spring program.

Time (EST)	Depth (ft)	Temp ($^{\circ}$ C)	Salinity ($^{\circ}$ /oo)	σ_t
29 March 1971 (low tide)				
1523	0	2.78	29.64	23.65
1526	10	2.68	29.86	23.84
1528	20	2.64	30.02	23.97
1530	30	2.61	30.16	24.08
1533	40	2.50	30.54	24.39
1537	0	2.66	30.00	23.95
30 March 1971 (high tide)				
1016	0	2.73	30.45	24.31
1018	10	2.74	30.44	24.30
1021	20	2.63	30.55	24.34
1023	30	2.61	30.55	24.35
1025	40	2.40	31.06	24.82
1027	0	2.65	30.52	24.37
30 March 1971 (low tide)				
1520	0	3.10	29.62	23.63
1522	10	2.88	29.83	23.79
1523	20	2.80	30.08	23.99
1525	30	2.65	30.21	24.13
1527	40	2.65	30.51	24.44
1530	0	3.04	29.80	23.77

Table A4.4 continued

Time (EST)	Depth (ft)	Temp ($^{\circ}$ C)	Salinity ($^{\circ}$ /oo)	σ_t
5 April 1971 (low tide)				
1037	0	4.69	29.44	23.33
1039	10	4.43	29.50	23.40
1041	20	3.98	29.99	23.84
1043	30	3.48	30.34	24.16
1045	40	2.80	31.30	24.97
1047	0	4.50	29.40	23.31